KAUNAS UNIVERSITY OF TECHNOLOGY

MONIKA MAZIUKIENĖ

# MODELING OF COMPLEX HEAT TRANSFER AND PHASE CHANGE TRANSITIONAL PROCESSES OF WATER DROPLETS IN HUMID AIR

Doctoral dissertation

Technological Sciences, Energetics and Power Engineering (T 006)

2019, Kaunas

This dissertation was prepared at Kaunas University of Technology in 2014–2018, at Faculty of Mechanical Engineering and Design, Department of Thermal and Nuclear Energy.
The studies were supported by Research Council of Lithuania.

**Scientific supervisor:**

Prof. Dr. Habil. Gintautas MILIAUSKAS (Kaunas University of Technology, Technological sciences, Energetics and Power Engineering – T 006).

Doctoral dissertation has been published in:

http://ktu.edu

Editor:

Armandas Rumšas (Publishing Office “Technologija”)



ISBN (įrašyti gautą ISBN kodą)

The bibliographic information about the publication is available in the National Bibliographic Data Bank (NBDB) of the Martynas Mažvydas National Library of Lithuania.

KAUNO TECHNOLOGIJOS UNIVERSITETAS

MONIKA MAZIUKIENĖ

# VANDENS LAŠELIŲ SUDĖTINIŲ ŠILUMOS MAINŲ IR FAZINIŲ VIRSMŲ PEREINAMŲJŲ PROCESŲ DRĖGNAME ORE MODELIAVIMAS

Daktaro disertacija

Techologijos mokslai, Energetika ir termoinžinerija (T 006)

2019, Kaunas

Disertacija rengta 2014-2018 metais Kauno technologijos universiteto (Mechanikos inžinerijos ir dizaino) fakultete (Šilumos ir atomo energetikos katedroje) katedroje. Mokslinius tyrimus rėmė Lietuvos mokslo taryba.

**Mokslinis vadovas:**

Prof. habil. Dr. Gintautas MILIAUSKAS (Kauno technologijos universitetas, technologijos mokslai, energetika ir termoinžinerija – T 006).

Interneto svetainės, kurioje skelbiama disertacija, adresas:

http://ktu.edu

Redagavo:

Armandas Rumšas (leidykla Technologija")



ISBN (įrašyti gautą ISBN kodą)

Leidinio bibliografinė informacija pateikiama Lietuvos nacionalinės Martyno Mažvydo bibliotekos Nacionalinės bibliografijos duomenų banke (NBDB).

## Contents

## Nomenclature

| | |
|---|---|
| $a$ | – thermal diffusivity, $m^2/s$; |
| $B_T$ | – Spalding heat transfer parameter; |
| $B_M$ | – Spalding mass transfer parameter; |
| $c_p$ | – mass specific heat, J/kg·K; |
| $D$ | – mass diffusivity, $m^2/s$; |
| $Fo$ | – Fourier number; |
| $F_s$ | – Radiation source function; |
| $g$ | – vapor flux, kg/s; |
| $I$ | − index of control time in a numerical scheme; |
| $I_\omega$ | – spectral intensity of radiation, *W*/(*m*·*ster*); |
| $J$ | − integer defining the radial coordinate of the droplet; |
| $k_c^-$ | – effective conductivity parameter; |
| $\kappa_\omega$ | – spectral index of absorption; |
| $L$ | – latent heat of evaporation, J/kg ; |
| $m_g$ | – vapor mass flux density, $kg/m^2s$; |
| $M$ | – integer defining the spectral subdivision of the radiation spectrum; |
| $n$ | – number of the term in infinite sum; |
| $N$ | – the number of assessable members in the infinity integral equation series; |
| $Nu$ | – Nusselt number; |
| $n_\omega$ | – spectral index of refraction; |
| $n_{\omega\kappa}$ | – complex spectral index of refraction; |
| $p$ | – pressure, Pa; |
| $Pe$ | – Peclet number; |
| $Pr$ | – Prandtl number; |
| $q$ | – heat flux density, $W/m^2$; |
| $R$ | – radius of a droplet, m; |
| $R_\mu$ | – universal gas constant, J/kmol·K; |
| $Re$ | – Reynolds number; |
| $r$ | – radial coordinate, m; |
| $r_\omega$ | – spectral index of light reflection; |
| $\chi_\omega$ | – spectral coefficient of absorption, $m^{-1}$; |
| $T$ | – temperature, K; |
| $\beta, \gamma, \varphi, \psi$ | – characteristic angles of thermal radiation in sphere rad; |
| $\beta_\omega$ | – Brewster's angle, rad; |
| $\eta$ | – dimensionless radial coordinate; |
| $\lambda$ | – thermal conductivity, W/K·m; |
| $\mu$ | – molecular mass, kg/kmol ; |
| $\rho$ | – density, $kg/m^3$; |
| $\tau$ | – time, s; |

$w$ – velocity, m/s.

**Subscripts**

$c$ – convective;
$co$ – condensation;
$C$ – droplet center;
$dp$ – dew point;
$e$ – equilibrium evaporation;
$f$ – phase change;
$g$ – gas;
$gv$ – gas-vapor mixture;
$i$ – time index in a digital scheme;
$it$ – number of iterations in numerical scheme;
$j$ – index of radial coordinate in numerical scheme;
$kt$ – contact temperature;
$l$ – liquid;
$m$ – mass average;
$R$ – droplet surface;
$r$ – radiation;
$sr$ – radiation source;
$v$ – vapor;
$\omega$ – spectral;
$\Sigma$ – total;
$0$ – initial state;
$\infty$ – far from a droplet;
$*$ – variable.

**Superscripts**

$+$ – external side of droplet surface;
$-$ – internal side of surface;
$\wedge$ – average droplet parameter value.

**Abbreviations**

$c$ – heating by convection;
$c+r$ – combined heating by convection and radiation;
HMT – heat mass transfer;
$k$ – heating by conduction;
$k+r$ – combined heating by conduction and radiation;
$P$ – parameter of heat and mass transfer;
$P_f$ – parameter of droplet phase transformations;
$P_F$ – droplet dynamic parameter;
$P_T$ – parameter of droplet thermal state;
$P_q$ – parameter of droplet energy state;

$\overline{P}$ – parameter normalized according to initial state of droplet parameter.

## Main Definitions

The main concepts used in the dissertation:

- **Droplet** – water volume having equivalent sphere radius $R_{ekv} = \sqrt[3]{3M_l/(4\pi\rho)}$ ;
- **Semi transparent liquid** – an equivalent diameter sphere that partially reflects, absorbs and transmit spectral radiation;
- **'Droplet' task** – the general name of dispersed liquid droplets HMT researches;
- **Phase transformation cycle** – the consistent change of phase transformation regimes on the droplet surface;
- **Combined transitional processes** – ongoing and interacting processes of heat transfer and phase transformations in condensation and in transitional to equilibrium evaporation regime;
- **Interaction of processes** – self-interaction that defines together the intensity of ongoing transfer processes;
- **Condensation regime** – droplet heating process by heat transfer and condensed vapor heat;
- **Transitional evaporation** – droplet evaporation case, when heat supplied for the droplet warms it and evaporates water;
- **Equilibrium evaporation** – droplet evaporation case, when supplied heat evaporates water;
- **Heating by conduction** – droplet heating case, when heat supplied only by conduction is evaluated;
- **Heating by convection** – droplet heating case, when heating by radiation is neglect;
- **Combined heating** – general droplet heat transfer case;
- **Iterative cycle** – at defined time moments executed iterative calculations by the fastest descent method for determination of instantaneous droplet surface temperature;
- **Droplet surface instantaneous temperature** – in the iterative cycle, the defined droplet surface temperature at which the calculated flows towards and from the droplet are different not less than by 0.05 percent.

## Introduction

In today's industry, it is important to develop renewable energy technologies to reduce the use of fossil fuels and its negative impact on the environment. Biofuel, together with renewable energy sources, is considered as a good alternative to replace fossil fuels. *Renewable Energy Directive 2009/28/EC* and *2001/80/EC* for industry emphasizes the need to reduce emissions from large combustion plants [1, 2]. This raises important questions regarding the development of an energetically sustainable environment, practical industrial application of newly developed technologies and the modernization of already operating plants.

Liquid spraying takes an important place in thermal technologies [3]. Fuel (used in furnaces and engines), along with water, is the most commonly sprayed liquid. Water spray is the first step towards modern micro-systems based on the technologies of transfer processes. In these technologies, the contact area between a one-piece carrier (commonly, a gas) and a discretionary (commonly, liquid droplets or solid particles) medium is strongly increased. This ensures fast heat and mass exchange between phases.

In the two-phase flow between droplets and the gases they are carrying, complex droplet heat and mass transfer processes take place under conditions of intense interaction. The interaction intensity is defined by a number of factors. Most important factors in this interaction are the *Stefan hydrodynamic flow* influencing the convective heating and evaporation of droplets, the impact of droplets slipping in the gas flow for external heat transfer and liquid forced circulation, as well as the forced liquid circulation and radiation absorption in semitransparent droplets.

A wide variety of boundary conditions are characteristic for the two different phase gas and droplets flows in the spraying technologies. However, the calculation methodology for defining processes in the general case can be named as the 'droplet' problem which consists of the droplet tasks of internal and external heat and the mass transfer and phase transformations ongoing on the droplet surface.

In the water dispersion case, the 'droplet' problem must be determined regarding the aspect of droplet phase transformations because their intensity defines the efficiency of the thermal technologies. Sprayed water droplets are usually warmed by a gas flow; therefore, surface evaporation takes place, or water vapor condensates on droplets. Thus gases around a droplet cool down and dry or humidize due to water vapor concentration variations. This leads to the result that the vapor flow flowing around the droplet's surface is the most important parameter for liquid spraying technologies. It is defined by the specifics of droplet heat transfer processes and the cycle peculiarities of phase transformation regimes. In sprayed water droplets, phase transformations, cycle condensation, transitional and equilibrium evaporation processes can be foreseen.

The 'droplet' problem has been investigated in many researchers' works. These studies cover more than a century of science history. The classical single 'droplet' evaporation models are presented in researches of Fuchs [4], Sirignano [5], Sazhin [6] and other works [7]. In the 'droplet' problem, the equilibrium evaporation process of a droplet has been widely investigated [8]. Slightly more profound analysis has been

made for transitional evaporation, while condensation regime studies are still at the initial stage of development, therefore, investigations of the transitional processes require more attention. There is lack of systematic assessment of the transfer processes interaction in the constantly changing phase transformations cycle of the droplet, which is the main goal of this thesis.

**Object of investigation** – Complex transitional transfer processes of a water droplet in constantly changing phase transformation regimes

**The aim of the work** – To investigate the transitional processes of heat and phase transformations inside water droplets in humid air flow and to highlight the interaction peculiarities and the defining factors.

**Objectives of the thesis**

In order to achieve the aim of the thesis, the following objectives have been outlined:

1. On the grounds of scientific literature analysis, to provide a physical interpretation of water droplet heat and mass transfer processes, which could define the cycle of continuous and uninterrupted droplet phase transformation regimes.
2. To analyze the peculiarities of the droplet energy state in the phase transformations cycle and to justify the Spalding transfer parameter based on the similarity theory, the relevance of the Stefan's hydrodynamic flow influence assessment in the condensation regime while in the 'droplet' mathematical model and its numerical solution algorithm, to define an opportunity of the variation of phase transformation regimes on the droplet surface.
3. To define the optimal number of members in the infinite sum in the line of integral equations which describes the unsteady temperature field gradient and to define the radial and time coordinate scheme grid in the numerical scheme.
4. To provide a mechanism for experiment control in each iterative cycle for the definition of the droplet instantaneous surface temperature and to justify the reliability of the results of numerical investigation.
5. To model droplet warming and phase transformations in humid air in water spraying technologies under common boundary conditions; to investigate the influence of air parameters, droplet dispersity and temperature as well as heat transfer peculiarities on the transitional transfer processes and to highlight the thermal state and phase transformations of water sprayed in humid air flow; to define factors of phase transformations.
6. To summarize the results of numerical research by dimensionless parameters which shall enable the prediction of thermal state and phase transformations as well as phase transformations, which is important for the engineering practice of optimal water spraying.

**Defensive propositions of the dissertation:**

1. The universal 'droplet' mathematical model for droplet phase transformation regimes is ensured by Stefan's hydrodynamic flow influence evaluated by the classical Spalding parameter expression modification based on the energy state variation in transitional regimes as well as phase transformations and the introduction of a correction ratio expressed by convectional heating fluxes and its relation with the droplet temperature gradient vector.
2. Continuous numerical research of droplet thermal and energetic state variation in phase transformation regimes is ensured by a vapor flux model from negative in the condensation regime to positive in the evaporation regime, as well as universal models of the temperature field gradient and the Spalding parameter.
3. Water droplet phase transformation processes and their interaction in humid air flow are defined by factors of air humidity, water and air temperatures, droplet dispersity and their complex heat transfer. Water parameters define the transitional phase transformation regimes, while air parameters define the droplet equilibrium evaporation temperature and the evaporation rate. For complex heat transfer, the importance of droplets slipping in humid air flow and their spectral absorption must be taken into consideration.
4. In semitransparent droplet absorbed radiation flux for the condensation phase, the transformation regime is not significant. However, in the transitional evaporation regime, due to its impact, the negative temperature field gradient forms, which makes preconditions to intensify the evaporation of the liquid surface and distinguishes between two individual periods in this regime. In the first iteration, water is evaporated only by the part of heat supplied for the droplet by external convection. In the second case, water is evaporated by the entire amount of external convection heat supplied for a droplet and a part of the heat supplied by radiation. Equilibrium evaporation only starts when the total absorbed radiation flux gets involved in the evaporation process.
5. The duration of the condensation regime on the droplet surface for a droplet slipping in a humid air flow increases due to forced water circulation caused by friction forces because it can intensify the heat lead to droplet internal layers, and its surface warming to the dew point temperature increases.
6. In a humid gas flow, the thermal state of sprayed water in the transitional phase transformation regime can be defined by the dew point and equilibrium evaporation temperatures normalized with regard to the sprayed water temperature.

**Scientific novelty of work:**

Based on the definition of the droplet energy state, the variation in the phase transformation cycle and the evaluation of Stefan's hydrodynamic flow assessment by the Spalding heat transfer parameter based by similarity theory relevance was specified, extended and applied for transitional transfer processes condensation regime.

On the basis of the complex evaluation of water droplet heat transfer conditions, the possible condensation regime duration growth for more intensively slipping droplets was highlighted.

**Practical significance of the work**:

The introduced dimensionless parameters $\overline{T}_{dp} = T_{dp}/T_{l,0}$ and $\overline{T}_e = T_e/T_{l,0}$ have a practical value for the optimal water spray in the field of engineering. From the scientific point of view, the practical value of the thesis is the developed systematic approach to the water droplet phase transformation regime cycle and a piece of software which is iteratively optimized with regard to these transformations .(

The equilibrium evaporation temperature variation dependence on the air temperature and humidity $T_e(\tau)$ parameters and the emphasis of droplet heat transfer conditions is of fundamental importance for practical aspects of the thematic area.

**Publication of the scientific work** – The topic of the dissertation was covered in 9 publications of the author of the thesis, including 3 publications in international and 7 in national databases of *Clarivate Analytics* in the publications of the *Web of Science Core Collection*, 2 publications in peer-reviewed international scientific information data referenced publications, and 11 publications based on international and Lithuanian conference papers.

**Volume of the scientific work** – This work consists of an introduction, review, methodology and results sections, conclusions and a list of the author's publications on the dissertation topic. This work is made up of 100 pages and 52 figures; 111 references are presented in the reference list.

**Structure of the dissertation –** The main body of the dissertation consists of an introduction, three chapters and conclusions. The first part of the dissertation *Literature Review on the Issue of Droplets* covers the development of practical application of sprayed water droplets in various technical systems. The question of the droplet task application in thermal technologies is highlighted. The 'internal' droplet task solution is treated as essential in this topic. In the second part of the work, the methodology of the main aspects of the 'droplet' theory and its relevant calculation pertaining to the 'internal' task basis is provided. The main assumptions discussed in the work are formulated. The methodology of the iterative numerical scheme calculation and optimization is also provided. The third chapter presents the most important numerical modeling results and delivers a summary of the key statements. In the last section of the dissertation, conclusions of this work are presented.

**Approbation of the scientific work** – Oral presentations n the dissertation topic have been delivered in 3 international conferences abroad, in 1 international conference in Lithuania in addition to 7 presentations in national conferences.

## 1. Literature Review on the Issue of Droplets

The meaning of water is very important in nature and in human activities [9]. Traditionally, not only natural phenomena but also a variety of technical applications deal with large volumes of water. In the nature, water is found in seas, oceans, or precipitation in the form of rain, while in thermal technologies it is found as a liquid boiling in large volumes. Transfer processes taking place in large volumes are denoted by some peculiarities.

The heat and mass transfer of a large volume flowing liquid is not effective because the contact surface interphase is relatively small. Therefore, it is important to improve thermal technologies by optimizing them, and this creates preconditions for the development of new and more efficient technologies. For this, it is important to split large volumes of liquid into smaller volumes. As a method of dispersion, fluid spraying is well-known and widely used [3–7]. In dispersed fluid technologies, the contact surface is often developed between the solid carrier (commonly, gas) and the discretionary (commonly, liquid droplets or solid particles) medias. Heat and mass transfer takes place at the junction of different phases. Temperature variation among phases is also very important. It is regarded to be a variation of the contact surface of a droplet and its surrounding gas flow temperature function in time.

The importance of liquid spraying in various technologies has already been highlighted. However, the optimization and development of different technologies encourages to take into account the peculiarities of specific technologies. Therefore, the following section of the dissertation presents an overview of traditional liquid spraying directions and the application of various water spraying technologies.

### 1.1. Practical Application of Water Spraying Technologies

Liquid in the form of droplets is important not only in natural phenomena, but also in practical human activities [1–25, etc.]. The most commonly sprayed liquids in thermal technologies are water and liquid fuel. The fuel spraying technology is considered to be the traditional one in internal combustion engines [5, 10, 11, 12, 13] and furnaces [14, 15, 16]. The water spraying technology is applied in air conditioning systems [17, 18], fire front suppression [19, 20, 21], gas cooling [22, 23, 24], agricultural irrigation [25, 26], surface treatment [27, 28] and protection [29], cooling towers [30, 31], water freezing and crystallization [32, 33, 34], aerosols [35, 36, 37, 38], gas turbines [39, 40], heat recovery from removed flue gases [41], reduction of $No_x$, CO, $CO_2$, SO and other oxides in fuel combustion products [42, 43], pollutants reduction in nuclear power plants [44], water and fuel emulsions [45, 46] and in other technologies.

In the last decade the thematic area of modern and promising water droplets heat and mass transfer processes has been increasingly developed. Such modern technologies are water droplet evaporation to regulate high temperature combustion parameters [47], formation of clusters [48], surface erosion studies [49], various technological processes in the food industry [50], medicine and pharmacy [51], laser

technologies [52], electro-technical industry [53], and plasma engineering [54, 55] can be considered.

Liquid spraying technology is assigned to compound two phase flows; it analyzes the dynamic interaction between the liquid droplet and gaseous phases. In the research of liquid fuel droplets, the following main trends of analysis can be distinguished: pure [56, 57], bi-component [58, 59], and multicomponent [60, 61].

In order to optimize the already existing technologies and make preconditions for effective development of new ones, the research problem is highlighted. Thus compound heat and mass transfer transitional processes in water droplet and in gas two-phase flow are evaluated. This requires cognition of the patterns of systematic and deep transfer processes. The knowledge and management of water spray mechanics is important for modern transfer processes in micro systems and nanotechnologies-based technologies and their practical application. This widely influences any scientific research in the 'droplet' thematic area.

The main issues raised by the modern society in terms of sustainable energy are environmental pollution and global warming. This is influenced by energetics-related demands to use different sources of renewable energy or energy saving devices in order to reduce fossil fuel use dependency and its negative impact on the nature. Energy transformation processes and the usage of various nature resources generates side products which usually increase the environmental pollution. Attempts to improve the current situation and reduce emissions into the environment in thermal technologies are regulated by various legal acts and directives providing strict technology control [1, 2].

In the context of environment protection, the development of modern technologies is very important for the sustainable development of mankind. When creating economically sustainable biofuel combustion technologies, not only economic performance indicators of boilers are improved, but also the thermal and chemical environmental pollution is reduced [62]. Therefore, water spraying becomes an important aspect of environmental protection. When burning various fuels, either liquid, gaseous or solid, flue gases are emitted; their list contains various oxides – such as CO, $CO_2$, SO, $NO_x$, various chemical compounds – HCl, HF, $H_2$, $N_2$, $H_2O$, and solid particles.

Condensing economizer technologies are based on direct water spraying into removed biofuel flue gases, where water vapor condensates directly on water droplets and is warmed by the condensate. In the contact type economizer water is directly sprayed into the flue gases, and humidity condensates directly on the droplets. In the recuperative type economizers, humidity condensates on the flue gases when they flow through tubes, while water is sprayed at the upper part of the economizer in order to improve the hydrodynamics of the condensate film and the flue gas flow. Furthermore, water spraying can be used to irrigate air that is supplied into a fireplace, or else to control the biofuel burning process, to clean flue gases from solid particles and to regulate the parameters of flue gas that is supplied into a condensing economizer. In most cases, water spraying is carried out in separate devices. However, the water spraying processes must be synchronized with each other in order to ensure optimal biofuel burning and the effective exploitation of the generated thermal energy.

This requires knowledge of complex heat and mass transfer processes in the water droplet phase change cycle regimes [63, 64].

One of the ways to reduce energy consumption is to increase the efficiency of air conditioning and refrigeration. Many researches have investigated interrelated heat and mass transfer processes in air conditioning systems [17, 18]. The efficiency of the system could be increased when spraying water into the condenser of the refrigeration device. When water is directly sprayed over the condenser, the heat transfer could be improved in two possible ways. In the first case, the sprayed water evaporates in air and reduces the air temperature via the adiabatic cooling process. In the second case, the sprayed droplets affect the heat exchanger's surface and increase the area of the heat and mass transfer due to water film formation and water evaporation on the surface. The optimization of heat and mass transfer processes involves structural improvement of the relevant device taking into account the heat transfer area, flow rates and other processes [18].

Water spraying technology is very important in researches related with $NO_x$ oxides reduction in combustion products [42]. The investigations carried out in this area improves general knowledge about the impact of water spraying on combustion chambers. Water spraying in internal combustion engines of various types controls the combustion temperature and pressure. This method is also used to control undesirable emissions. Various water spraying cases are applied for $NO_x$ reduction in internal combustion engines and furnaces [43].

Fire suppression by water spraying includes several combined phenomena [21]. This process affects the gaseous phase, including flame or fuel, or both of them at the same time. Fire flame suppression is affected by a strong evaporation process. Thermal water characteristics, such as high water specific evaporation heat, have an impact on the reduction of the flame energy and temperature. One of the most important characteristics of the sprayed water application for fire front reduction is the ratio of the large surface area and the volume, which is crucial for efficient heat and mass transfer [65]. During the evaporation of water droplets, a large amount of vapor is released, which affects the mixing of fuel vapor and oxygen. This, in turn, affects the combustion process and causes fire front suppression. In the course of fire front suppression, water droplets are strongly affected by the impact of radiation. Therefore, it is important to take into account the effects inside the droplet and their impact on the droplet's lifetime duration. Thus the deeper cognition and modeling of fire front suppression with the help of water droplets requires to evaluate the radiation impact and the spectral optical characteristics of a semi-transparent liquid.

The formation of toxic or flammable gas clouds is a common undesirable phenomenon in the industry [67]. To avoid this effect, the phenomenon of sprayed water curtains in various industry sections is being applied. Sprayed water curtains are deemed to be a useful technique for the reduction of large and unwanted industrial hazards [68]. This technology is used in chemical and gas production in order to prevent the release of heavy toxins or flammable vapors into the environment. In terms of the water curtains technology, the mechanism of heat transfer is characterized by the energy transfer theory which combines conduction, convection and radiation

processes. When seeking the development and experimental application of an effective methodology of water spraying in water curtains, it is necessary to understand complex physical and heat transfer processes related with the variations of gas concentration and temperature.

Therefore, the variety of spray technologies is very large. The application of liquid dispersion across the technologies is very broad, and it includes a wide range of industries. Each technology has some specific aspects denoted by important peculiarities; therefore, the problem of the definition of various boundary conditions arises. The optimal usage of each specific technology requires good understanding of heat and mass transfer processes in liquid technologies so that to define their regularities and evaluate the boundary conditions influencing them. This problem can be solved individually, or combined together with the peculiarities and conclusions of the investigation so that the general regularities could be highlighted. It is a hard and long road. The 'reverse' forward-looking approach is denoted by good perspectives as a systematic approach to the ongoing processes of sprayed fluid technologies is being developed. Initially, the regularities of the general complex transfer processes are discussed; further in the text, the specificity of each technology is taken into account. In the literature, this definition is known as the 'droplet' problem, or the 'droplet' task researches.

## 1.2. 'Droplet' HMT Problem

Water droplets are commonly used in various thermal and other technologies as discussed in the previous section. Traditionally, the 'droplet' problem is considered to be a classical task which is therefore investigated in many authors' works.

The first theoretical model of droplet evaporation in the gaseous medium was described in 1877 by J.S. Maxwell. This work discussed and presented simple stationary and spherical droplet evaporation as compared to the continuous infinite medium [4]. According to the author, the vapor concentration on the droplet's surface is equal to the vapor concentration in equilibrium with the droplet. Previous droplet investigations focused on external heat and mass transfer for stagnant droplets [68]. Meanwhile, subsequent studies assessed the impact of more complex heat and mass transfer boundary conditions on the droplet heating intensity and phase transitions [5]. The instability of the heat and mass transfer process directed researchers' attention towards the necessity of solving the droplet problem in order to describe the heat flows distribution during the process of droplet heating and evaporation.

Investigations covering transfer processes of gas and droplet flows are called by general 'droplet' term. When modeling heat and mass transfer processes in sprayed liquid flows, the 'external' and 'internal' problems of droplets could be relatively distinguished. The objective of the droplet 'external' task is to define the intensity of the transfer processes between the droplets and the fluid that carries them. The target of the droplet 'internal' problem is to characterize the intensity of the transfer processes in droplets. The 'droplet' problem could also treated in a narrower and in a broader sense. In the first case, the aim is to purify the regularities of the droplet transitional processes so that the influence of droplet heat and mass transfer for the

parameters of carrying the flow is neglected. In practice, it is the case when the amount of liquid injected into the flow is quite little so that the effect of the droplet heat transfer and phase transformations for the fluid flow parameters is not significant. In the second case, the intensity of fluid flow parameters variation is defined.

It is assumed that the interface temperature of different phases is defined as phase contact temperature $T_{fK}$. The definition of *surface temperature* is directly related with total heat fluxes $q_{\Sigma}$ which flow forward and toward the droplet surface. These fluxes can only be described by complex analysis of combined transfer processes. In the general case, a balance of the heat flux in a quasi-stationary assumption framework can be described by equation:

$$\sum_{ii}^{II} \vec{q}_i(\tau) = 0. \qquad (1)$$

The water droplet temperature can be calculated by using simplified models [14]:

- A model based on the assumption that the droplet surface temperature is uniform and does not change over time;
- The 'Infinite conductivity' model which is based on the assumption that there is no temperature gradient inside a droplet;
- The 'Effective conductivity model' when $k_c \equiv f(Pe)$ [68];
- The 'Vortex model' which describes circulation in the droplet by the well-known Hill vortex and describes circulation dynamics inside a droplet [69];
- Temperature gradient definition with numerical methods inside a droplet.

The stationary temperature distribution inside a droplet can be described with analytical equations only in the simplest droplet stationary heat transfer case 'k' when the heat in the droplet spreads only by conduction. This is a case of idealized heating in which heat transfer by convection and radiation is denied. In a non-radiating medium, slipping droplet convection heating is defined as the '*c*' heat transfer case. In the case of radiant media, complex heating cases by conduction and radiation, or convection and radiation, are distinguished. They are defined as '$k+r$' and 'c+$r$' droplet heating cases.

In the thermal technologies, the applicability of stationary heat transfer models is rather limited because the thermal state of sprayed liquid droplets changes over time in most cases [70]. Therefore, the temperature distribution inside a droplet can be described by the radius and time function $T(r,\tau)$ which defines the unsteady temperature field. In the simplest '*k*' heat transfer case, the unsteady temperature field function $T_{'k'}(r,\tau)$ inside a droplet is calculated according to the well-known integral type mathematical model [71] which can be calculated numerically.

In the 'droplet' problem, the tasks of 'internal' and 'external' solutions are outlined. For all the thermal technologies, the most important parameter is vapor flux *g* (kg/s); therefore, it could be stated that the main task of the 'droplet' problem is to define the phase transformations ongoing on the droplet surface. However, this task

could not be separated from the ‘droplet’ internal and external problems; thus the ‘droplet’ HMT problem must be investigated in a complex way.

### 1.3. Droplet phase transformations

For the practical application of thermal technologies, it is important to evaluate the intensity of phase transformations, because the liquid vapor flow density on the droplet surface defines the efficiency of the spray technologies. Vapor flux *g* may be generated or condensate on the water surface at the contact with humid gases [72]. (

Phase transformations on the water surface are defined by vapor flow flowing toward a droplet in the condensation regime, and from a droplet in the evaporation regime. Therefore, liquid vapor flow *g* on the droplet’s surface is considered as one of the most important parameters in liquid spraying technologies. The driving force of phase transformations is the difference of water vapor near the droplet’s surface and partial pressure in gases (Fig. 1.1).

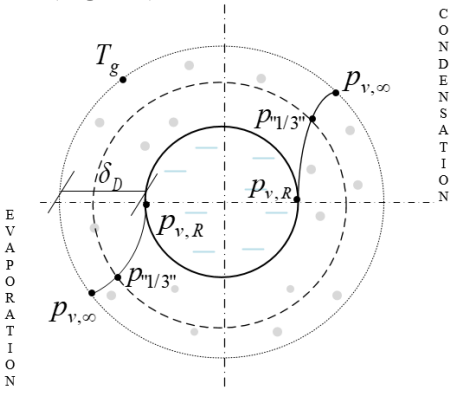


Fig. 1.1. Phase transformation model on the droplet surface

The water vapor flux is characterized according to the difference of partial pressure of water vapor in humid air and vapor near the droplet’s surface: $\Delta p_v(\tau) = p_{v,g}(\tau) - p_{v,H}(\tau)$ (Fig. 1.1). In the diffusion layer $\delta_D$ that surrounds the droplet, the vapor flux near the droplet $p_{g,R}$ increases to water vapor partial pressure $p_{v,\infty}$ in the course of the condensation process. The condensation process takes place when condition $p_{v,\infty} > p_{v,R}$ is valid. Then the driving force of the process is defined as the difference between the water vapor partial pressure in the droplet-surrounding air and the partial vapor pressure near the droplet’s surface $\Delta p_v = p_{v,\infty} - p_{v,R} = p_{v,\infty} - p_{sot}(T_R)$. The evaporation process takes place when $p_{v,R} > p_{v,\infty}$, while the driving force is the difference between the water vapor partial pressure near the droplet’s surface and the water vapor partial pressure in the surrounding air $\Delta p_v = p_{v,R} - p_{v,\infty} = p_{sot}(T_R) - p_{v,\infty}$.

The intensity of phase transformations on the water surface is defined by vapor flux density, kg/(s m$^2$) which is defined as the vapor flux ratio with the contact surface area between phases:

$$m_v = \frac{g_v}{A} \qquad (2)$$

The vapor flux density in Stefan's formula is defined by the surrounding $H$ thickness diffusion layer $\delta_D$ through the liquid surface; it can be described analytically [72]:

$$m_v = -\frac{D_{vg}\mu_v}{R_\mu T_v}\frac{p}{l}\ln\frac{p - p_{v,\infty}}{p - p_{v,sat}} \quad . (3)$$

Water vapor flux density on the surface of a spherically symmetric droplet in [73] is defined by expression:

$$m_{v,R} = \frac{D_{vg}}{T_{vg}}\frac{\mu_v}{R_\mu R}\left\{p_{v,R} - p_{v,\infty} + \frac{\mu_v}{\mu_g}\times\left[p\ln\frac{p - p_{v,\infty}}{p - p_{v,R}} - \left(p_{v,R} - p_{v,\infty}\right)\right]\right\}. \quad (4)$$

When assumptions $\delta_D \equiv R$ and $T_{v,H} \equiv T_{vg,R}$ are valid, the vapor flux density (5) equation matches the vapor flux density expression (4) approximation that is provided in [74].

$$m_{v,R} = \frac{D_{vg}}{T_{vg}}\frac{\mu_v p}{R_\mu R}\ln\frac{p - p_{v,\infty}}{p - p_{v,R}} \qquad (5)$$

The vapor and gas mixture temperature near the droplet is equated with the droplet surface temperature: $T_{vg,R} \equiv T_R$. The water vapor pressure near a droplet is expressed by a part of vapor volume $\overline{p}_v$ in the gas mixture which is expressed as the ratio of water vapor partial pressure and the gas pressure. The partial pressure of water vapor generated on the droplet surface is expressed as function $p_{v,R} \equiv p_s\left(T_R\right)$. In order to describe the relation of saturated vapor and temperature in the interval of $0 \div 95\ ^0$C, the high confidence Gerry empirical correlation is applied: $\lg p_s = 0.0141966 - 3.142305\left(\frac{10^3}{T_s} - \frac{10^3}{T - 373.16}\right) + 8.2\lg\left(\frac{373.16}{T_s}\right) - 0.0024804\left(373.16 - T_s\right)$ [75]. Phase transformations heat flux density is described as the product of vapor flux density and water latent heat:

$$q_f^{surf.} = m_v \cdot L \qquad (6)$$

The phase transformations ongoing on the droplet surface areclosely related with the concurrent droplet heat transfer processes inside the droplet and in its surroundings. For this reason, the 'external' and 'internal' tasks must be concretized.

### 1.4. ‘Droplet’ internal problem

The droplet ‘internal’ problem is a complex heat transfer task where the interaction of radiation and transfer processes in a semi-transparent liquid is very important [65]. The general case of the heat transfer inside a droplet is described by a system of energy and integro-differential equations of motion. In the complex heat transfer case, this system of equations is not analytically solved, while its numerical solution is complicated. Therefore, alternative solution methods are being sought. In the ‘droplet’ problem, this is the application of combined analytical and numerical research methods. Usually, in the integral type, analytical solutions are searched for. It is desirable to control the convergence of the numerical solution schemes. For the internal ‘droplet’ problem, the complex heat transfer case by conduction and radiation is considered as the basic one.

When the liquid is stable inside a droplet, then the temperature gradient in the droplet can be defined by the integral type model that is convenient for numerical research [8]. The integral type model combines the heat spread in the droplet by conduction and radiation. However, liquid can circulate in a droplet. These presumptions are made on the grounds of non-isothermality in a droplet and are based on friction forces that develop on the droplet’s surface [76, 77]. Archimedes’ forces rise in a non-isothermal droplet. Their effect on the liquid’s stability depends on the droplet dispersity. In the commonly applied technologies, such as liquid fuel burning, in fireplaces or in air conditioning systems, droplets are fairly small. The rising Archimedes’ forces in droplets are weak and do not cause fluid circulation [14, 13]. Forced fluid circulation develops in a sliding droplet. This circulation is described by the Navier-Stokes equation system.

The main task of the ‘internal’ droplet problem is to evaluate the temperature inside the droplet which changes over time. The unsteady temperature field is described by the energy equation inside a droplet:

$$\rho_l c_{p,l} \frac{\partial(T)}{\partial \tau} = \frac{1}{r^2} \frac{\partial}{\partial r} \left( r^2 \lambda_l \frac{\partial T}{\partial r} \right) + F_s . \qquad (7)$$

In the equation, value $F_s$ is the function of the radiation source. When specifying the function of the radiation source, it is necessary to take into account the applied radiation flow model. Its expression is $F_s = -\left(1/r^2\right)\partial\left(r^2 q_r\right)/\partial r$. The source function in expression (7) takes into account the heat impact of the absorbed radiation in a semi-transparent liquid for the droplet’s thermal state. The expression of function $F_s$ depends on the radiation flux $q_r$ model. The most commonly used $q_r$ models are based on theories of geometric optics or electromagnetic waves. In the first case, the local radiation flux density inside a droplet is described, while the second expression is applied for the description of heat flux absorbed in the droplet’s volume [78]. The

local radiation flux inside a droplet can be described by the transcendental system of differential and integral equations [71]:

$$q_r = \int_0^{\infty}\int_0^{\pi}\int_0^{2\pi} I_\omega \sin\Theta\cos\Theta d\Theta d\varphi d\omega \tag{8}$$

$$\frac{\partial I_\omega}{\partial s} = \chi_\omega\left[n_\omega^2 I_{\omega 0} - I_\omega\right] \tag{9}$$

$$\chi_\omega = 4\pi k_\omega \omega \tag{10}$$

$$q_r = \bar{n}_\omega = n_\omega - ik_\omega \tag{11}$$

The system of equations (7–11) is transcendental. Therefore, tasks describing the spherical droplet unsteady temperature field and the local radiation flux spread inside the droplet are solved separately. When solving equation (7), the assumption is made that the local radiation flux and droplet surface temperature are already defined parameters. Then, equation (7) can be solved by introducing an auxiliary function $\theta(r,\tau) = r[T(r,\tau) - T_R(\tau)]$. Then, the system of equations is easily transformed into the Dirichlet heat transfer case with the defined source function [71]:

$$\frac{\partial\Theta}{\partial\tau} = a_1^2\frac{\partial^2\Theta}{\partial r^2} + F_s, \text{ when } F_s \equiv -\frac{1}{c_{p,l}\rho_l r}\frac{\partial\left(r^2 q_r\right)}{\partial r} - r\frac{dT_R}{d\tau}. \tag{12}$$

This system of equations can be solved only numerically, therefore, the iterative method can be applied. Thus unambiguous conditions for the previously provided equations system (7–11) is formulated. They are formulated with regard to the yet unknown functions of the droplet surface temperature $T_R(\tau)$ and spectral radiation intensity at the internal surface of the droplet $I_{\omega R}(\tau)$:

$$\begin{aligned} &R(\tau \equiv 0) = T_{l,0};\ T_l(\tau \equiv 0) = T_{l,0};\quad T(r \equiv R^-, \tau) = T_R(\tau); \\ &I_\omega(r \equiv R^-, \tau) = I_{\omega,R^-}(\tau),\ \partial T(r \equiv 0, \tau)/\partial r = 0 \end{aligned} \tag{13}$$

The unsteady temperature field $T(r,\tau)$ is described by an infinite line of integral equations [79]:

$$T_l(r,\tau) = T_R(\tau) + \frac{2}{r}\sum_{n=1}^{\infty}\sin\frac{n\pi r}{R}\int_o^{\tau} f_n \exp\left[-a\left(\frac{n\pi}{R}\right)^2(\tau - \tau_*)\right]d\tau_* \tag{14}$$

In expression (14), the function of member $f_n$ in the infinite sum evaluates the droplet heating rate and radiation absorption intensity within the droplet [70]:

$$f_n = (-1)^n\frac{R}{n\pi}\frac{dT_R}{d\tau} + \frac{1}{c_{p,l}\rho_l}\int_0^R q_r\cdot\left(\frac{n\pi r}{R}\cos\frac{n\pi r}{R} - \sin\frac{n\pi r}{R}\right)dr. \tag{15}$$

The solution of equations (8–12) fully defines the temperature field inside the droplet in the case of symmetrical droplet heating of the '*k*+*r*' complex heating case. For the complex 'c+*r*' heating case, the methodology developed in the '*k*+*r*' case could also be applied.

Friction forces developing on the droplet's surface affect the droplet liquid, therefore, the liquid starts to circulate, and the heat transfer inside the droplet intensifies. In the classical Fourier law, water circulation inside a droplet is evaluated by the convection correction factor which is expressed as $\lambda_{ef} = \lambda_l \cdot k_c^-$. Convection correction coefficient $k_c^-$ is described by empirical dependence from the Peclet number for liquid $k_c^-(\tau) = 1.86 + 0.86\tanh[2.245\lg(Pe_l(\tau)/30)]$ [14]. The droplet slipping factor is evaluated by Peclet $Pe_l = Re_l Pr_l = 2Rw_R/\nu_R$ number expression. Reynolds number for liquids is $Re_l = 2Rw_R/\nu_l$. Prandtl number for liquids is determined by $Pr_l = \nu_l/a_l$. In the air flow, the slipping droplet convective heat flow inside the droplet is described by modified Fourier law:

$$q_c^{in.} = -\lambda_{ef} \left.\frac{\partial T_R(r,\tau)}{\partial r}\right|_{r=R}. \qquad (16)$$

The maximum velocity flow on the droplet's surface caused by friction forces is described by expression $w_R = \mu_g C_l \,\mathrm{Re}_\infty \Delta w_l / 32\mu_l$ [14].

When a droplet does not slip in gases, then it is not necessary to take into account the convective heat transfer inside the droplet; thus $k_c^- \equiv 1$. Due to the non-isothermality of the internal layers of droplets, the Archimedes' force rises, which is insufficient for self-caused internal droplet circulation [79].

Droplet 'internal' problem solutions define the intensity of heat transfer and liquid vapor fluxes between the liquid and gaseous phases. In the case of an already known droplet temperature, the 'internal' droplet problem is considered as defined. Boundary conditions in thermal technologies often change, and a description of the droplet's thermal state only with the 'internal' task is impossible. Therefore, the heat transfer intensity outside the droplet must be taken into account. For this, the solution of the 'external' task must be analyzed.

In cases of complex heating, for example, heating by conduction and radiation '*k*+*r*', the unsteady temperature field function $T(r,\tau)$ can also be described according to the integral '*k*' heat transfer case when, additionally, the component of radiation '*r*' is considered. The calculation of radiation inside the droplet is based on calculation methods requiring complex and profound knowledge. Therefore, the following section provides a methodology for estimating the radiation flux absorption inside the droplet and the most important influencing optical characteristics.

### 1.4.1. Radiation impact on semitransparent spherical droplet

When analyzing cases of complex heating, such as conduction and radiation '*k*+*r*', or convection and radiation '*c*+*r*', the problem of radiation flux assessment in

a semitransparent droplet rises. The impact of radiation on the energy state of semitransparent droplets can be evaluated by different models of spectral radiation: approximations based on by geometric optics [65, 80, 81], the classical *Mie* theory, and other models [82, 83].

The classical *Mie* theory is often applied for the radiation flux description inside a droplet [84, 85]. This theory can be precisely described by analytical solution of Maxwell equations adjusted to describe the dispersion of radiation in spherical particles. Theoretical and experimental studies have shown that this theory can only be applied to small droplets with a much smaller diameter than the falling wavelength $d << \lambda_B$.

Thermal radiation is important not only in environmental physics, but also in various thermal technologies. Some thermal technologies have been specifically designed to operate only at high temperatures and provide good thermal efficiency [86]. Therefore, radiation should be evaluated when calculating thermal effects in rocket nozzles [87], power plants [88], engines [89] and high temperature heat exchangers [90]. Radiation significantly contributes to energy transmission in furnaces [91], combustion chambers [91], and emissions after a nuclear explosion [92].

Complex cases of heat and mass transfer involving radiation are the most difficult heat transfer cases. Two theories can be applied to estimate the radiation flow: the classical electromagnetic waves theory or quantum mechanics [93]. The quantum theory is based on the emitted or absorbed finite mass elementary particles of thermal energy transfer in the radiation process. The wave theory is based on the theory of electromagnetic wavelength with a defined length, amplitude and wave frequency. Electromagnetic radiation can be classified by wave length $\lambda_B$, its frequency $v$ or wave number $\omega = 1/\lambda_B$. The wavelength range of interest includes an extended range of visible light from $\lambda_B = 0.4 \div 07\ \mu m$ to the end of the infrared wavelength 1000 $\mu m$ [94].

The compound integral radiation flux to the spherical body per unit area $dA$ pertime unit can be described according to the infinite wave spectrum [93]:

$$q_{r,0} = \int_0^{\infty} \int_0^{4\pi} I_{\lambda_B,\Omega} d\Omega d\lambda_B . \qquad (17)$$

The solution of equation (17) is the analytical expression of the black body radiation law of Stefan-Bolzman $q_{r,0}=\sigma \cdot T^4$. The radiation flux density emitted by the absolute black body is proportional to the fourth degree of the body temperature. Since black bodies are practically unacceptable in nature, therefore, the radiation intensity of such bodies does not match the case of a black body. For this purpose, a coefficient which defines the spectral degree of blackness of real bodies $\varepsilon_{\lambda_B} = I_{\lambda_B} / I_{\lambda_B,0} \cong const.$ is set when $0 \le \varepsilon_{\lambda_B} \le 1$. Therefore, the radiation integral flux for a real body is defined by expression:

$$q_r = \int_0^{\infty} \int_0^{4\pi} \varepsilon_{\lambda_B} I_{\lambda_B,\Omega} d\Omega d\lambda_B . \qquad (18)$$

Black body radiation is considered as supporting, with which the main characteristics of radiating bodies is compared. A real body's radiation depends on many factors, such as: composition, surface uniformity, temperature, wavelength of radiation, angle at witch radiation is absorbed or radiated, and the body transparency factor.

As a strategy to describe the radiation intensity variation in a freely chosen direction, Kesten suggested that the radiation intensity variation in a symmetrical environment should be changed into the dimension direction of the semitransparent body. This author performed radiation modeling on an infinite cylindrical body [95]. In the case of a spherical droplet, sphere coordinate *r* and change $dr$ are analytically linked to path change $ds$ of a light beam in freely chosen direction *s*. The light beam direction is evaluated by angles $\beta$ , $\Theta$ and $\gamma$ for the radiation modeling in a spherical droplet. Therefore at compound's integral radiation flux can be calculated according to the infinite wave spectrum, angle of azimuth φ and $\Theta$ :

$$q_r = \int_0^{\infty} \int_0^{\pi} \int_0^{2\pi} I_{\lambda_B} \sin\Theta \cos\Theta d\Theta d\varphi d\lambda_B \qquad (19)$$

The influence of radiation on an evaporating droplet was also studied by Viskanta [65]. It is considered that water is not opaque but semi-transparent, and radiation absorption is not a surface phenomenon, but rather a volumetric phenomenon. The impact of radiation absorption on the droplet's lifetime is provided in (Fig. 1.2). The data clearly shows that if a droplet is considered as semi-transparent (without radiation), its lifetime is much longer than that of a semi-transparent droplet, especially for the droplets with a larger initial diameter. The convection impact is more prominent brighter for smaller droplets compared to radiation absorption. External radiation absorption only slightly influences the droplet evaporation rate and its lifetime. If a droplet is considered as opaque, then its lifetime (when the droplet's diameter is *D*=1000 μm) may be about 20% longer compared to that of a semi-transparent droplet [65].

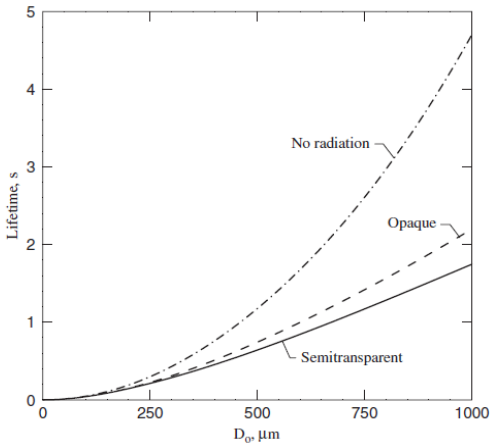


Fig. 1.2. Lifetime of droplets when $T_0$=280 °K and $T_g$=150 °K [65]

When calculating the radiation flux inside a droplet, it is assumed that radiation absorption in water droplets is a complex multi-factor process. If the radiation intensity is weak, then radiation absorption inside a droplet can be considered as linear. In case of intense radiation, the absorption of radiation may be described by non-linear curves. This uneven treatment of radiation absorption in water droplets is influenced by the optical spectral characteristics of water, the temperature of the radiation source, and the droplet size [96, 97].

It is important to evaluate the interphase contact of the surface spectral optical effects when modeling complex transfer processes inside a droplet and in its surroundings. Deeper knowledge of spectral optical properties in a liquid and its environment allows evaluating and calculating radiation absorption in droplets more precisely.

### 1.4.2. Spectral optical characteristics of a semitransparent water droplet

Water is considered as a standard semi-transparent liquid. This is influenced by the fact that the optical characteristics of water are well-known, and water is extensively used in the dispersed form in various technologies. In recent years, the exploration of the optical properties of water has been receiving major interest of researchers due to its high practical application [47, 96, 97].

It is known that semi-transparent media absorb and radiate energy themselves across the entire range of their volume, therefore, heat can spread by radiation, conduction and convection in such bodies [98]. There might be a case when a liquid does not circulate inside droplets; in these cases, convection may be neglected. The complex case of heat transfer of conduction and radiation '*k*+*r*' will always be manifested inside a droplet. The interaction of these heat transfer processes is highly dependent on the radiation absorption process inside a droplet. The main principles valid for other semi-transparent media are also applicable, and heat transfer of droplet in the droplet's heat and mass transfer. Heat and mass transfer take into account the

radiation flux decreasing from the external side, which is partially reflected on the surface of semi-transparent media and is partially absorbed into the droplet. This is a consequence of the fact that radiation spread in the droplet is gradually absorbed and supplemented by its own liquid radiation flux. When modeling complex transfer cases in semi-transparent droplets, it is necessary to take into account the spectral optical characteristics of the liquid.

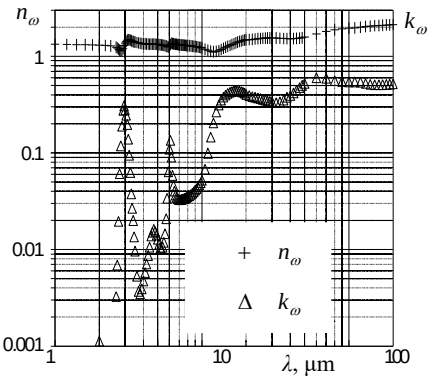


Fig. 1.3. Spectral fraction and absorption indexes of 25 °C water temperature [101]

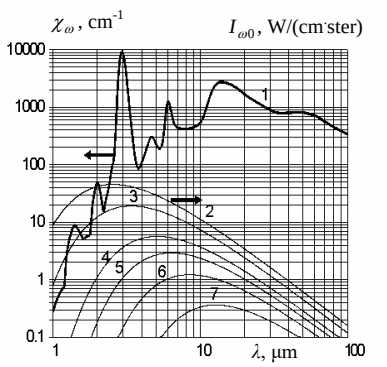


Fig. 1.4. The intensity of absolute black body spectral radiation and the variation of water spectral absorption index T, K: *1* – 298; *2* – 2000; *3* – 1500; *4* – 1000; *5* – 800; *6* – 600; *7* – 400

The main optical properties of a substance are evaluated by the complex spectral index of refraction which is described by expression $\bar{n}_\omega = n_\omega - ik_\omega$. The real part of expression – the spectral index of refraction – defines the reverse of a light beam moving from one environment into another, i.e., into one which possesses different $n_\omega$ values, and is also denoted by variations of the electromagnetic wavelength and velocity. In the range of light wavelength variation from 0.2 to 200 μm, the values of the optical characteristics of 25 °C temperature water are provided in 169 spectrum sections [94]. The values of water refraction and absorption indexes change through all the energetically important spectrum of radiation (Fig. 1.3).

The imaginary complex spectral index of the refraction part is called the spectral index of absorption. The spectral index of absorption together with $n_\omega$ determines the optical spectral effects on the surface of interphase and describes the ability of semi-transparent media to absorb the flowing radiation in them. Size $k_\omega$ defines the spectral index of absorption. It can be provided via expression $\chi_\omega = 4\pi k_\omega n_\omega \omega_0$. The value of the water spectral index of absorption variates within hundreds of times according to a complex curve with many extremity points (Fig. 1.4). For example, when a light beam's length is $\lambda \approx 3$ μm, then $\chi_\omega \approx 10^4$ cm$^{-1}$; when $\lambda \approx 1$ μm, then $\chi_\omega \cong 0.3$ cm$^{-1}$. It is very important that the absorption coefficient varies in the short wave area of the thermal radiation spectrum where the maximum intensity of radiation is characteristic of thermal technologies.

When a light beam falls at angle $\beta$ from the environment with a complex spectral index of refraction $\bar{n}_1$ to an environment which has a complex index of refraction $\bar{n}$, then light refraction can be described according to the law:

$$\frac{\sin(\varphi)}{\sin(\beta)} = \frac{\bar{n}}{\bar{n}_1} = \frac{n - ik}{n_1 - ik_1}. \quad (20)$$

On the mirror surface of a droplet, the refraction coefficient of a falling light beam at angle $\beta$ is equal to the refraction coefficient of a light beam at angle $\varphi$ falling onto the internal surface of a semi-transparent sphere. On the mirror surface of a droplet, spectral light refraction coefficients are calculated according to parallel and perpendicular plane-polarized light wave reflection coefficients:

$$r_\omega(\beta) = \frac{1}{2}\left[r_{\omega\perp}(\beta) + r_{\omega//}(\beta)\right]. \quad (21)$$

The reflection coefficient of a polarized light wave parallel to the falling plane is obtained as follows:

$$r_{\omega//}(\beta) = \frac{\left[n\cos(\beta) - n\cos(\varphi)\right]^2 + \left[k\cos(\beta) - k_1\cos(\varphi)\right]^2}{\left[n\cos(\beta) + n\cos(\varphi)\right]^2 + \left[k\cos(\beta) + k_1\cos(\varphi)\right]^2}. \quad (22)$$

The reflection coefficient of a polarized light wave perpendicular to the falling plane is calculated as follows:

$$r_{\omega\perp}(\beta) = \frac{\left[n\cos(\varphi) - n_1\cos(\beta)\right]^2 + \left[k\cos(\varphi) - k_1\cos(\beta)\right]^2}{\left[n\cos(\varphi) + n_1\cos(\beta)\right]^2 + \left[k\cos(\varphi) + k_1\cos(\beta)\right]^2}. \quad (23)$$

The value of the light reflection coefficient on the water surface variates in a wide range, and a specific value depends on the radius of falling angle $\beta$ (Fig. 1.5), while, for the same angle, it is highly dependent on the wavelength: $r_\omega$ is a variable in the shorter area, yet it evenly increases in longer wavelengths (Fig. 1.6).

For light beams falling to the internal side of a droplet, the full effect of their refraction can be observed and must be evaluated. This is a valid condition for light beams falling at an angle equal or larger than Brewster's angle. Its expression is presented as:

$$\beta_\omega^{kr} = \arcsin\left(\frac{\bar{n}_1}{\bar{n}_\omega}\sin\frac{\pi}{2}\right) = \arcsin\frac{\bar{n}_1}{\bar{n}_\omega}. \quad (24)$$

Light beamsfalling at angle $\beta > \beta_\omega^{kr}$ are mirrored back to a semi-transparent droplet. Calculation results have confirmed that angle size $\beta_\omega^{kr}$ is highly dependent on the wavelength of a light beam (Fig. 1.6).

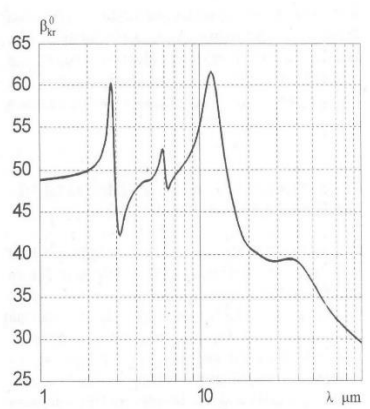


Fig. 1.5. Variation of Brewster's angle in radiation spectrum for 25 °C water [79]

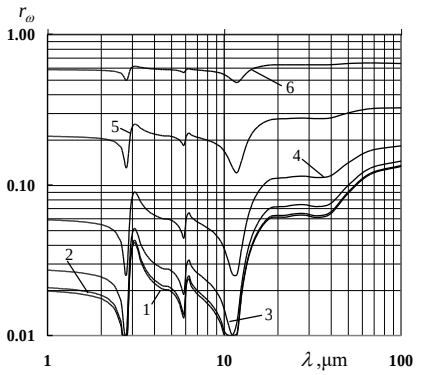


Fig. 1.6. Dependence of spectral water refraction coefficient $r_\omega$ on light beam falling angle $\varphi$,$^0$: *1* – 5; *2* – 30; *3* – 45; *4* – 60; *5* – 75; *6* – 85 [79]

When calculating light beam spectral intensity $I_{\omega,R}$ from a semi-transparent droplet's surface, it is necessary to take into account the radiation of the droplet. For example, spectral intensity $I_{\omega,kr}$ of radiation falling from outside at angle $\beta$ to the droplet's surface is a part of it is mirrored on the droplet surface $I_{\omega,at}$. The remaining part enters inside the droplet at a direction described by angle $\varphi$. In the direction of this angle to the droplet surface of a semi-transparent liquid from the droplet's internal side, the falling light radiation spectral intensity part leaves the droplet in angle direction $\beta$, while the remaining part is mirrored and reflected at the droplet's internal side of the surface.

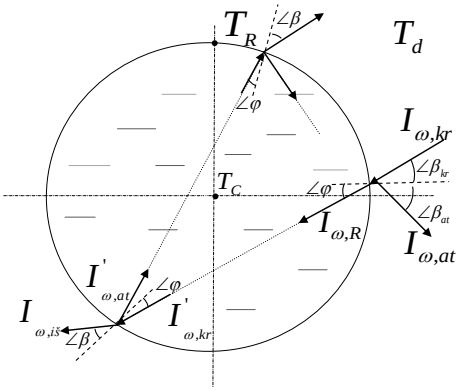


Fig. 1.7. Scheme of radiation absorption in a droplet of a semi-transparent liquid

The multiple light reflection inside a droplet is evaluated by spectral optical density $\tau_{r_1}^{r_2}$ which depends on the droplet's diameter [98]:

$$\tau_{r_1}^{r_2} \equiv \int_{r_1}^{r_2} d\tau_r^R = \int_{r_1}^{r_2} \frac{\chi_\omega dr_*}{\left(1 - r^2 \sin^2 \gamma / r_*^2\right)^{1/2}}. \qquad (25)$$

In the expression of optical thickness, values $r_1$ and $r_2$ include optical thickness plot validity limits.

For the assessment of optical effects, the most important spectral parameters are Brewster's angle $\beta_\omega$, spectral index of absorption $\chi_\omega$, and light reflection coefficients.

### 1.5. Solution of 'droplet' external problem

Droplet 'external' problem evaluation should take into account the movement of a droplet into an air flow. Droplets move at speed $w_l$ in a gas flow running at speed $w_g$. This speed difference defines the velocity of a droplet slipping in gas flow $\Delta w_{l_{sl}} = |w_l - w_g|$. The droplet's movement in a gas flow is described by differential equation [14] (Fig. 1.8):

$$\frac{dw_{l_{sl}}(\tau)}{d\tau} = \frac{3}{16} \frac{\mu_g(\tau)}{\rho_l(\tau)} \frac{w_g(\tau) - w_l(\tau)}{R^2(\tau)} \mathrm{Re}_\infty(\tau) C_l(\tau) \qquad (26)$$

The Reynolds number is defined by a modified expression which evaluates the droplet diameter, slip velocity, gas density and gas dynamic velocity of a gas mixture $\mathrm{Re}_\infty = 2R\rho_g \Delta w_l / \mu_{vg}$. Gas density is defined by gas temperature: $\rho \equiv \rho(T_g)$ when the dynamic viscosity of the gas mixture $\mu_{vg} \equiv \mu(T_{vg})$ is selected for a liquid vapor and gas mixture.

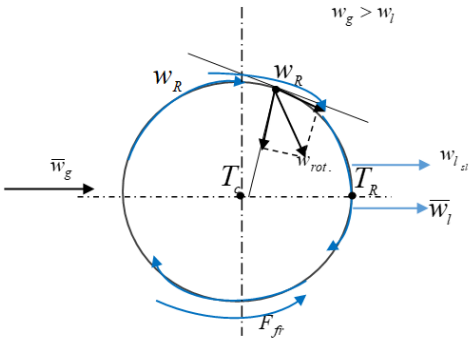


Fig. 1.8. Droplet movement in gas flow

The composition and temperature of a gas mixture conform to the rule: $Y_{vg} \equiv Y_{vg,R} + (Y_{vg,\infty} - Y_{vg,R})/3$, $T_{vg} \equiv T_{vg,R} + (T_g - T_{vg,R})/3$. Full friction drag coefficient $C_l$ for a moving droplet is evaluated by empirical expression $C_l = 24\left((1 + 0.2\,\mathrm{Re}^{0.63})/\mathrm{Re}(1 + B_T)^{0.2}\right)$ [100]. This coefficient evaluates the resistance that is caused by friction and pressure forces of a slipping droplet in a gas flow.

Phase transformations on the droplet's surface have an impact on the convection heating intensity. The flowing water vapor from an evaporating droplet resists against the hot gas flowing towards the droplet's surface; therefore, the boundary layer increases, and the convection heating intensity of an evaporating droplet decreases compared to solid particles in the analogous heating case. In many cases which are important for practice, convection heating, when ignoring the influence of droplet phase transformations, is defined by the dimensionless Nusselt number which depends on Reynolds and Prandtl numbers Nu=*f*(Re,Pr). For a non-evaporating solid particle, the well-known convection heating models are discussed in work [14]. The Nusselt number for solid particles is defined by well-known empirical expressions. If Re=0 for a stagnant and non-evaporating droplet, the case of a solid particle is applied when $Nu_0=2$. For the larger values of the Re number, but in cases of laminar flow, the Nu number is proportional to value $Re^{1/2}Pr^{1/3}$ [4]. The convective heating intensity of a non-evaporating droplet is defined by expression $Nu = 2 + 0.552\,\mathrm{Re}^{1/2}\,\mathrm{Pr}^{1/3}$ [4]. In phase transformations, external convection heating is defined by the classical Newton law $q_c^{ext.} = \alpha\left(T_g - T_R\right)$. Then, the convection heat flux from gases to the droplet is as follows:

$$q_c^{ext.} = \lambda_{vg}\frac{Nu_f}{2R}\left(T_g - T_R\right) \qquad (27)$$

When phase transformations take place on the droplet's surface, $\mathrm{Nu}$ is defined according to a solid particle's Nusselt number equations, when Stefan's hydrodynamic flow influence is evaluated by the Spalding heat transfer parameter $B_T$ function $Nu_f \equiv 2\cdot f_{B_T}$ [101]. Function $B_T$ is traditionally defined according to the classical model $f_{B_T} = \ln\left(1+B_T\right)/B_T$ or according to the empirical correlation form $f_{B_T} = \left(1+B_T\right)^{-0.7}$ [14, 100]. The classic $f_{B_T}$ function form is well-fitted for the case of negligible levels of the slipping of droplets in a gas flow. The empirical correlation model is applied in the case of strong slipping of droplets in a gas flow.

The expression of Spalding heat transfer parameter is well-known for the equilibrium evaporation of complex heating in the case of conduction and radiation '$c+r$': $B_T = c_{p,vg}\cdot\left(\left(T_v - T_{fK}\right)/L\right)\left(1+q_r/q_c\right)\right)$ [102]. The classic expression of the mass transfer is $B_M = B_M\left(1+Q_R/Q_C\right)$ [100]. The Spalding heat transfer parameter $B_T$ application methodology is not fully developed for transitional phase transformation regimes. Therefore, a need for the universal transfer parameter function expression for any of phase transformation regime arises. This requires a more detailed interpretation in the variation of energy fluxes in each of the phase transformation regimes.

## 1.6. Review of experimental investigations of droplets

The most common droplet evaporation models in the gaseous media are the diffusion models based on Maxwell's assumptions in the works of such authors as Spalding [101], Fuchs [4] and others. They are based on the assumption that the whole energy supplied for liquid and vapor interaction is used in the evaporation process [94], [100], [103]. Many researchers have studied the evaporation phenomena related with liquid droplets and solid materials. Such studies were performed in natural or free convection conditions at low environment temperatures [6]Investigations were further extended to more complex cases of heating by convection and radiation at higher temperatures [34, 104].

Diffuse and kinetic models explore heat and mass transfer fluxes between a droplet and its gaseous surrounding. Therefore, it is fairly difficult to predict the water droplet evaporation rate in high temperatures (over 600 °K) by using only empirical correlations. According to some authors, the deviation between theoretical and experimental data may reach 60–80% at high temperatures [105]. Thus it is very important to solve these problems because they have a significant impact on various technologies using gas and vapor systems.

Over the past few years, various optical systems have led to unique experimental results. For two-phase flow monitoring (liquid-gas), various disciplines are applied: speed imagine recording systems, particle imagine rate measurement, particle trace measurement, interferometric particle imaging and shadow photography. These precise metrology techniques allow obtaining the latest information about the intensive evaporation of the gas/vapor and droplet mixture and the ongoing chemical reactions [34, 106].

In the latest experiments investigating water droplet evaporation, the characteristic evaporation rates are specified [104]. In the performed investigations, droplets move in high temperatures (about 800–1200 °K) in gaseous media consisting of hot air and combustion products. It was confirmed that the evaporation rate for the flow of one droplet or several droplets was significantly different. The main reason why this happens is due to the impact of the temperature factor. The temperature is considerably different when one droplet evaporates versus when a droplet evaporates while being surrounded by other droplets. Study [104] indicates how such factors as the initial droplet size, velocities of high-temperature gas flows, volume concentration of droplets, combustion products temperature, and the initial water temperature exert influence on the integral characteristics of the temperature traces of droplets.

Experimental investigations of conditions of droplet equilibrium evaporation are quite rare. Original experimental studies of water vapor equilibrium evaporation rate were carried out by Russian researchers Ivanov and Smirnov in [106]. The equilibrium evaporation rate of large water droplets was experimentally investigated in the case of complex heating.

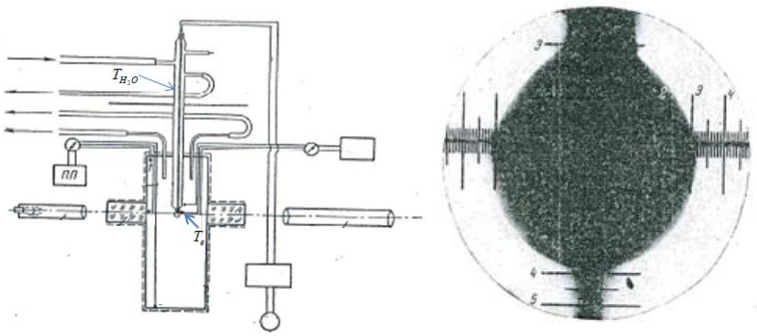

Fig. 1.9. Test section of experiment and droplet enlarged projection [107]

The experiment was performed in an original test section where water was fed into the center of a chamber heated up to a temperature of 405–860 °C via a capillary system. An evaporating water droplet of 600–2900 μm diameter was formed at the outlet of a 3 mm diameter copper capillary tube (Fig. 1.9). The droplet was heated with the radiation from the chamber walls, and the convective heat of the air-water vapor mixture flowing around the chamber was extracted. The extraction of the vapor flow was carried out at low speeds to ensure the stability of the air-water parameters. The droplet was heated to such a temperature that additionally supplied feeding water of 25–30 °C temperature from the capillary system for evaporating the droplet would not change the droplet's temperature which was measured with a thermocouple. After ensuring the stability, the 30–50 times enlarged projection of the illuminated droplet on a screen was observed, and the velocity of the droplet evaporation was equated to the measured feed water flow rate [106].

## 1.7. Generalization of literature review

For the evaluation of liquid spraying systems, the systematic approach is important. This uniform approach can be provided and revealed through analysis of sprayed droplets which consists of the analysis of droplet thermal and energy states. It is possible when the solutions of 'internal', 'external' and 'phase transformations' problems are analyzed together regarding the aspect of compound heat fluxes balance interphase contact condition (Fig. 1.10). In the expression of the total heat flux (1), it is necessary to take into account the vector direction of heat fluxes which flow towards and from the droplet's surface. Therefore, expression (1) could be reorganized and written as:

$$\vec{q}_f^{ext.} + \vec{q}_\Sigma^{ext.} + \vec{q}_\Sigma^{in.} = 0 \qquad (28)$$

For all thermal technologies, the most important parameter is vapor flux $g$ (kg/s); therefore, it could be stated that the main task in the 'droplet' problem is the problem of phase transformations. However, it is impossible to separate it from the droplet 'internal' and 'external' problems. Thus the droplet heat and mass transfer problem must be investigated in a complex way.

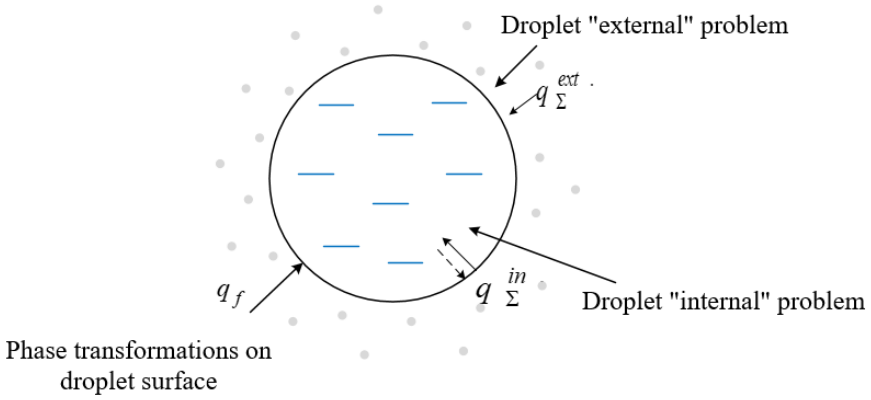


Fig. 1.10. Interpretation of the ‘droplet’ problem

In the general case, either in a droplet or in gases, complex heat transfer takes place. Heat transfer is carried oud by convection or radiation. External or internal heat fluxes can be described as $q_{\Sigma}^{ext.} = q_r^{ext.} + q_c^{ext.}$ and $q_{\Sigma}^{in.} = q_r^{in.} + q_c^{in.}$, respectively. Since the spectral absorption coefficients of a semi-transparent droplet are finite values, a popular assumption is applied $q_{r,R}^{ext.} \approx q_{r,R}^{in.}$.

It is important to note that expression (28) unambiguously defines instantaneous temperature $T_R$ of the interphase contact surface which directly influences the fluxes of heat transfer and phase transformations and ensures their interconnection.

When summarizing the literature review, it could be stated that:

- The numerical solution schemes of the specific ‘droplet’ problem can only be created after clarifying expression (28). For this reason, it is necessary to dispose with the Spalding transfer parameter function adaptation methodology for all the phase transformation regimes that are possible on a droplet’s surface. For the transitional phase transformation regime, such a methodology has not been developed yet, therefore, the need for a universal Spalding transfer parameter expression rises for the full phase cycle of transformation regimes. In this case, the variation of the energy interpretation of heat fluxes inside a droplet is very important in phase transformation regimes.
- It should be noted that heat and mass transfer processes and their interaction could be analyzed when combining phase transformations on the droplet’s surface in the cycle of phase transformations. The beginning of the cycle of droplet phase transformation regimes is defined by liquid spraying moment $\tau = 0$, while the end of the cycle is determined by droplet evaporation moment $\tau = \tau_f$. Then a continuous variation of water droplet consistent phase transformation regimes can be derived by expression:

$$\tau \equiv 0 \div \tau_{co} \div \tau_{nf} \div \tau_f \qquad (29)$$

- A droplet phase transformation cycle consists of the regimes of condensation and transition to the equilibrium evaporation (which is also known as the unsteady phase transformation regime), and the equilibrium evaporation regimes: when $\tau \equiv 0 \div \tau_{nf}$ and $\tau \equiv \tau_{nf} \div \tau_f$, respectively.
- Droplet heating is defined by combined heat transfer and phase transformations processes. They take place due to intensive self-interaction as well as due to the heat and mass transfer boundary conditions. The influence of Stefan's hydrodynamic flow, Knudsen layer, droplet slipping in the gas flow, and the thermal radiation flux absorption in a semi-transparent liquid are important for the interaction of combined droplet transfer processes**.**
- Spectral radiation absorption in a semi-transparent liquid exerts direct influence on the warming of internal layers and creates preconditions for forming the negative temperature field gradient in the droplet. For the definition of the thermal state of a droplet, an integral model of complex droplet heating by conduction and radiation can be considered as the basis in the phase transformation cycle.
- Droplet slipping in a gas flow intensifies convection heating and creates preconditions for forced liquid circulation to arise. For the heat convection evaluation inside a droplet, the well-known theory of effective heat conduction is used.
- Temperature and pressure jumps in the Knudsen layer are more significant for phase transformations of the small/micron-row droplets. Therefore, for our analysis, a conditional classification of sprayed water droplets was outlined: (small, when $2R<10<50$; average $50<2R<250$; large $250<2R<1000$; very large $2R>1000$ micrometers). This allows to neglect the Knudsen layer's impact on the investigated water droplets.
- Stefan's hydrodynamic flow accelerates the diffusion evaporation process and suppresses the droplet convective heating. The impact of Stefan's hydrodynamic flow on the droplet's convection heating and evaporation is traditionally taken into account with the empirical expression of the Spalding transfer parameter.
- Droplet phase transformations and heat transfer are individual. It is difficult to outline and provide a physical interpretation of the process taking place on a droplet's surface which would allow to define preconditions for the creation of a universal mathematical model suitable for the entire cycle and to develop an appropriate methodology for numerical modeling. For this reason, it is important to provide for a droplet the physical interpretation of the entire phase transformation cycle which consists of its geometrical, thermal and energy components.

### 1.8. Author's contribution to the topic

This dissertation was written at Kaunas University of Technology, department of Thermal and Nuclear Energy, when participating in the scientific group *Complex Transfer Processes in Radiating Disperse Systems* (led by prof. G. Miliauskas). This dissertation is continuous work. It is based onthe transfer processes numerical modeling for evaporating water droplets in a complex heating case by radiation and conduction as developed by dr. V. Šabanas. For the analysis of the obtained results in the Fourier time scale and the definition of duration of the transitional evaporation regime, recommendations based on dr. K. Norvaišienė's dissertation were applied. The ideas listed above were creatively developed for the entire droplet phase transformation cycle while emphasizing the peculiarities of the condensation regime. For the investigation described in this work at the iteration cycles, an assumption of the droplet radius definition methodology according to the calculation results of a previous iteration was used while changing the classical $R_{i,it} = R_{i-1}$ assumption into requirement $R_{i,it} = R_{i,it-1}$ across all the iterative cycles for the definition of the droplet surface instantaneous temperature. The interaction between the radiation absorption and convection heat transfer processes in semitransparent water and the negative temperature field gradient formation are related with the ongoing phase transformations regime energetic variation on the droplet surface and the intensification of the evaporation process. The increase of the condensation regime duration on the droplet's surface is based on the process of a more intensively slipping droplet in humid air.

## 2. Methodology of the 'Droplet Problem' Research

A systematic approach is very important for sprayed water droplets. Consistent phase transformation regime change and equivalent treatment of different regimes for thermal and energy states must be ensured. The approach can be developed by using physical interpretation including water droplet geometrical, thermal and energy analysis.

The object of this work is the complex transfer processes in the transitional processes in a humid air flow. In this work, the main assumptions provided for a combined numerical research are:

1) Droplets are spherical volumes which are heated spherically symmetrically. The symmetrical heating condition is assumed to be: $\partial T(r \equiv 0, \tau) / \partial r \equiv 0$;
2) The droplet surface is a time dependent function $T_R(\tau)$; it ensures the requirement of expression (28); its changes are determined by interaction of transfer processes;
3) Radiation absorption by water surface is insignificant; therefore, radiation fluxes on the droplet surface satisfies the condition $q_r^- \equiv q_r^+$;
4) Free convection is not significant in the water droplet heating process;
5) Water does not circulate inside a droplet carried by a gas flow;
6) The impact of the Knudsen layer on the interaction of transfer processes is insignificant;
7) Heat fluxes on the droplet's surface satisfy the condition of transfer processes in the quasi-steady state.

### 2.1. Geometric and Thermal State Interpretation of the Droplet

For the efficiency of thermal technologies, the dispersion process is applied, during which, large volume droplets are dispersed into smaller volumes. Dispersion is the initial process when a physical droplet of certain dimensions is formed (Fig. 2.1). During the process of droplet dispersion, five different outcome regimes can be outlined as droplets may: bounce, partly merge, fully merge, split up, and disperse [107].

Assumption of droplet volume sphericity $V = 4\pi R_{equ}^3 / 3$ is made, while the surface area of a droplet is described by expression $A_l = 4\pi R_{equ}^2$. The total area of a liquid droplet is estimated as the composite surface area of all the droplets considering the need to optimize and improve thermal technologies, it is important that the contact surface of liquid droplets with their surrounding environment should be much higher than liquids in large volume.

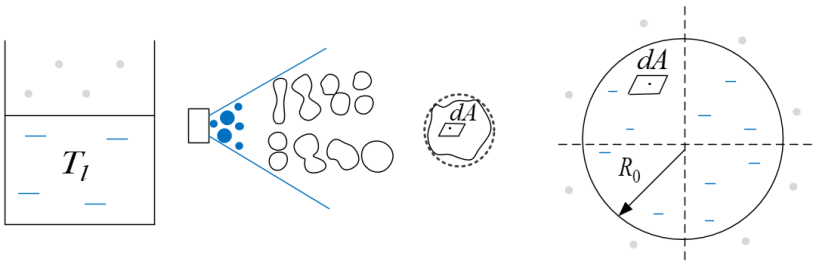


Fig. 2.1. Dispersion of liquids and the geometric interpretation of a droplet

Liquid volumes may fuse or split until the regular two-phase liquid droplets and the gas flow form, which can be defined according to various mass $M_{l,i} = V_{l,i} \cdot \rho_0$ of droplet concentration in groups. When a droplet's mass is known, its equivalent radius can be evaluated by expression $R_{equ,i} = \sqrt[3]{3M_{l,i}/(4\pi\rho_{l,0})}$. The dispersity of sprayed water droplets is characterized by their initial diameter $2R_{0,i}$. For the creation of a universal model, the geometrical interpretation must be taken into account. When an assumption of a spherical droplet is made, then, for the definition of the droplet phase transformation cycle (29), assumption $R(\tau = 0) = R_0 \equiv R_{equ}$ is created. The variation of droplet radius in whole droplet phase transformation cycle is presented in (Fig. 2.2).

In the phase transformations cycle (29), the droplet mass varies due to the phase transformations ongoing on its surface, while the droplet diameter variation is additionally influenced by the process of expansion of warming water. The ongoing phase transformations are defined by vapor flux density $g$; which condensates or evaporates on the droplet's surface. Conditionally, while providing the negative condensed vapor flux in the condensation regime, the consistent variation of the droplet mass and volume can be described by the droplet phase transformations equation in the phase transformations cycle (29):

$$\frac{dM_l(\tau)}{d\tau} \equiv \frac{4\pi}{3}\frac{d\left[\rho_l(\tau)R^3(\tau)\right]}{d\tau} = -g(\tau) \qquad (30)$$

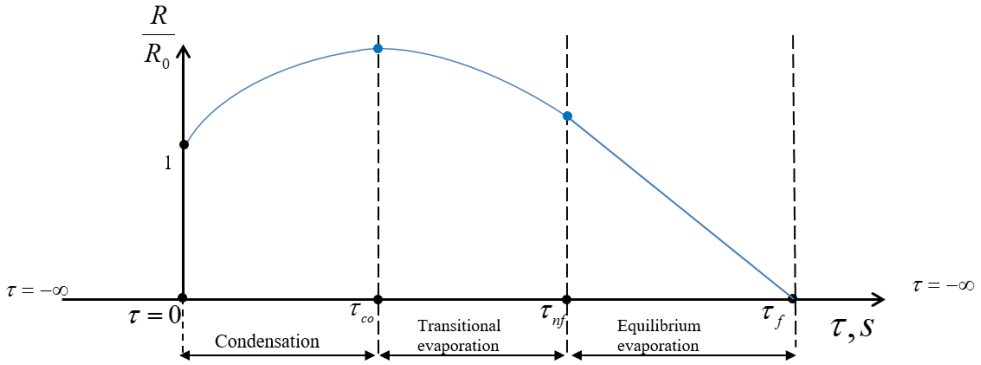


Fig. 2.2. Variation of droplet radius in droplet phase transformation regime cycle

For the definition of vapor flux $g$, it is required to take into account the thermal state of a droplet. Therefore, an interpretation of the droplet thermal state variation is outlined and presented in (Fig. 2.3) and (Fig. 2.4).

When modeling and evaluating thermal technologies, the problem of the droplet surface temperature definition arises. The variation of temperature in a two-phase flow between different phases is evaluated as contact function $T_{fK}$ of the droplet's surface and its surrounding gas flow temperature (Fig. 2.3). At the initial stage of the droplet research, contact $T_{fK}$ surface temperature can be freely selected, but in some works it was equated with saturation temperature $T_{sat.}$ or described by empirical equations [75]. In the cases of undertaking more rigorous analysis, $T_{fK}$ can be calculated from the energy flow balance (28) condition, and this inevitably led to complex assessment of the internal and external sides of a droplet. The driving force of the external heat transfer is characterized according to a droplet's surface and the temperature difference from the surrounding temperature $T_g(\tau)$-$T_R(\tau)$. The temperature difference between the droplet's surface and its center $\left|T_R(\tau)-T_C(\tau)\right| \equiv \Delta T_l$ defines the driving force of the droplet's internal heat transfer, or, otherwise, the non-isothermality of the droplet [14].

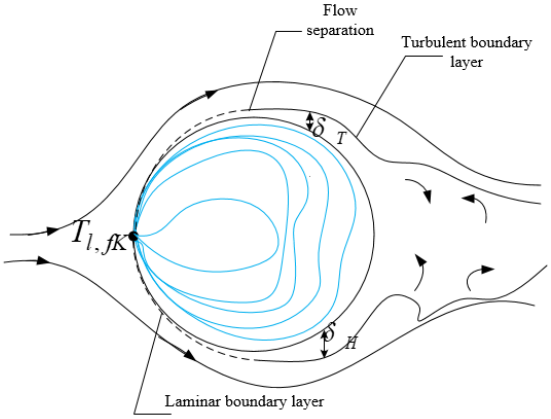


Fig. 2.3. In a two-phase flow, the thermal state interpretation of a flowing droplet

In the general case, when a gas flows around a droplet's interphase surface, the heat transfer conditions for convective heating may be highly different. Therefore, the temperature for individual elementary surface areas will be different as well. Accordingly, in the general case, local temperature $T_{fK}$ of a non-isothermal surface will be described by time and space coordinates $T_{fk}(\tau, X, Y, Z)$; here, $X$, $Y$ and $Z$ are the defining coordinates of the interphase surface contact. It is expected to define the thermal state of a droplet's surface by the average surface temperature for the whole surface $T_R$. Then, the interphase surface average temperature is defined by time coordinate function $T_{fk}(\tau) \equiv T_R(\tau)$. In the general case, the temperature distribution inside a droplet is described with a function of time and space coordinates $T_l(\tau, X, Y, Z)$. A conception of the average temperature of a droplet's internal layers

is provided, and the field of unsteady temperature is described by time and radial coordinates $T_l(\tau, r)$ where condition $\partial T_l(\tau, r)/\partial r\big|_{r=0} = 0$ is valid. In a phase transformation cycle, the variation of the thermal state of a non-isothermal droplet can be defined according to its mass average $T_{l,m}(\tau)$ temperature function:

$$T_m(\tau) \equiv \int_0^R R^3(\tau)\rho_l(r,\tau)T(r,\tau)dr \Big/ \int_0^R R^3(\tau)\rho_l(r,\tau)dr \,. \quad (31)$$

The droplet phase transformations model (30) allows outlining the qualitatively regular droplet diameter variation across all the phase transformation cycle regimes $\tau \equiv 0 \div \tau_f$ (29) (Fig. 2.2). In the phase transformations regime cycle, a sprayed droplet's diameter $R_0$ is equated to the time moment $\tau \equiv 0$, at which droplet is sprayed, while the droplet's instantaneous diameter $2R$ and initial $2R_0$ diameter ratio are equated to 1. In the condensation regime, the droplet warms up, and vapor condensates; therefore, the droplet's diameter grows up to $2R_{co}$. Hence $R_{co}/R_0>1$. The condensation phase transformation regime finishes when the droplet's surface has warmed to the dew point temperature $T_R(\tau \equiv \tau_{co}) = T_{dp}$ which is defined by a partial pressure of water in humid air $T_{dp} = T_{sat}(p_{v,g})$. In the transitional evaporation regime, a droplet warms up to the equilibrium evaporation temperature $T_e$ which is defined by the air temperature and humidity and is also influenced in the case of the warming droplet heat transfer (Fig. 2.4). Droplets heated by conduction only ('*k*' heat transfer case) evaporate at equilibrium near the lowest $T_{e,\text{'}k\text{'}}$ temperature $T_{e,"k"} \cong T_{e,\min}$. In more complex cases of heating than heating by conduction only, a droplet warms to the higher equilibrium evaporation temperature in the transitional evaporation regime: $T_{e,"c+r"} > T_{e,"c"} > T_{e,"k"}$. In the equilibrium evaporation regime, the heat transfer boundary conditions are changing. This is influenced by the suffocating decreasing droplet slipping in air, which is caused by friction forces, while in the case of complex heating, radiation absorption in droplets is weakening due to the impact of evaporation on the decreasing droplets. Therefore, it is impossible to foresee in advance the thermal state variation in the equilibrium evaporation regime. It can only be stated that, in the equilibrium evaporation regime, the droplet's thermal state will be variating between the marginal "$c+r$" and "$k$" case temperatures $T_e$ (Fig. 2.4).

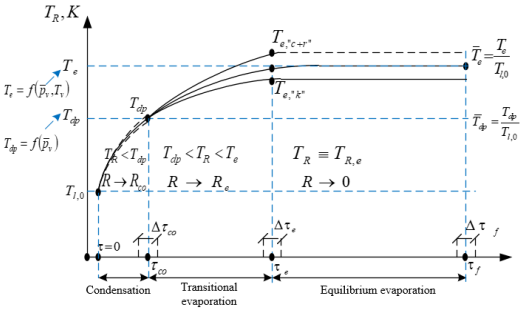


Fig. 2.4. The variation of droplet surface in a cycle of phase transformation regimes

At the beginning of equilibrium evaporation, the droplet's volume variation is influenced by two different factors: due to the further water warming expansion, the droplet's volume is increasing, while the beginning of surface evaporation leads us to an assumption that the droplet's volume is decreasing. Therefore, the droplet's volume could be increasing for some time, while evaporation will outweigh the expansion effect of water at the end of transitional evaporation. It could be predicted that, at the end of transitional evaporation, the droplet's volume will be close to the initial value, therefore, $R_e/R_0 \approx 1$ (Fig. 2.2). In the equilibrium evaporation regime, the droplet consistently decreases until it fully evaporates; therefore, $R_f/R_0 = 0$.

The ratio of temperature $T_{dp}$ with $T_R$ temperature is defined as parameter $\overline{T}_{dp} \equiv T_{dp}/T_R$ which defines the nature of the phase transformations on the droplet's surface: for the condensation phase transformation regime, condition $\overline{T}_{dp} > 1$ is necessary, while, in the evaporation regime, $\overline{T}_{dp} < 1$. At the time moment when $\overline{T}_{dp} = 1$, variation of phase transformations from condensation to the evaporation regime takes place. The initial parameter $\overline{T}_{dp} \equiv \overline{T}_{dp,0} = T_{dp}/T_{l,0}$ value is very important. When $\overline{T}_{dp,0} > 1$ the surface of sprayed liquid warms to the dew point $T_{dp}$ temperature in the condensation regime. When $\overline{T}_{dp,0} < 1$, the sprayed liquid starts to evaporate immediately. The evaporation regime is defined by the ratio of temperature $T_e$ with $T_R$ temperature expressed by parameter $\overline{T}_e \equiv T_e/T_R$. For equilibrium evaporation during which the supplied heat evaporates the liquid, condition $\overline{T}_e = 1$ is necessary. When the parameter is $\overline{T}_e < 1$, the transitional evaporation regime takes place, and the droplet warms to $T_e$ temperature. The initial value of parameter $\overline{T}_e \equiv \overline{T}_{e,0} = T_e/T_{l,0}$ is very important as well. In the condensation regime, condition $\overline{T}_{e,0} > 1$ is always satisfied, however, additional condition $\overline{T}_{dp,0} > 1$ is necessary. When $\overline{T}_{e,0} > 1$ and $\overline{T}_{dp,0} < 1$, the sprayed liquid phase transformations cycle starts with the transitional evaporation regime when the droplet warms up to the equilibrium evaporation temperature. When condition $\overline{T}_{e,0} = 1$ is valid, the sprayed liquid's droplets evaporate immediately at equilibrium. When condition $\overline{T}_{e,0} < 1$ is satisfied, the sprayed liquid's droplets also evaporate immediately, but, in the initial stage, they cool down to $T_e$ temperature.

The unsteady temperature field function $T_l(r,\tau)$ is closely related with droplet thermal parameters $P_T(\tau) \equiv T_R(\tau) = T(r = R^-, \tau)$ and $P_T(\tau) \equiv gradT_{r=R^-}(\tau) = \partial T/\partial r_{r=R^-}$. The expression of thermal parameters functions $P_T(\tau)$ of semi-transparent droplets flowing in radiating gas flux without slipping can be described with a model of integral type based on the infinite series:

$$P_T(r,\tau)=P_{T,R}(\tau)+\sum_{n=1}^{\infty}F(n,r)\int_0^{\tau}\left[(-1)^n\frac{R}{n\pi}\frac{dT_R}{d\tau}-\frac{1}{R\rho_l c_{p,l}}\right.$$
$$\left.\times\int_0^{R}q_r\left(\sin\frac{n\pi r_*}{R}-\frac{n\pi r_*}{R}\cos\frac{n\pi r_*}{R}\right)dr_*\right]\exp\left[-a_l\left(\frac{n\pi}{R}\right)^2(\tau-\tau_*)\right]d\tau. \quad (32)$$

For $P_{T,R}$ and $F(n,r)$ functions, a different meaning is provided when various thermal parameters are analyzed:

$$P_{T,R}(\tau)\equiv T_R(\tau) \text{ when } F(n,r)\equiv\frac{2}{r}\sin\frac{n\pi r}{R}, \text{ and } P_T(r,\tau)\equiv T(r,\tau); \quad (33)$$

$$P_{T,R}(\tau)\equiv T_R(\tau) \text{ when } F(n,r)\equiv\frac{2n\pi}{R}, \text{ and } P_T(r,\tau)\equiv T(r=0,\tau)=T_C(\tau); \quad (34)$$

$$P_{T,R}(\tau)\equiv 0 \text{ and } F(n,r)\equiv 2\frac{n\pi}{rR}\cos\frac{n\pi r}{R}-\frac{2}{r^2}\sin\frac{n\pi r}{R}, \quad (35)$$
$$\text{when } P_T(r,\tau)\equiv gradT_r(\tau)=\frac{\partial T(r,\tau)}{\partial r};$$

$$P_{T,R}(\tau)\equiv 0 \text{ and } F(n,r)\equiv(-1)^n\frac{2\pi n}{R^2}, \quad (36)$$
$$\text{when } P_T(r,\tau)\equiv gradT(r=R,\tau)=\left.\frac{\partial T(r,\tau)}{\partial r}\right|_{r=R};$$

$$P_{T,R}(\tau)\equiv 0 \text{ and } F(n,r)\equiv 0, \quad (37)$$
$$\text{when } P_T(r,\tau)\equiv gradT(r=0,\tau)=\left.\frac{\partial T(r,\tau)}{\partial r}\right|_{r=0}.$$

Integrals in expression (32) can be changed to finite integral sums:

$$\int_0^{R}q_r\cdot\left(\frac{n\pi r}{R}\cos\frac{n\pi r}{R}-\sin\frac{n\pi r}{R}\right)dr\to R\sum_{j=2}^{J}q_r^j\int_{r_{j-1}}^{r_j}\left(\frac{n\pi r}{R}\cos\frac{n\pi r}{R}-\sin\frac{n\pi r}{R}\right)dr, \quad (38)$$

$$\int_0^{\tau}f_n\exp\left[-a\left(\frac{n\pi}{R}\right)^2(\tau-\tau_*)\right]d\tau_*\to\frac{R_0^2}{a_{et}}\sum_{i=2}^{I}f_n^i\int_{\tau_{i-1}}^{\tau_i}\exp\left[-(n\pi)^2\frac{a}{a_{et}}\frac{R_0^2}{R^2}(\tau-\tau_*)\right]d\tau_* \quad (39)$$

Sums of finite integrals in expressions (38) and (39) are easily solved analytically when:

$$\int_0^{\tau}f_{n,\tau}d\tau=\sum_{i=2}^{I}\int_{\tau_{i-1}}^{\tau_i}f_{n,\tau,i}d\tau=\Sigma\bar{f}_{n,i}\int_{\tau_{i-1}}^{\tau}d\tau=\sum\bar{f}_{n.i}(\tau_i-\tau_{i-1}) \text{ when } \bar{f}_{n,i}\equiv\frac{f_{n,i}+f_{n,i-1}}{2} \quad (40)$$

$$\int_0^R f_{n,\Sigma,\tau,R}\,dr = \sum_{j=2}^{J}\int_{r_{j-1}}^{r_j} f_{n,\Sigma,\tau,r}\,dr = \Sigma\bar{f}_{n,\tau,r}\int_{r_{j-1}}^{r_j} dr = \sum \bar{f}_{n,\tau,j}\left(r_j - r_{j-1}\right) \text{ when } \bar{f}_{n,\tau,j} \equiv \frac{f_{n,\tau,j} + f_{n,\tau,j-1}}{2} \quad (41)$$

In the regimes of phase transformations cycle (29), the droplet's volume and thermal state are changing consistently. The variation offunction $T_R(\tau)$ describing the droplet's surface temperature and its matching at phase transformation moments to dew point $T_{dp}$ and to equilibrium evaporation, $T_e$ is fundamentally important for the definition of the change of phase transformations. The function of the droplet surface temperature is defined by solutions of equation (28). In the general case, finding $T_R(\tau)$ is possible only by applying the iterative numerical method because the instantaneous droplet surface temperature should be defined by the definition of heat fluxes. Therefore, for the definition of the heat flux balance condition on the droplet surface (28), rigorous analysis of the droplet energy state in the cycle of phase transformations regimes (29) is needed.

### 2.2. Droplet energy state analysis

To emphasize the droplet energy state variation in the phase transformation cycle (29) on the droplet's surface conditionally external and internal droplet sides are distinguished which are defined as radius $R^+$ and $R^-$, respectively. Therefore, it could be rewritten as: $\left|R^+\right| = \left|R^-\right| = R$.

The definition of the droplet's surface is directly related with total heat fluxes $q_\Sigma$ that flow toward and from the droplet's surface. This requires an interpretation of the droplet energy state which depends on phase transformation regimes (Fig. 2.5). In the radiating gas flow in the case of complex heating, the supplied heat flux for a slipping droplet's surface is defined by radiation, convection and conductive components:

$$q^+_{"c+r",\Sigma}(\tau) \equiv q^+_{"c+r"}(\tau) = q^+_{"c+r",r}(\tau) + q^+_{"c+r",c}(\tau) + q^+_{"c+r",k}(\tau). \quad (42)$$

For a droplet slipping in the air flow, the rising friction forces causes forced water circulation; therefore, in the general case, the intensity of the heat inside the droplet is defined by the complex heat flux density. The flux comes from the internal surface, which also involves the components of radiation, convection and conduction:

$$q^-_{"c+r",\Sigma}(r,\tau) \equiv q^-_{"c+r"}(r,\tau) = q^-_{"c+r",r}(r,\tau) + q^-_{"c+r",c}(r,\tau) + q^-_{"c+r",k}(r,\tau). \quad (43)$$

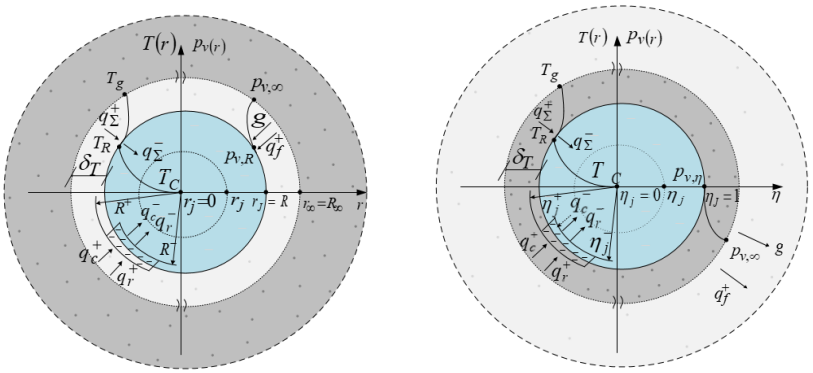


Fig. 2.5. Geometrical interpretation of water droplet heat transfer and phase changes: a) condensation regime; b) evaporation regime

A droplet of an equivalent diameter is surrounded by thermal $\delta_T$ and diffusion $\delta_D$ thickness boundary layers which are symmetrical regarding the aspect of the droplet center and ensure the average calculated heat fluxes that are caused by interacting transfer processes on the droplet's surface (Fig. 2.5).

In the thermal boundary layer, the temperature of the water vapor and air mixture becomes equal to the droplet's surface temperature. In the diffusion layer, the partial pressure of water vapor equalizes with the saturated water vapor pressure as defined by temperature $T_R$. However, in the diffusion layer, the variation of vapor pressure depends on the phase transformations regime: in the condensation regime, the partial pressure of water vapor in air is higher than that near the droplet's surface; therefore, in the diffusion layer, vapor pressure decreases to $p_{v,R}$ (Fig. 2.5 a.). Meanwhile, in the evaporation regime, the water vapor partial pressure is higher near the droplet's surface. Yet, in the diffusion layer, vapor pressure decreases to $p_{v,g}$ (Fig. 2.5 b). The difference of water vapor partial pressures $\left|p_{v,g} - p_{v,R}\right|$ defines a driving force of the ongoing phase transformations on the droplet's surface and determines the direction of the vapor flux: in the condensation regime, water vapor will diffuse towards the droplet and condensate on it, while, in the evaporation regime, water vapor will be generated in the process of surface evaporation and will spread out, away from the droplet.

Heat flux $q_f$, W/m$^2$ of phase transformations is defined according to the product of vapor flux density $m_v$, kg/(m$^2$s) and the water latent heat of evaporation $L$, J/kg. When the vapor flux density is described by Shorin-Kuzikovski correlation [73, 74], the universal phase transformations heat flux model is created for the entire phase transformations cycle (29):

$$q_f^+ \equiv m_v^+ L = L\frac{D_{vg}\mu_v}{T_{vg,R}R_\mu R}\left[p_{v,R} - p_{v,\infty} + \frac{\mu_v}{\mu_g}\left(p\ln\frac{p - p_{v,\infty}}{p - p_{v,R}} - p_{v,R} + p_{v,\infty}\right)\right]. \quad (44)$$

When concretizing the heat fluxes balance expression (28), it is important that the selected mathematical model should also ensure the negative calculated vapor flux in the condensation regime and the positive value in the evaporation regime. This is ensured by Stefan's logarithm in expression (44) which reaches the zero value of vapor flux when crossing from the condensation regime to the evaporation regime (then, the droplet warms to the dew point temperature; therefore $p_{v,\infty} \equiv p_{v,g} = p_{v,R}$ and $m_v = 0$).

The convection heat flux inside the droplet is defined by taking into account the variation of the temperature field gradient in the phase transformations cycle (29) regimes. In the case of complex heating by radiation and conduction when defining the droplet temperature field gradient $\partial T(\tau, r)/\partial r$ on the basis of expression (14) and when applying condition $r \equiv R^-$, the heat convection flux inside the droplet is defined by the universal model for whole phase transformations cycle (29):

$$q^-_{"c"} = \left.\frac{T(r,\tau)}{\partial r}\right|_{r=R^-} = \frac{2\pi}{R^2}\sum_{n=1}^{\infty}(-1)^n n \int_o^{\tau} f_n \exp\left[-a\left(\frac{n\pi}{R}\right)^2(\tau-\tau_*)\right]d\tau_* \quad (45)$$

It is important that the system of expressions (15, 45) defines the calculated convection heat flux of the negative sign for the case when the temperature field gradient inside the droplet is positive, and it also ensures a self-contained change of this flux vector when a negative temperature field gradient forms in the transitional evaporation regime due to the impact of radiation absorption.

When providing for the fact that the air temperature is higher than the droplet temperature ($T_g > T_R$), the water vapor and air mixture will always cool down to temperature $T_R$, while the difference between temperatures $T_g$-$T_R$ will define the driving force of the heat transfer in all the phase transformation regimes. When the Nusselt number for an evaporating droplet is described according to Abramzon-Sirignano correlation [14], the external convectional heat flux density of a droplet slipping in gas flow is defined according to the model based on the Newton law:

$$q^+_c = \lambda_{vg}\frac{T_g - T_R}{2R}\cdot\left[2\frac{\ln(1+B_T)}{B_T} + 0.57\frac{\mathrm{Re}^{1/2}\,\mathrm{Pr}^{1/3}}{(1+B_T)^{0.7}}\right] \quad (46)$$

The Spalding heat transfer parameter evaluates the influence of Stefan's hydrodynamic flow, and its expression is well-known for an equilibrium evaporating droplet in the case of convection heating [5]:

$$B_{T,"c",e} = c_{p,vg}\frac{T_g - T_R}{L}. \quad (47)$$

In the case of complex heating, the impact of radiation must be considered in the energy balance of equilibrium evaporation [108]:

$$B_{T,"c+r",e} = c_{p,vg}\frac{T_v - T_R}{L - q_r / m^+_{v,e}}. \quad (48)$$

In the transitional phase transformation regimes of $B_T$ model, additional consideration must be taken regarding the complex heat flux provided for a droplet which not only evaporates but also heats water. For that, rigorous evaluation of the energy state variation in the phase transformations cycle regimes must be performed, and attention to the stimulation of heat fluxes in the evaporation process must be taken into account.

Then the local radiation flux can be described according to the spectral radiation model in a semitransparent sphere:

$$\begin{aligned} q_r(r) &= 2\pi \int_0^{\infty} \int_0^{\frac{\pi}{2}} \sin\gamma \cos\gamma \cdot F_{\omega}(r,\gamma) d\gamma d\omega, \\ F_{\omega}(r,\gamma) &= I_{\omega,R,\gamma} \exp\left(-\tau_r^R\right) + \int_r^R n_{\omega}^2 I_{\omega 0} \exp\left(-\tau_r^{r_*}\right) d\tau_r^{r_*} - I_{\omega,R,\gamma} \exp\left(-\tau_{r\sin\gamma}^R - \tau_{r\sin\gamma}^r\right) \\ &- \int_{r\sin\gamma}^r n_{\omega}^2 I_{\omega 0} \exp\left(-\tau_{r\sin\gamma}^r - \tau_{r\sin\gamma}^{r_*}\right) d\tau_r^{r_*} - \int_r^R n_{\omega}^2 I_{\omega 0} \exp\left(-\tau_{r_*}^r\right) d\tau_{r_*}^r \end{aligned} \quad (49)$$

It is based on the geometric theory of optics [71]. The local radiation flux model in the droplet and its surroundings provides estimates of spectral radiation as well as peculiarities of the complex spectral index of refraction of a semi-transparent liquid and the occurring optical effects on the internal and external sides of a droplet's surface.

During the condensation phase transformation regime, water is being heated by the absorbed radiation heat, besides, by all the gas convective heat and additionally contributed condensed water vapor from phase transformations heat on the droplet surface, therefore:

$$\begin{aligned} q_{\Sigma}^-(\tau \equiv 0 \div \tau_{co}) &= q_r^-(\tau \equiv 0 \div \tau_{co}) + q_c^+(\tau \equiv 0 \div \tau_{co}) + q_f^+(\tau \equiv 0 \div \tau_{co}); \\ q_c^-(\tau \equiv 0 \div \tau_{co}) &= q_r^-(\tau \equiv 0 \div \tau_{co}) + q_c^+(\tau \equiv 0 \div \tau_{co}). \end{aligned} \quad (50)$$

In the transitional evaporation regime, a part of the external convection heat is already involved into the water evaporation process, and the evaporation heat is proportional to the difference of external and internal heat fluxes, therefore:

$$\begin{aligned} q_{\Sigma}^-(\tau \equiv \tau_{co} \div \tau_e) &= q_r^-(\tau \equiv \tau_{co} \div \tau_e) + q_c^-(\tau \equiv \tau_{co} \div \tau_e) \\ q_f^-(\tau \equiv \tau_{co} \div \tau_e) &= q_c^+(\tau \equiv \tau_{co} \div \tau_e) - q_c^-(\tau \equiv \tau_{co} \div \tau_e). \end{aligned} \quad (51)$$

The interpretation of heat fluxes flowing towards and from the droplet's surface in the phase transformation regimes is provided in (Fig. 2.5).

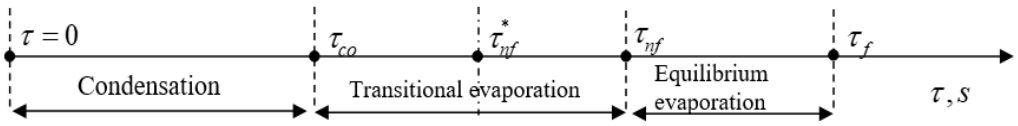


Fig. 2.6. The Interpretation of droplet phase transformation regimes cycle duration

It should be noted that in the case of complex heating in the transitional evaporation regime at time moment $\tau_{nf}^*$ (Fig. 2.6), a negative temperature field gradient forms [109]. This makes preconditions for the absorbed radiation flux partial

outflow to the droplet's surface by internal heat convection participation in the water surface evaporation process. Therefore, at time moment $\tau_{nf}^{*}$, the direction of the convection heat flux vector changes, while the energetic nature of $q_c^-$ flux changes too: at time period $\tau \equiv \tau_{co} \div \tau_{nf}^{*}$, the internal heat convection flux matches the part of the external convection flux that warms the water, while during the time interval $\tau \equiv \tau_{nf}^{*} \div \tau_e$ already corresponds, to a part of radiation flux which evaporates the water, therefore:

$$\begin{aligned} q_c^-\left(\tau \equiv \tau_{co} \div \tau_{nf}^{*}\right) &= q_c^+\left(\tau \equiv \tau_{co} \div \tau_{nf}^{*}\right) - q_f^+\left(\tau \equiv \tau_{co} \div \tau_{nf}^{*}\right); \\ q_c^-\left(\tau \equiv \tau_{nf}^{*} \div \tau_e\right) &= q_f^+\left(\tau \equiv \tau_{nf}^{*} \div \tau_e\right) - q_c^+\left(\tau \equiv \tau_{nf}^{*} \div \tau_e\right). \end{aligned} \qquad (52)$$

Equilibrium evaporation starts only when all the absorbed radiation flux participates in evaporation, therefore:

$$\begin{aligned} q_f^+\left(\tau \equiv \tau_e \div \tau_f\right) &= q_c^+\left(\tau \equiv \tau_e \div \tau_f\right) + q_c^-\left(\tau \equiv \tau_e \div \tau_f\right); \\ q_\Sigma^-\left(\tau \equiv \tau_e \div \tau_f\right) &= q_c^-\left(\tau \equiv \tau_e \div \tau_f\right) - q_r^-\left(\tau \equiv \tau_e \div \tau_f\right) \approx 0. \end{aligned} \qquad (53)$$

It should be noted that, in the context of the heat fluxes energy balance, the difference of heat fluxes $q_c^-\left(\tau \equiv \tau_e \div \tau_f\right) - q_r^-\left(\tau \equiv \tau_e \div \tau_f\right)$ determines the impact of enthalpy in the equilibrium evaporating droplet and, which is possibly lost in the cooling process. The assessment of a droplet's energy state variation in cycle regimes (29) is generalized by expressions (49–53). This equation system makes preconditions for universal approximation creation of the Spalding transfer parameter. In a broader sense, function $q_r(\tau)$ in expression (48) can be considered as function $q(\tau)$ which defines all the heat fluxes which participate in the phase transformations, except for external heat convection $q(\tau) \equiv q_f^+(\tau) - q_c^+(\tau) = m_v^+(\tau)L(\tau) - q_c^+(\tau)$. Therefore, expression (48), which is already considered to be the classical expression of equilibrium evaporation, is analytically reorganized into the universal form of the Spalding heat transfer parameter for the entire cycle (29):

$$B_T(\tau) = \frac{c_{p,vg}(\tau)}{L(\tau)} \frac{T_v - T_R(\tau)}{1 - \dfrac{q(\tau)}{m_{v,e}^+(\tau)L(\tau)}} = B_{T,"c"}(\tau)\frac{q_f^+(\tau)}{q_c^+(\tau)}. \qquad (54)$$

We should note that the heat flux of phase transformations on a droplet's surface is defined by the difference of flowing in and flowing from heat fluxes $q_{f,l}^+(\tau) = q_{\Sigma,g}^+(\tau) - q_{\Sigma,l}^-(\tau)$; in the framework of assumption $q_r^-(\tau) \cong q_r^+(\tau)$, expression (54) is transformed into an equation which is well-known in the transitional evaporation regime [108].

$$B_T(\tau) \cong B_{T,"c"}(\tau)\left[1+\frac{q_c^-(\tau)}{q_c^+(\tau)}\right] = B_{T,"c"}(\tau)\left[1-k_c^-(\tau)\lambda_l(\tau)\frac{\partial T_l(r,\tau)}{\partial \tau}\bigg|_{r=R} / q_c^+(\tau)\right], \quad (55)$$

Spalding heat transfer $B_T$ parameter expression (55) justifies a close connection between internal and external heat transfer processes and a droplet's thermal state. Expression (55) which defines parameter $B_T$ is universal throughout all the droplet phase change cycle regimes.

If we consider the selected heat flux models (44–46, 49), the formal heat flux balance condition (28) is transformed into the balance model of heat fluxes on a droplet's surface, which is universal for all phase transformations:

$$\left(q_r^+ - q_r^-\right) + \frac{\lambda_{vg} Nu_f}{2R}\left(T_g - T_R\right) - k_c^-\lambda_l \frac{\partial T_r}{\partial r}\bigg|_{r=R} - m_v L = 0. \quad (56)$$

In condition (56), the system of integral and algebraic equations is hidden, which, together with the selected phase transformations model (28), is universal for the entire droplet cycle (29). Thus function $T_R(\tau \equiv 0 \div \tau_f)$ is unambiguously defined; this determines the temperature variation on a droplet's surface. Therefore, function describing the local radiation flux $q_r(\tau, r)$ must be defined. While providing that system of equations (56) can only be solved numerically by applying the iterative method, function $q_r(\tau, r)$ is defined at selectively selected control time moments as a radial coordinate function $q_r(\tau \equiv \tau_i, r)$ according to integral model based on geometric optics [72]. The calculations require equivalent diameter $2Ri$ of the droplet and its instantaneous $T(\tau_i,r)$ temperature field. Both of them are selected as already known parameters at $\tau_{i-1}$ time moment.

### 2.3. Numerical solution of the 'droplet' problem

When solving the 'droplet' problem, quick solutions are being sought. The aim is to avoid iterative calculations because they greatly increase the solution time of sprayed liquid systems when software packages are being used [10, 57]. For modeling the liquid fuel combustion process in cylindrical engines, the volume is divided into hundreds or thousands, or even into several million elementary volumes, whereas the droplet evaporation rate for each of them must be calculated in order to define the amount of burnt fuel and the amount which is evaporated in the combustion process. For this reason, accurate models are replaced by approximating expressions. An issue of the reliability of these expressions rises. It requires experimental research or detailed numerical modeling. This necessity leads to the creation of an iterative numerical scheme and its solution.

The inevitability of iteration calculations is caused by a fact that, at certain time moments heat fluxes can only be calculated when parameters $T_{R,i}$ and $R_i$ are defined. In addition, heat fluxes $q_{c,i}^+$ and $q_{f,i}^+$ must be already defined so that it makes possible

to calculate parameter $B_{T,i}$ according to our expression. Expression (56) is a transcendental equation whose solution can be defined numerically only by an iterative scheme.

### 2.3.1. Explanation of iterative cycle

The numerical iterative cycle is carried out in the droplet phase transformation cycle at all pre-released control time moments $\tau_i$ (29),

$$it \equiv it = 1 \div it = IT \qquad (57)$$

whose definition requires specific number $I$ of control time $\tau_i$ moments.

While foreseeing the variation stability of time coordinate step $\Delta\tau_i$ in all the droplet phase tranformations regimes (Fig. 2.7), in the general case, $\Delta\tau_i$ is defined when the duration of phase transformations $\tau_f$ is guesstimated:

$$\Delta\tau_i = \frac{\tau_f}{I-1};\ \text{when}\ \sum_{i=2}^{I}(\tau_i - \tau_{i-1}) = \tau_f\ . \qquad (58)$$

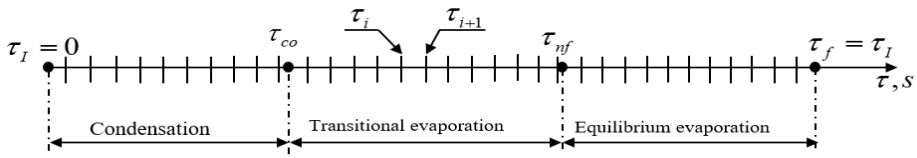


Fig. 2.7. A schematic diagram of iterative numerical scheme in phase transformation regimes cycle

In the numerical scheme, the initial value of time coordinate $\tau = 0$ is identified with the beginning of the phase transformations cycle (29). All the HMT parameters are determined at the initial time moment. When a possible droplet surface temperature variation interval $T_{R,min} \div T_{R,max}$ is defined, iterative cycle (57) is carried out by the fastest descent method consistently for each control $\tau_i$ time moment starting from $\tau_{i=2}$ . The calculated temperature of droplet surface $T_{R,i}$ is considered as the temperature selected at the final iteration $T_{R,i,it=IT}$ of a cycle (57).

$$T_{R,i} \equiv T_{R,i,it=IT}\ ;\ \text{when}\ \left|1 + \frac{q^{-}_{c,i,it=IT} - q_{f,i,it=IT}}{q^{+}_{c,i,it=IT}}\right| \times 100\% < \delta_{allowed} = 0.05\% . \qquad (59)$$

For the determination of the transfer parameters inside a droplet, number $J$ of the control division points is distinguished in the radius of an equivalent sphere, whereas the control number of concentric sections $J$ (Fig. 2.8) is defined by radial $r_j$ coordinates:

$$\Delta r_j = \frac{R}{J-1};\ \text{when}\ \sum_{j=2}^{J}\left(r_j - r_{J-1}\right) = R\ . \qquad (60)$$

It is inconvenient to define the grid of time and radial coordinates in real life according

to expressions (58) and (60) in the numerical scheme. Droplet's diameters are changing throughout the entire droplet phase transformations cycle (29), while the duration of these phase transformation regimes can be prominently different. Additionally, in the numerical scheme, the uncertainty of stability still remains, when the vapor flux on a droplet's surface is passing the zero value as the condensation regime is changing to the evaporation regime. These problems are solved by introducing the dimensionless radial coordinate $\eta$, and an idea of the universal phase tranformations cycle with uniform unit-length regimes is being applied [110].

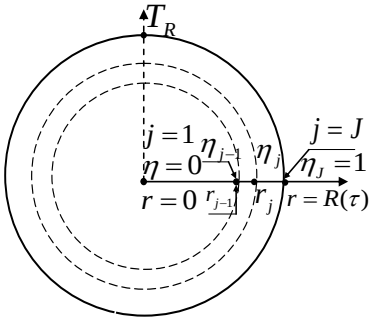


Fig. 2.8. Schematic diagram of droplet radial coordinate division

The universal radial coordinate $\eta$ is created when radial coordinate $r$ is normed with time $R(\tau)$ function which describes the variation of the equivalent dimension:

$$\eta = \frac{r}{R(\tau)} \qquad (61)$$

For the case of a universal radial coordinate, the center of a droplet is defined with the value $\eta = 0$, while a droplet's surface is defined with value $\eta = 1$ (Fig. 2.8); therefore, throughout the entire droplet phase transformation cycle (29), the unit dimensionless radius of the droplet remains constant. This allows to ensure the variating grid of the droplet radial coordinate according to a constant step defined in the universal radial coordinate case:

$$\Delta\eta_j = \frac{1}{J-1}; \rightarrow \eta_{j>1\div J} = \eta_{j-1} + \Delta\eta_j; \rightarrow \Delta r_{i,j} = \Delta\eta_j R_i; r_{i,j>1\div J} = r_{i,j-1} + \Delta r_{i,j}. \quad (62)$$

The duration of phase transformation regimes may be considerably different. Hence a problem of a universal approach towards the duration of individual regimes arises. For its solution, the idea of a universal phase transformation regimes cycle is applied.

### 2.3.2. Universal phase transformation regimes cycle of unitary duration

For the creation of a universal phase transformation regime cycle (63), the universal time scale based on the modified Fourier number cycle in expression (29) is reorganized as:

$$Fo = \frac{a_0}{R_0^2} \cdot \tau; \rightarrow Fo \equiv 0 \div Fo_{co} \div Fo_e \div Fo_f \quad (63).$$

The classical Fourier number $Fo = \left(a / R^2\right) \cdot \tau$ expression for the formation of a transformed cycle $\tau \equiv 0 \div \tau_f$ is inappropriate. During the droplet warming time, phase transformations take place on its surface. They influence the variation of $a / R^2$ interface parameter in the Fourier time scale. Therefore, the modified Fourier number $Fo = \left(a_0 / R_0^2\right) \cdot \tau$ is used. For the modified number, the multiplier $a_0 / R_0^2$ is formed according to the initial state of a droplet, therefore, it does not change during the phase transformation process. The Fourier number $Fo=(a_{stand.}/R_0^2)\cdot\tau$ is calculated for a standard liquid. Water at 278 °K temperature is considered as a base liquid. The linking multiplier for the real phase transformation time and the modified number is initial droplet radius function $a_0 / R_0^2 = f\left(R_0\right)$. Then, the droplet phase transformation regimes cycle (29) is transformed into the Fourier time scale cycle (63).

The heat transfer case "$k$" is well-known and has been extensively investigated. It allows providing peculiarities of heat and mass transfer parameters presented in works [109, 110]. The droplet's heat and mass transfer parameters can be grouped into thermal $P_T$, energetic $P_q$, dynamic $P_D$ and $P_f$ phase parameters. A droplet's thermal $P_T$ parameters are related with the non-stationary temperature field function $T(r,\tau)$ which describes the temperature change inside a droplet. Dynamic $P_D$ parameters describe a droplet's movement in the gas flow and the forces operating on a droplet's surface; Energy $P_q$. parameters define the droplet's energy state variation which is related with the heat fluxes inside the droplet and in its surroundings; Phase $P_f$ parameters are related with phase transformations [72].

For example, the functions of thermal parameter groups $P_T$ are noted as exclusive ones. In the real time scale, their dispersity is very significant for the droplet heating process. In the droplet phase transformation cycle, at the time scale expressed by the Fourier number, the warming process of droplets of different dispersity is identical, $P_T(Fo)$. A droplet's surface temperature depends only on the surrounding gas temperature and the vapor partial pressure $P_{T,"k"}(Fo) = f\left(T_d, \overline{p}_{g,\infty} / p\right)$. This illustrates the principal graphs provided in (Fig. 2.9). For other droplet parameter groups, such as $P_q(Fo)$ and $P_f(Fo)$, it seems that functions independent from droplet dispersion cannot be devised. However, they become universal in the normed form $P/P_0$: $\overline{P}_T(Fo)$ and $\overline{P}_q(Fo)$, and then they are universal for the droplet dispersity.

Therefore, in the well-known "$k$" heat transfer case, functions of heat and mass transfer parameters are normed $\overline{P}_{"k"}(Fo)$ and can be provided in the time scale expressed by the Fourier number (Fig. 2.9). The main advantage of this time scale is that for all heat and mass transfer parameter functions $P(\tau)$, dimensionless form functions $\overline{P}(Fo) = P(Fo) / P_0$ can be applied, and then all the functions become sensitive to droplet dispersion. This principle could be applied to all the droplet transfer

parameter functions $\overline{P}_{k''}(Fo)$. This allows optimizing the numerical research experiment; however, a problem of the application of this method for more complex cases arises.

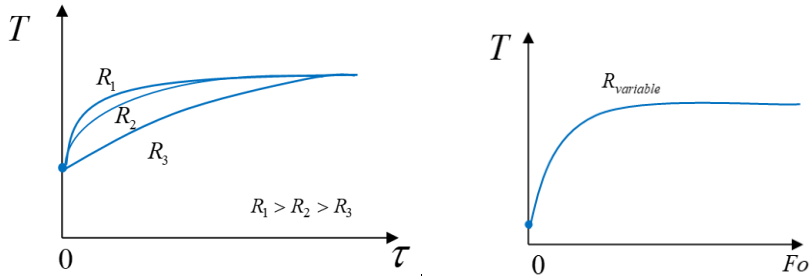


Fig. 2.9. Variation of principal droplet temperature dependence on thedroplet diameter in real time and Fourier number time scale 'k' heat transfer case

For a numerical experiment of the 'droplet' problem scheme creation, the time and radial coordinates involving universal grid is important. The universal cycle of unitary duration regimes is important for the time coordinate grid creation across all the cycle regimes. According to expression (63), the generated universal droplet life time cycle is:

$$\overline{Fo} = \frac{Fo}{Fo_n} \cdot \rightarrow \overline{Fo} \equiv 0 \div 1 \div 2 \div 3. \qquad (64)$$

The modified Fourier number is applied for the creation of a universal unit length phase transformation cycle [110]. Therefore, for different regimes, a different normative criterin $Fo_n$ is used: for the condensation regime $Fo_n \equiv Fo_{co}$ and $\overline{Fo} = 0 \div 1$; for the transitional evaporation regime, $Fo_n \equiv Fo_{nf} - Fo_{co}$ and $\overline{Fo} \equiv 1 + (Fo - Fo_{co})/(Fo_{nf} - Fo_{co}) = 1 \div 2$; for the equilibrium evaporation regime, $Fo_n \equiv Fo_f - Fo_{nf}$ and $\overline{Fo} \equiv 2 + (Fo - Fo_{nf})/(Fo_f - Fo_{nf}) = 2 \div 3$. In this cycle interval, $0 \div 1$ is the condensation phase transformation regime of the universal dimensionless unit length; $1 \div 2$ is the transit phase transformation regime of the universal dimensionless unit length; $2 \div 3$ is the equilibrium evaporation phase transformation regime of the universal dimensionless unit length. Interval $0 \div 2$ determines the universal regime of transit phase transformations. Time dimensionless parameter $\overline{Fo}$ in the phase transformation cycle regime is formed individually. Then, in the numerical scheme, time grid (29) can be a grid defined according to the universal and already defined first step of cycle (64).

$$\Delta\overline{Fo} = \frac{1}{I_{co} - 1}; \rightarrow \Delta Fo = \Delta\overline{Fo} \cdot Fo_{co}; \rightarrow \Delta\tau = \frac{\Delta Fo}{a_0 / R_0^2}; \rightarrow \tau_{i>1} = \tau_{i-1} + \Delta\tau \quad (65)$$

If a droplet's phase transformation cycle starts with the transitional evaporation regime, then in scheme (65), $\Delta\overline{\mathrm{Fo}} = 1/(I_{nf} - 1)$ and $\Delta\mathrm{Fo} = \Delta\overline{\mathrm{F}} \cdot \mathrm{Fo}_{nf}$. It could be expected

that the time variation step $\tau_f$ according to the phase transformation time is inconvenient because it is virtually impossible to predict the exact droplet evaporation time, while at least $\tau_f$ could indicate only when all the iterative cycles are carried out for the droplet's surface temperature definition by the fastest descent method. Therefore, the time step is determined for the first regime of a universal cycle (65), while it is unchanged in other regimes.

For the definition of optimal parameters $\Delta\tau$ and $\Delta r$, additional analysis is necessary. They are defined by special investigation which is provided in the results section (Section 3.1). Based on this grid, a numerical iterative scheme is carried out. This numerical scheme needs to be optimized by optimal radial coordinate grading $J_{op}$, optimal time step $I_{op}$, and $N_{op}$ selection of members in the infinite integral equations series describing the unsteady temperature field gradient. Based on the selected mathematical model, the iterative numerical scheme requires the selection of optimal parameters.

### 2.3.3 Numerical iterative scheme

For each control time moment $\tau_i$, the iterative cycle is carried out. It is performed for the droplet surface instantaneous temperature definition, and, in parallel, all the important parameters of thermal, energy and phase transformation parameters are calculated as well. The necessity of the iteration calculation is caused by the fact that, for energy fluxes calculation at time moment $\tau_i$, the instantaneous droplet surface temperature $T_{R,i}$ and instantaneous droplet diameter $R_i$ must be known. Convection heat flux $q_{c,i,it}$ must be defined by $B_T$ parameter in each iteration *it*. Therefore, at each time moment $\tau_i$, the iterative cycle is performed for the definition of a droplet's surface instantaneous temperature $T_{R,i}$.

A droplet's heat and mass transfer processes in two phase water droplets and in humid air flow are defined by parameter $P(\tau)$ functions. For any of the droplet transfer parameter, an iterative numerical calculation system is created. The unknown parameters $P_{i,it=1}$ required for the first iteration are attributed. In other iterations, parameters are defined by condition $P_{i,it} = P_{i,it-1}$. They are indicated by the values of the iterative cycle already defined in the previous iteration, for example, $T_{R_{i,it-1}}$, $R_{i,it-1}$, $q_{c,i,it-1}$. To define droplet transfer parameters $P_{i>1}$, starting from $\tau_{i=2}$, iterative cycle $it \subset 1 \div IT$ is executed for each time moment $\tau_i$ to define a droplet's surface temperature $T_{R,i}$. According to expression (56), the developed numerical scheme is:

$$\left(q^{+}_{r,J,i}-q^{-}_{r,J,i}\right)+\lambda_{vg,i}\frac{T_g-T_{J,i,it}}{2R_{i,it-1}}\cdot\left[2\frac{\ln\left(1+B_{T,i,it}\right)}{B_{T,i,it}}+0.57\frac{\mathrm{Re}^{1/2}_{i,it}\,\mathrm{Pr}^{1/3}_{i,it}}{\left(1+B_{T,i,it}\right)}\right]-$$
$$-\frac{D_{vg,i,it}\mu_v}{T_{J,i,it}R_{\mu}R_{i,it-1}}\left[p_{v,J,i,it}-p_{v,\infty}+\frac{\mu_v}{\mu_g}\cdot\left(p\ln\frac{p-p_{v,\infty}}{p-p_{v,R,i,it}}-p_{v,R,i,it}+p_{v,\infty}\right)\right]=q^{-}_{c,J,i,it}. \quad (66)$$

In scheme (66), size is:

$$q^{-}_{c,J,i,it}=-2k^{-}_{c,i,it}\lambda_{J,i,it}\sum_{n=1}^{\infty}(-1)^n\frac{n\pi}{R^2_{i,it-1}}\times\sum_{ii=2}^{i}\left[(-1)^n\frac{\hat{R}_{ii}}{n\pi}\frac{T_{J,ii}-T_{J,ii-1}}{\tau_{ii}-\tau_{ii-1}}+\frac{f_{q_r,i,ii}}{\hat{\rho}_{l,ii}\hat{c}_{p,l,ii}\hat{R}_{ii}}\right]$$
$$\times\frac{1}{\hat{a}_{l,ii}}\left(\frac{\hat{R}_{ii}}{n\pi}\right)^2\left\{\exp\left[\hat{a}_{l,ii}\frac{n^2\pi^2}{\hat{R}^2_{ii}}\left(\tau_{ii}-\tau_i\right)\right]-\exp\left[\hat{a}_{l,ii}\frac{n^2\pi^2}{\hat{R}^2_{ii}}\left(\tau_{ii-1}-\tau_i\right)\right]\right\};. \quad (67)$$

A droplet's surface temperature $T_{R,i,it}$ is selected for an iteration, while the necessary parameters are defined as $R_{i,it}\equiv R_{i,it-1}$, $q^{+}_{c,i,it}\equiv q^{+}_{c,i,it-1}$ ir $q^{+}_{f,i,it}\equiv q^{+}_{f,i,it-1}$.. In expression (67), sizes $\hat{\rho}_{l,ii}=0.5\left(\rho_{l,ii}+\rho_{l,ii-1}\right)$, $\hat{c}_{p,l,ii}=0.5\left(c_{p,l,ii}+c_{p,l,ii-1}\right)$ and $\hat{a}_{l,ii}=0.5\left(a_{p,l,ii}+a_{l,ii-1}\right)$ are liquid density, specific heat and temperature coefficients, respectively. For each size, we carry out iteration *it* according to scheme (66); unknown droplet radius $R_{it}$ is specified as $R_{i,it}\equiv R_{i,it-1}$. This allows taking into account the droplet dimension variation in cycle regimes. A droplet's volume after each iteration is:

$$R^3_{i,it}=R^3_{i-1}-\frac{R^2_{i-1}+R^2_{i,it-1}}{\rho_{l.m,i-1}+\rho_{l.m,i,it}}\left(3\frac{m^{+}_{v,i-1}+m^{+}_{v,i.it}}{2}+\frac{R_{i-1}+R_{i,it-1}}{4}\times\frac{\rho_{l,m,i,it}-\rho_{l,m,i-1}}{\tau_i-\tau_{i-1}}\right)\left(\tau_i-\tau_{i-1}\right). \quad (68)$$

In all the phase transformation regimes, the iterative cycle of the Spalding heat transfer parameter variation is evaluated:

$$B_{T,i,it}=\frac{c_{p,gd,i,it}\left(T_d-T_{R,i,it}\right)}{L_{i,it}}\left(1-\frac{q^{-}_{c,i,it}}{q^{+}_{c,i,it}}\right). \quad (69)$$

The effective heat conduction parameter is expressed:

$$k^{-}_{c,i,it}=1.86+0.86\tanh\left(2.225\log_{10}\frac{Pe_{l,i,it}}{30}\right). \quad (70)$$

Peclet number expression is $Pe_{l,i,it}=\left(R^2_{i,it-1}\Delta w^2_{l,i,it}/8\right)\cdot\left(\rho_g/a_{l,i,it}\mu_{l,i,it}\right)\cdot C_{F,i,it}$. Reynolds and Prandtl numbers are calculated by expressions: $\mathrm{Re}_{i,it}\equiv 2R_{i,it-1}\Delta w_{l,i,it}\rho_g/\mu_{vg,i,it}$ and $\mathrm{Pr}_{i,it}=\nu_{vg,i,it}/a_{vg,i,it}$, respectively. The maximum liquid flow on a droplet's surface is evaluated by expression:

$$w_{l,i,it} = w_{l,i-1} + \frac{3}{8}\rho_d \frac{\hat{C}_{l,i,it}\Delta\hat{w}_{l,i,it}\left|\Delta\hat{w}_{l,i,it}\right|}{\hat{R}_{i,it}\hat{\rho}_{l,i,it}}\left(\tau_i - \tau_{i-1}\right) \qquad (71)$$

In the expression, a droplet's full drag coefficient is $C_{l,i,it} = 24 + 4.8\,\mathrm{Re}_{i,it}^{0.63}/\left(1 + B_{T,i,it}\right)^{0.2} \cdot \mathrm{Re}_{i,it}$. The average droplet slipping velocity is: $\Delta\hat{w}_{l,i,it} = 0.5\left(w_{l,i-1} + w_{l,i,it}\right) - w_d$, while the average full drag coefficient is $\hat{C}_{l,i,it} = 0.5\left(C_{l,i-1} + C_{l,i,it}\right)$. The average radius of a droplet is evaluated by expression $\hat{R}_{i,it} = 0.5\left(R_{i-1} + R_{i,it-1}\right)$, while average water density equals $\hat{\rho}_{l,i,it} = 0.5\left(\rho_{l,i-1} + \rho_{l,i,it}\right)$. Instantaneous mass mean temperature $T_{l,m,i}$ of a droplet is calculated according to scheme:

$$T_{l,m,i} = 0.5\frac{\sum_{j=2}^{J}\hat{\rho}_{l,j,i}\cdot\left(V_{l,j,i} - V_{l,j-1,i}\right)\cdot\left(T_{j,i} + T_{j-1,i}\right)}{\sum_{j=2}^{J}\hat{\rho}_{l,j,i}\cdot\left(V_{l,j,i} - V_{l,j-1,i}\right)}. \qquad (72)$$

A droplet's mass is adjusted at the end of each iterative cycle $it \equiv 1 \div IT$ according to expression $M_i = M_{i-1} - 4\pi\hat{R}_i^2\hat{m}_{g,i}^{+}\left(\tau_i - \tau_{i-1}\right)$.

A numerical scheme for the determination of droplet dynamics and heating intensity definition is created according to the mathematical model. The provided numerical schemes are universal for the entire phase transformation cycle (29). An iterative calculation scheme is used to define a time grid.

## 3. Results of Investigation and Systematic Evaluation

For the definition of a droplet's geometric, thermal and energy states, the phase transformation regimes cycle (29) is modeled for different droplet heating cases. It ensures a consistent phase transformations variation across the entire cycle. The Fourier number is applied for the universal cycle of the generation of unitary duration regimes. The iterative calculation scheme is created according to the mathematical model and implemented by the fastest descent method. The control and optimization of the numerical scheme was performed for the first time in this thesis.

### 3.1. Justification of numerical iterative scheme grid

For the calculation of the time and radial coordinate step, a numerical scheme which uses the iterative cycle methodology has been created. However, the functionality of the numerical iterative scheme and the reliability of the results of the numerical modeling of droplet phase transformations depends on the selection of parameters *N, J, M* and *I*. In the iterative cycle, it is virtually impossible to predict the optimal values of these parameters due to the non-linearity of complex heat and mass transfer processes in semi-transparent droplets flowing in a two-phase flow. The numerical scheme optimal parameters $N_{op}$, $J_{op}$, $M_{op}$ and $I_{op}$ can only be defined with a rigorous numerical experiment. The determining parameters of the time grid for a numerical scheme are influenced by the droplet heating case and the defining parameters of the sprayed liquid and gas flow boundary conditions.

Any thermal parameter $P_T(\tau)$ can be expressed by an infinite series related to integral equations. When calculating the unsteady temperature field and its gradient, it is necessary to evaluate number *N* of the assessable finite members in the infinity integral equation series. Therefore, any thermal parameter can be described by equation:

$$P_T = \sum_{n=1}^{\infty} f_n(\tau, r) = f_{n=1} + f_{n=2} + ... + f_N + ... + f_\infty \quad (73)$$

The real numerical scheme cannot be associated with an infinite number of members (infinity). Therefore, infinity is defined as a specific integer N ( $\infty \to N$ ). It is the number of the members of an infinite sum. Therefore, equation (73) can be provided as expression (74):

$$P_T = \sum_{N=1}^{N} f_n(\tau, r) \quad (74)$$

In the case of complex droplet heating, when calculating the local radiation flux $q_{r,i,j}$, recommendations provided in work [72] are followed.

The infinite spectrum of radiation is defined by the lengths of light waves of $l_{\min} = 0.8\ \mu m$ and $l_{\min} = 200\ \mu m$ because the definition of optical effects on the droplet's surface and the determination of the light absorption coefficient demands

rigorous analysis of the water complex spectral index of refraction in this wave interval [95]. When grading the radiation spectrum, the components of the water spectral index of absorption and the spectral index of light refraction change according to the curves which are very complex and have a lot of extremity points [95]. Therefore, integration of a light beam according to the radiation wavelength in a range of short waves should be multiplexed. Thus an interval of waves $l_{\min} \div l_{\min}$ is changed to the interval of wave number $\omega_{\min} = 1/l_{\max} \div \omega_{\max} = 1/l_{\min}$ which has an unchanging step:

$$\Delta\omega = \frac{\omega_{\max} - \omega_{\min}}{M - 1},\ m^{-1} \qquad (75)$$

This step ensures non-linear and highly thickened radiation spectrum grading according to the wavelength. This creates preconditions for the calculation of the radiation flux model according to our system-based (8–11) model [72] which allows to take into account the impact of the optical light spectral effects (the refraction in the external and internal side surfaces, refraction passing through the air to water, absorption in water, and full internal refraction when light falls at an angle larger than the Brewster's angle).

In numerical calculations, number M is chosen to be equal to $M$=101 and is selected according to the recommendation of work [95]; therefore, it must be $M$>80, and the speed of today's computer calculation must be evaluated as well. However, due to the specific aspects of the iteration method, when calculating the impact of the radiation flux for iterative cycle $it_i$, condition $q_{r,i,j,it} \equiv q_{r,i-1,j}$ is maintained, while $q_{r,i,j}$ is defined at the end of the iterative cycle. For the definition of parameters $N$ and $J$, the same method was applied. It was based on the fact that, when evaluating more members in the infinite integral line and dividing the universal unit droplet radius in smaller steps $\Delta\eta$ according to scheme (62), thermal parameters defined by expressions (14–15) will be calculated more precisely.

The phase transformations of a sprayed liquid can be modeled according to the four-step numerical experiment methodology which ensures adequate treatment of individual phase transformation regimes. Each step provides optimal parameters $N_{op}$, $J_{op}$, $M_{op}$ and $I_{op}$ of the numerical scheme graduation. The optimized numerical scheme ensures a high balance condition of the calculated heat fluxes on the droplet's surface and allows saving the computing time.

### 3.2.1 Parameter *N* selection

For the definition of parameter $N$ selection in the numerical scheme which defines the optimal number of members in the infinite sum, the phase transformations cycle of pure liquid droplets in the heat transfer '$k$' and '$k$+$r$' cases was modeled. Unsteady phase transformations of a water droplet with the initial diameter of 300 μm and temperature $T_0 = 290\ K$ dispersed in humid ($\bar{p}_{v,\infty} = 0.25$) and dry air (with pressure parameters 0.1 MPa and temperature 1000 °K) were modeled. A black body

source was foreseen. The values of parameters $M$ and $I$ were maintained constant ($M$=101, $I$=41, when $Fo_{nf,"k"}$≡0.7), while the values of parameters $N$ and $J$ were varied in two ways. In the first case, parameter $J = 61$ was selected independently, while N was consistently increased and defined by the optimal value of $N_{op}$=121. In the second case, parameter N was defined as $N$=121, while $J$ was consistently changed and defined as $J_{op}$=41.

For the definition of optimal number $N_{op}$ of the assessable members in the infinite sum, an in-depth analysis of the droplet heat and mass transfer thermal parameters $P_T(Fo, N)$ function was accomplished. It was validated that $N_{op}$ value is related with the allowed error of the numerical experiment. The droplet unsteady temperature field function $T(\eta, Fo)$ graph was used and formed for different $N$ values. Therefore, for a comparative analysis of functions $T(\eta, Fo, N)$, such basic functions were considered as $T(\eta, Fo, N \equiv 151)$. They were changed in terms of time and depended on the droplet heating case (Fig. 3.1). For our further analysis, time moments $\overline{Fo}_{i=9} = 0.2$ and $\overline{Fo}_{i=41} = 1$ were selected.

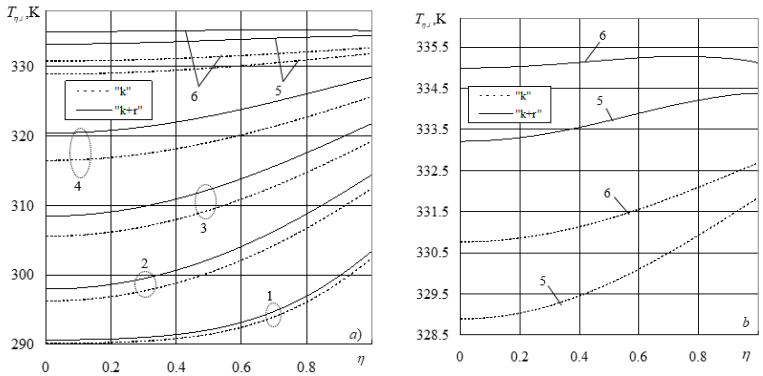


Fig. 3.1. The impact of droplet warming case on its thermal state in transitional evaporation regime *a*) and at the end of it *b*). $T_d = 1000$ K, $T_0$=290 K, $\overline{p}_{g,\infty} = 0.25$. $\overline{Fo}_i$: (1) 0.075, (2) 0.2, (3) 0.325, (4) 0.5, (5) 0.875, (6) 1

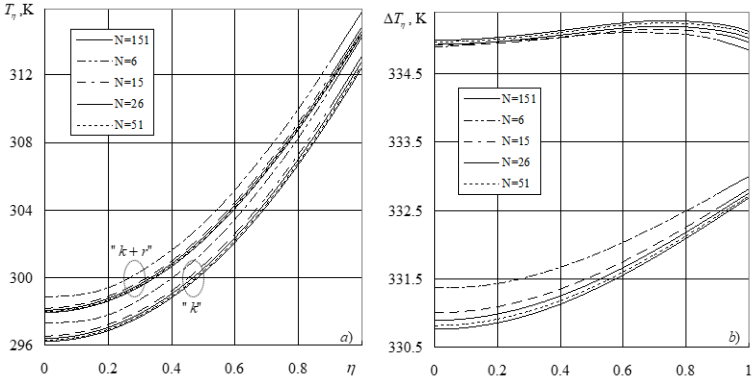


Fig. 3.2. The impact of selected number $N$ on the calculated temperature, when $\overline{Fo} = 0.2$ (a) and $\overline{Fo} \equiv 1$ (b). $\Delta T_\eta = T(\eta, Fo, N = 151) - T(\eta, Fo, N)$. $\overline{p}_{g,\infty} = 0.25$

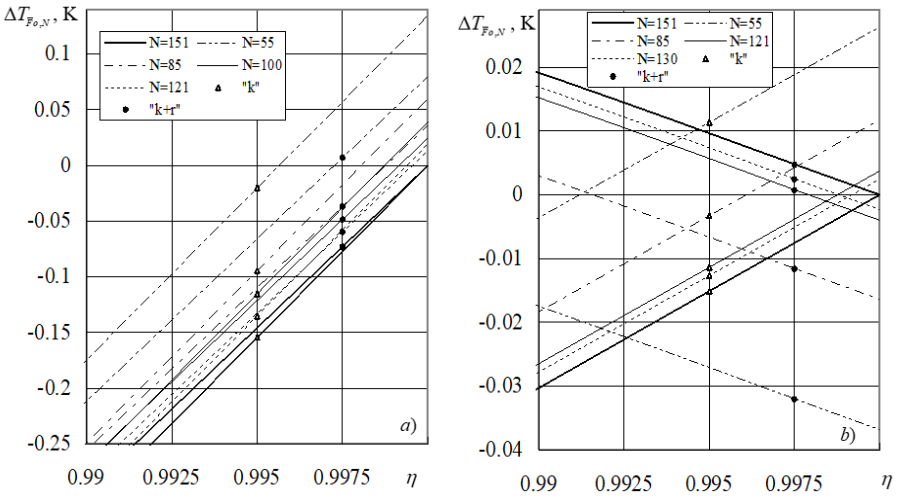


Fig. 3.3. The deviation of function $T(\eta, \bar{F}o, N)$ versus $T(\eta, \bar{F}o, N=151)$ in the surface layers of the droplet. Heating time: (*a*) $\bar{F}o=0.2$, (*b*) $\bar{F}o=1$. $\Delta T_\eta \equiv (\eta, N) - T(\eta, N=151)$

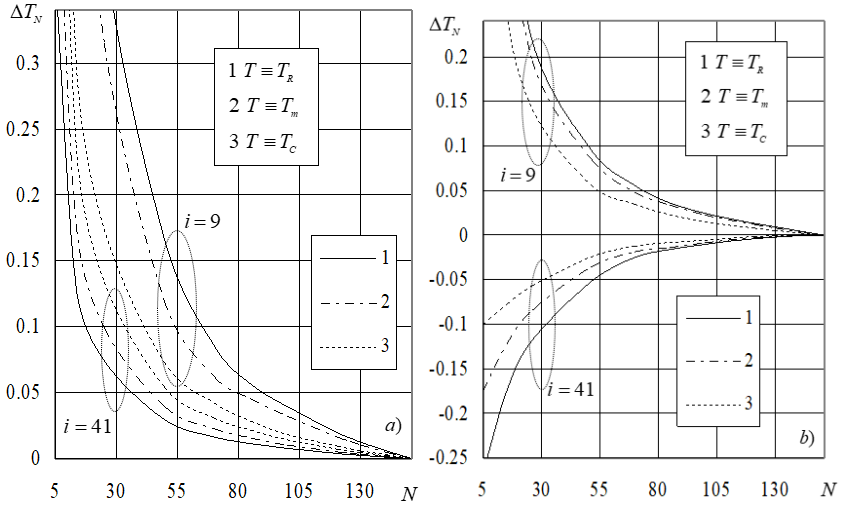


Fig. 3.4. The influence of selected N value for the calculated droplet characteristic temperatures: *a*) "$k$" case of conductive heating, b) case of complex heating "$k+r$". $T_d = 1000$ K, $T_0$=290 K, $\bar{p}_{g,\infty} = 0.25$

The first time moment $\bar{F}o_{i=9} = 0.2$ represents the initial intensive droplet heating stage when the surface layers of the droplet intensively warm up (Fig. 3.2 a). The absorbed radiation flux inside the droplet causes only quantitative thermal stage changes (Fig. 3.3 a), while the nature of the temperature field qualitatively does not change: $T_{\min} \equiv T_C$, o $T_{\max} \equiv T_R$. Therefore, in the initial heating case, the temperature field gradient remains positive inside the droplet. The second time moment $\bar{F}o_{i=41} \equiv 1$

represents the final stage of the modeled phase transformation regimes (Fig. 3.3 b). In the final stage of the transit evaporation regime, the droplet's thermal state depends on the method of droplet's heating.

In conduction heating ('k' heat transfer case), the droplet's non-isothermality consistently decreases, while the temperature field gradient maintains a positive value. In the case of complex heating ('k+r' heat transfer), the absorbed radiation flux inside the droplet qualitatively changes the droplet's thermal state during the final transit evaporation stage. Therefore, a negative temperature field gradient forms within the droplet (Fig. 3.3). This creates preconditions for the absorbed radiation flux participation in the liquid evaporation process [74].

When investigating the influence of the number of assessable members in the infinite sum for functions $T_{i,"k"}(\eta)$ and $T_{i,"k+r"}(\eta)$, the number of members $N$ was consistently increased from 5 to 151. Selected number $N$ has a significant impact on the calculated thermal state of a droplet in all the cycle of modeled phase transformation regimes. For higher selected N values, the calculated temperature field graph $T(\eta, \bar{F}o, N)$ approachesfunction $T(\eta, \bar{F}o, N=151)$ graph (Fig. 3.4). A deviation of functions $T(\eta, \bar{F}o, N)$ versus $T(\eta, \bar{F}o, N=151)$ graph is evaluated by temperature difference $\Delta T_{\bar{F}o,N}(\eta) = T(\eta, \bar{F}o, N) - T(\eta, \bar{F}o, N=151)$. This difference depends on the droplet heating duration and the type and changes ongoing individually inside the droplet (Fig. 3.4).

In the primary heating stage, a lower number of assessable members $N$ of the infinite sum determines a higher calculated temperature of the droplet for both modelled '$k$' and $"k+r"$ cases (Fig. 3.4 a). In the final '$k$' heating stage, a lower number of assessable members determines a higher calculated droplet temperature, however, in the case of $"k+r"$ heat transfer, a lower calculated droplet temperature is observed (Fig. 3.4 b). Analysis of graphs of functions $\Delta T^{"k"}_{\bar{F}o,N}(\eta)$ and $\Delta T^{"k+r"}_{\bar{F}o,N}(\eta)$ shows that the choice of $N_{op}$ can be associated with the strict requirements imposed on the 'droplet' problem.

In the developed 'droplet' problem, the essential role is played by droplet surface temperature $T_R$ because it determines the phase transformation regimes, and, in the surface layers of a droplet, the biggest part of the droplet's mass is accumulated. When looking for optimal $N_{op}$, it is reasonable to take into account the variation of the thermal parameters in the droplet's surface layers. This is illustrated by graph (Fig. 3.4). When looking for optimal $N_{op}$, it is worth paying attention to the influence of other characteristic temperatures as well (Fig. 3.5).

For the initial evaluation of the droplet phase transformation cycle stage, modeling results of N<55 were analyzed. Case $N_{op}$ = 51 was recognized as acceptable because it ensured less than 0.15 °K calculated temperatures $T_{R,N}$, $T_{C,N}$, and $T_{m,N}$, deviation from relevant temperatures $T_{R,N=151}$, $T_{C,N=151}$ and $T_{m,N=151}$ in the initial evaporation regime stage and less than $|\pm 0.05|$ °K deviation in the final stage of the transit evaporation regime.

A range of 55 < N < 105 values was selected for the primary evaluation of the droplet phase transformation regimes cycle. Case $N_{op}$=101 was assessed as optimal because it ensures less than 0.04 °K temperature deviation from $T_{R,i,N=151}$ temperature in the initial evaporation stage and less than $|\pm 0.02|$ °K deviation in the final transit evaporation stage (Fig. 3.5).

Half a percent reliability is already acceptable in scientific analysis. When tenths of percent reliability of (59) condition are requested, variations of the droplet surface temperature less than $10^{-2}$ °K must be taken into account (Fig. 3.5). Therefore, value $N_{op}$=121 is required (Fig. 3.5), which ensures at the same time a high accuracy of the droplet unsteady temperature field gradient calculation in the phase transformation regimes cycle (Fig. 3.6). This gradient defines the heat transfer component of heat flux in the droplet. According to peculiarities of $gradT_\eta$, it is possible to define the time change moment of the transit evaporation to the equilibrium evaporation regime: in the case of 'k' heat transfer case $gradT_{r=R,"k"}(Fo \to Fo_e) \to 0$, while in the complex heating case it must ensure derivation of the absorbed radiation flux to the droplet's surface by conduction $gradT_{r=R,"k+r"}(Fo \to Fo_e)\lambda_l \to q_r(Fo \to Fo_e)$.

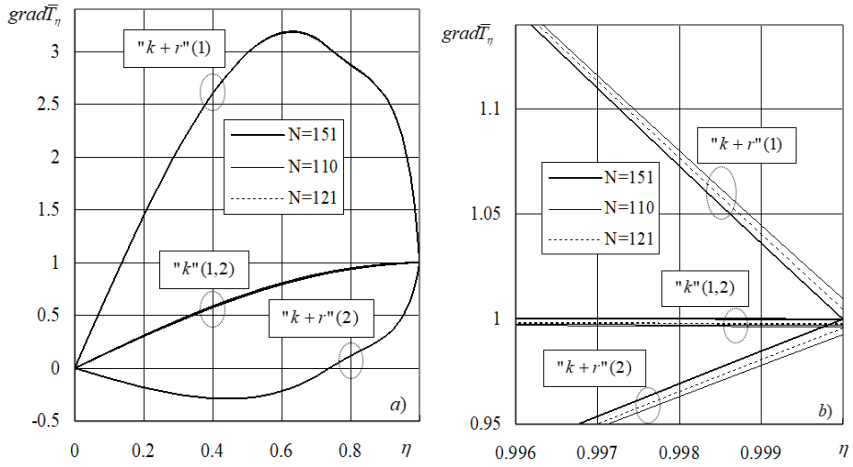


Fig. 3.5. The impact of selected $N$ on temperature local gradient a) inside a droplet and b) in the surface layers of a droplet. Warming time $\overline{Fo}$: (1) 0.2, (2) 1. $\overline{gradT}_\eta \equiv gradT(\eta, N)/gradT(\eta = 1, N = 151)$. $gradT_{"k"}(\eta = 1, N = 151)$, K/m: (1) 412124.1, (2) 41457.2; $gradT_{"k+r"}(\eta = 1, N = 151)$, K/m: (1) 386942.2, (2) -28314.7. $\overline{p}_{g,\infty} = 0.25$

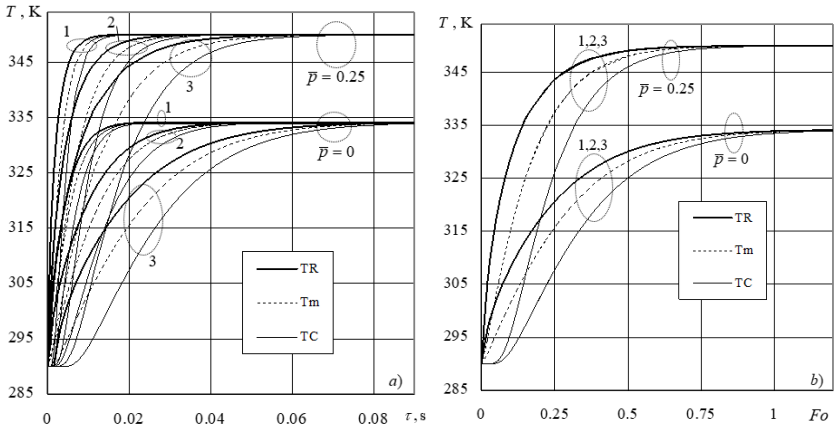


Fig. 3.6. Influence of air humidity on droplet heating in a) real time and b) Fourier time scale. The case of conductive heating. $T_g$=1000 K, $T_0$=290 K, $\bar{p}_{g,\infty} = 0.25$, $N$=121, $J$=81, I=61, $R_0 \cdot 10^6$ m: (1) 50, (2) 70, (3) 100

Among the many parameters that influence the droplet heat and mass transfer, the exclusive role belongs to the droplet-surrounding temperature $T_g$ and vapor concentration $\bar{p}_{v,\infty}$. Temperature difference $T_g$ - $T_R$ is an important characteristic of the environment impact on a droplet which determines the rate of the droplet's heating and evaporation intensity. When the partial vapor pressure in the droplet surrounding gas is $p_{v,\infty} > 0$, the condensation phase transformation regime is taking place on the droplet's surface, and the droplet warms up to a higher temperature in the transit evaporation regime compared to $p_{v,\infty} = 0$ (Fig. 3.6).

In the thermal technologies, droplet flows of different dispersivity are encountered. In the general case, in these flows, the droplet's function $T(r,\tau)$ is determined by numerical experiments, while taking into account their size in the entire diameter spectrum. In the 'k' heat transfer case, the experimental size can be reduced to freely chosen one-diameter droplet phase transformations cycle modeling. In order to achieve that, real time and droplet dimension function $T_{,,k"}(r,\tau)$ must be transformed into a universal time and universal droplet dimension radial coordinates function $T_{,,k"}(\eta,\tau)$. Functions $T_{R,"k"}(Fo)$, $T_{C,"k"}(Fo)$ and $T_{m,"k"}(Fo)$ are insensitive to the droplet dispersity when parameters $T_g$, $p_{v,\infty}$ and $T_{l,0}$ are defined.

By using dimensionless function $grad\bar{T}_R(Fo) = gradT_R(Fo)/gradT_{R,0}$, the temperature field gradient functions insensitive to the droplet diameter can be created (Fig. 3.7 b). Here, it is necessary to discuss the conception of the primary gradient $gradT_{R,0}$. In case of the strict assessment, the gradient of the isothermal initial state within the droplet is zero. In this case, the initial gradient $gradT_{R,0} \equiv \left(q^+_{\Sigma,0} + q^+_{co}\right)/\lambda_{l,0}$ is understood as the parameter of the droplet's thermal state defined by energy flows

which are calculated in the initial interaction moment of the droplet and its surroundings.

When parameters $T_g$, $\overline{p}_{v,\infty}$ and $T_{l,0}$ are defined, functions that are independent from the droplet dispersity $\overline{P}_{"k"}(Fo) \equiv P_{"k"}(Fo)/P_0$ can be formed according to the heat and mass transfer modeling results of a freely chosen droplet diameter. These functions are suitable for evaluating the influence of droplets and their surrounding interaction for the droplet phase transformations cycle in more complex heating cases than the 'k' heat transfer case.

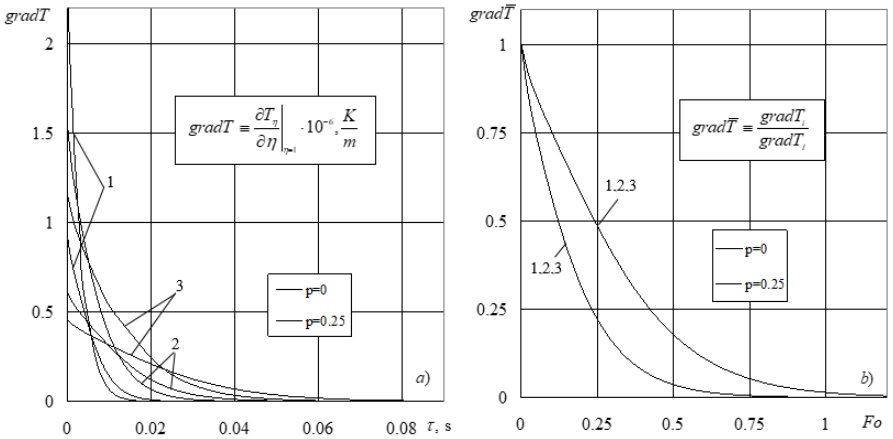


Fig. 3.7**.** The impact of air humidity on the unsteady temperature field gradient inside droplet: (a) in real time, (b) in Fourier number time scale. '*k*' heating case. $T_g$ = 1000 K, $T_0$ = 290 K, $\overline{p}_{g,\infty}$ = 0.25 , N = 121, J = 81, I = 61, $R_0 10^6$ m: (1) 50, (2) 70, (3) 100

The optimal number of a finite number of members in the infinite integral equations series for the droplet temperature field and its gradient was defined by a numerical experiment. The primary, engineering and strict scientific cases of the droplet problem solution cases were provided: $N_{op}$ 51, 101 and 121, respectively. For this reason, the water droplets transit phase transformation regime in air for heating cases '*k*' and '*k*+*r*' was modeled. When optimal number $N_{op}$ is provided, then the further droplet problem numerical scheme optimization can be performed.

### 3.2.2 Parameter *J* selection

The numerical iterative scheme functionality and the reliability of results of the droplet phase transformations numerical modeling depends on the appropriate selection of parameter *J*. Providing that the radiation factor is essential for the heat transfer inside a droplet, the optimal grading of the radial coordinate is expressed by the complex 'k+r' heating case for droplet warming in the air. Sprayed 290 °K temperature water droplet with an initial diameter of 150 micrometers was modeled. Its phase transformation cycle was modeled in dry 1000 °K air. In comparable analysis, the numerical scheme grid of parameters *N*=121, *J*=61, *I*=81, M=81 was considered to be the basic value.

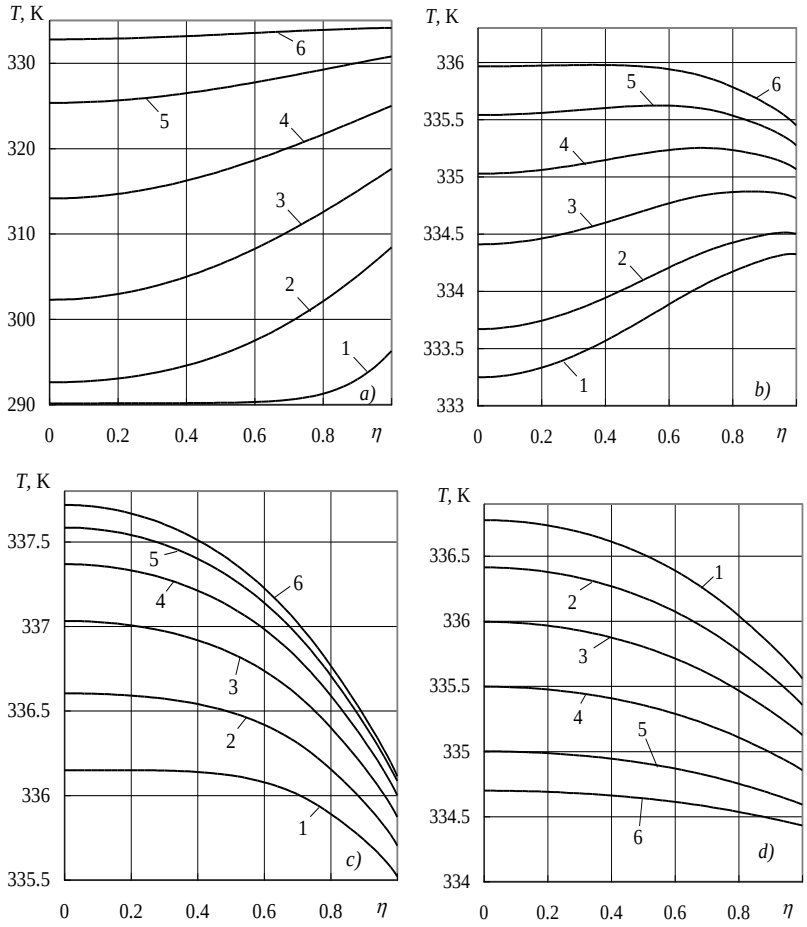


Fig. 3.8**.** The unsteady temperature field inside a water droplet in its (a) primary, (b), transit, (c) and final stage of transit evaporation, as well as in (d) equilibrium evaporation regime in case of complex droplet heating by radiation and conduction. (a) Fo = 0.0175; 0.0875; 0.175; 0.28; 0.42; 0.595, (b) Fo = 0.6125; 0.63; 0.665; 0.7; 0.735; 0.77, (c) Fo = 0.7875; 0.84; 0.91; 0.9975; 1.1025; 1.335, (d) Fo = 3.625; 4.25; 4.875; 5.5; 6; 6.25 (resp. curves 1–6); $T_g = 1000$ K; $p = 0.1$MPa; $\bar{p} = 0$; $T_0 = 290$ K; $T_{sr} \equiv T_g$; *N*=121; *J*=61; *I*=81; *M*=81

In the primary transit evaporation period, the surface layers of the droplet warm up the most intensively, therefore, the maximum value of function $T(\eta,Fo)$ is on the surface of the droplet (Fig. 3.8 *a*): $T(\eta=1,Fo) \equiv T_{max}(Fo) \equiv T_R(Fo)$. In this period, the radiation flux absorbed in the droplet accelerates the heating of its central layers, however, the temperature field gradient remains positive (Fig. 3.9 a). The interaction of complex transfer processes in the transit thermal state changing period is very intensive and causes unsteady temperature field deformations in the central droplet layers (Fig. 3.8 *b*). These deformations characterize the essential changes of the

temperature field local gradients (Fig. 3.9 *b*). During the transit, the droplet's thermal state change period, the maximum temperature from the droplet's surface consistently shifts to its center. Due to the observed peculiarities of the temperature local gradient in the droplet (Fig. 3.9 *b*), the thermal energy of the absorbed radiation flux is redistributed in two directions by thermal conduction: in the surface layers – towards the surface of the droplet (the temperature field gradient is negative in them), whereas in the central layers – towards the center of the droplet (the temperature field gradient is still positive). The final droplet's thermal state change period begins when the unsteady field maximum temperature reaches the center of the droplet. Regimes of transit (Fig. 3.8 c)) and equilibrium (Fig. 3.9 (d)) evaporation can be distinguished. At the beginning of the transit regime, the droplet is still heating up. Inside the droplet, a formulated negative temperature field gradient creates preconditions to output a part of the absorbed radiation thermal energy to the droplet's surface by conduction. This part of radiation flow is already involved in the liquid's evaporation process. The droplet heats up maximally at the end of the transit evaporation regime (Fig. 3.8 (c), 6th curve). From this moment on, the entire thermal energy provided for the droplet participates in the water evaporation process, therefore, $q_f^+ = q_c^+ + q_r$ because $q_k^- \equiv q_r$ . In the equilibrium evaporation regime, the droplet cools down (Fig. 3.12 (d)). The cooling of a droplet is caused by the reduced radiation absorption in the decreasing droplet. The negative gradient temperature field remains the same (Fig. 3.9 (d)).

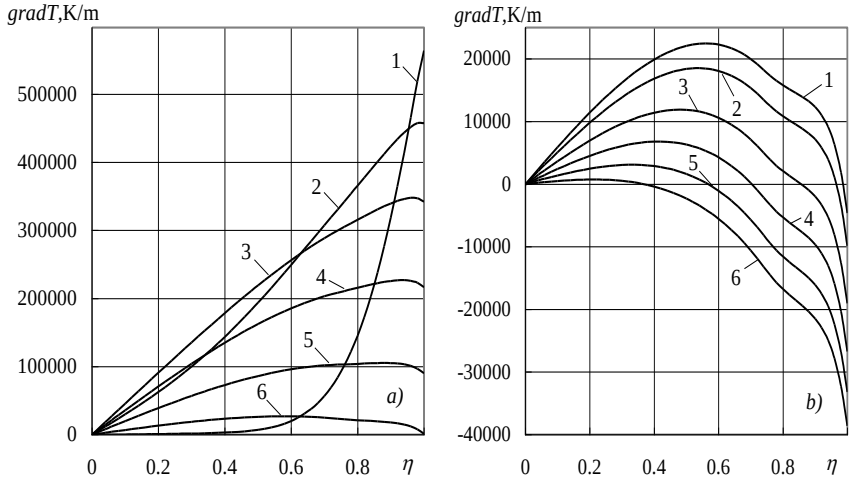

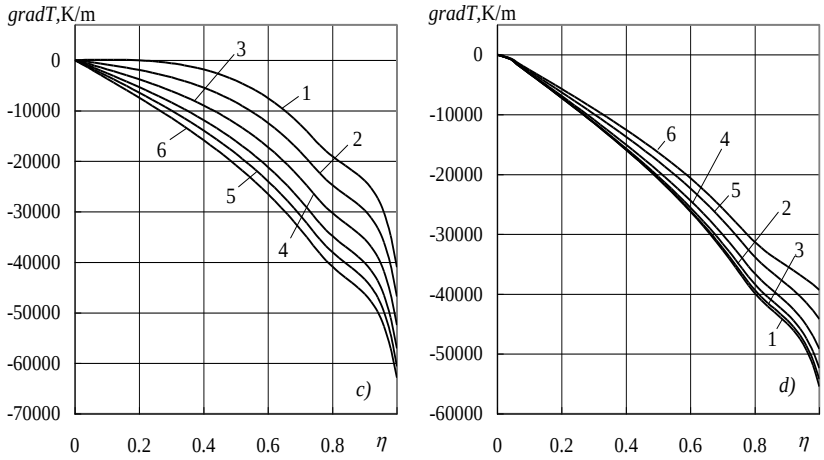


Fig. 3.9**.** The unsteady temperature field gradient inside a water droplet in its primary a), transit b), and final transit evaporation c), as well as in equilibrium evaporation d) regimes in case of complex droplet heating case '*k*+*r*' $gradT \equiv \partial T(\eta, Fo)/\partial\eta$, K/m. $T_g = 1000$ K; $p = 0.1$ MPa; $\bar{p} = 0$; $T_0 = 290$ K; $T_{sr} \equiv T_g$; *N*=121; *J*=61; *I*=81; *M*=81

When defining parameter $J_{op}$, the radial coordinate was gridded linearly: $\eta_j = (j-1)/(J-1)$, when $j = 1, J$. Parameter *J* was changed from 11 to 61. The influence of dividing number *J* on the calculated $P_T$ parameter functions is evaluated at the initial and transit droplet thermal state change periods, when the droplet heats up more intensively (Fig. 3.10). In these regimes, the droplet heats up more intensively when *Fo*≡0.28 (Fig. 3.10) and *Fo*≡0.84 (Fig. 3.11), respectively. It is clear that J > 41 is not worth considering. Therefore, the case of $J_{op}$ = 41 is accepted as the optimal droplet radial coordinate grid.

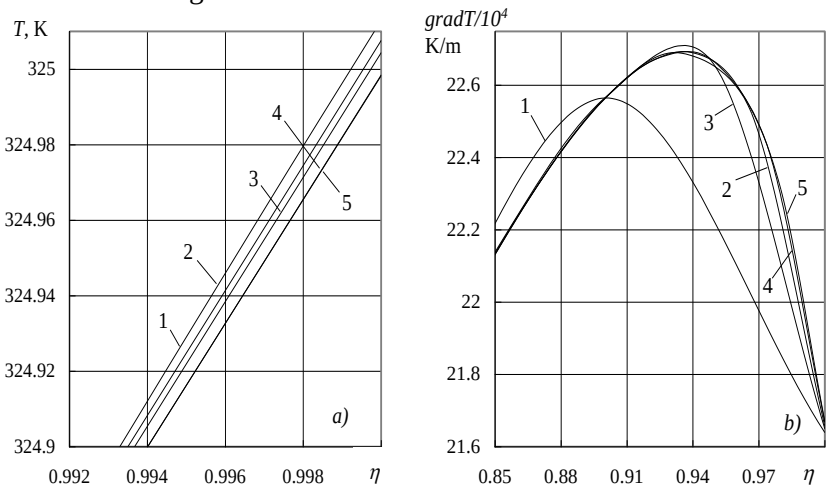


Fig. 3.10**.** The impact of a droplet's radial coordinate grading for the temperature field inside a droplet a) and for its gradient b) in the droplet's thermal state change initial period,

when *Fo*=0.28; $T_g = 1000$ K; $p = 0.1$MPa; $\bar{p} = 0$; $T_0 = 290$ K; $T_{sr} \equiv T_g$; *J*: (*1*) 11, (*2*) 21, (*3*) 31, (*4*) 41, (*5*) 61

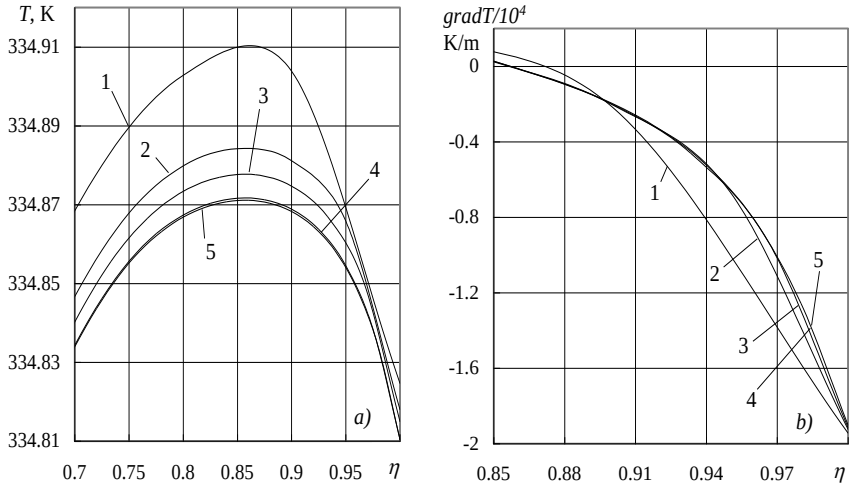


Fig. 3.11**.** Droplet's radial coordinate grading influence on the temperature field in the droplet a) and for its gradient b) during the droplet's thermal state change initial period, when *Fo*≡0.84; $T_g = 1000$ K; $p = 0.1$MPa; $\bar{p} = 0$; $T_0 = 290$ K; $T_{sr} \equiv T_g$

The optimal time coordinate grading should ensure equivalent attention to the transfer process interaction throughout the entire droplet phase transformation regime cycle. The duration of the phase transformation regimes may be distinctly different in both real and Fourier criteria time scales. Therefore, during the numerical experiment, this ought to be taken into account.

### 3.2.3. Parameter *I* selection

When dividing the time coordinate, peculiarities of a droplet phase transformation cycle must be evaluated, and the unequal duration of regimes must be taken into account. It is necessary to consider that, when the phase transformation regime changes to evaporation, the vapor flux on the droplet's surface gains the zero value. Therefore, at time moment $\tau_i \approx \tau_{co}$, the selected temperature $T_{J,i,it}$ in iterations may start to fluctuate regarding the dew point temperature. The final iterative cycle of the condensation regime may become indefinitely infinite $it_{i=\tau_{co}} \to \infty$. The durations of the individual phase transformations regimes may be different. Therefore, a definition problem of the uniform different phase transformation regimes arises. The previously discussed Fourier number is used. It ensures the continuous dimensionless time unit for each phase transformation regime in the entire cycle. The time grid of the numerical scheme is graded based on the modified Fourier number coordinate, changing *i* from *i* to *I*-1.

Modeling a continuous $\bar{\bar{F}}o \equiv 0 \div 3$ droplet phase transformation cycle is

problematic due to the indeterminations that are related with the condensing regime conversion to the transit evaporation regime at time moment $\overline{Fo}=1$ and initial moment selection of equilibrium evaporation $\overline{Fo}=2$. Therefore, at the beginning, only the condensation phase transformation regime is modeled when $I \equiv I_{0\div1}=21$. Its duration is defined by Fourier number $Fo_{co}$ and is selected by the consistent approximation method, thus setting the requirement $T_{dp}-T_{J,i,IT} \to \Delta T_{\min}>0$. When duration $Fo_{co}$ of the condensing phase transformation regime has already been defined, then the transit $\overline{Fo} \equiv 0\div1\div2$ droplet phase transformation regime is modeled. After defining the duration $Fo_{nf}=Fo_{co}+Fo_{e,u}$ of the droplet's transit phase transformation, droplet phase transformation cycle $\overline{Fo} \equiv 0\div1\div2\div3$ is modeled. For transit phase transformation regime $\overline{Fo} \equiv 0\div2$, steps $\Delta\overline{Fo}_{0\div1}$ and $\Delta\overline{Fo}_{0\div2}$ are maintained, while for equilibrium evaporation regime $\overline{Fo} \equiv 2\div3$, step $\Delta\overline{Fo}_{2\div3}$ is selected thus raising condition $R\left(\overline{Fo}_{i=I_f<225}=3\right)\cong 0$.

For each cycle regime, different number $I$ control time steps $I \equiv I_{0\div1}$, $I \equiv I_{1\div2}$, $I \equiv I_{2\div3}$ can be selected and defined by individual time steps $\Delta\overline{Fo}_{0\div1}$, $\Delta\overline{Fo}_{1\div2}$ and $\Delta\overline{Fo}_{2\div3}$, respectively. It should be noted that the end time of condensation and transit evaporation regimes defines their changes regarding the beginning regime; therefore, cycle control time moments are $I_f=I_{0\div1}+I_{1\div2}+I_{2\div3}-2$.

The provided numerical calculation methodology is influenced by the time of computing performed by the software. Especially the droplet's radius and the time coordinates variation steps exert influence on the numerical solution of the 'droplet' problem. The minimum time step is limited by the ongoing transfer processes and relaxation time, while the maximum time step must ensure the average droplet's mass warming up by 1 °K in order to maintain the high reliability of the droplet parameters calculation. The numerical scheme is adjusted by providing optimal parameters and cycle optimization.

The numerical experiment is carried out in three stages. In each of them, constant parameters of the numerical scheme is maintained: $N_{op}$ = 121, $J_{op}$ = 41, and $M$ = 81. The time grid grading parameter is chosen individually.

When $T_{dp}/T_0>1$, the first phase transformation cycle regime is condensation. It is modeled independently. The time grid in the numerical scheme is graded in the aspect of the condensation regime when control $Fo_i$ time moment number is provided for universal unit length $\Delta\overline{Fo}_i=1/\left(I_{co}-1\right)$. Then, the modeled phase transition regime $0\div Fo_{co,sp}$ and time step $Fo_i=\Delta Fo_i \cdot Fo_{co,sp}$ are defined by the guessed Fourier criterion $Fo_{co,sp}$. It is guessed that the condensation regime will end within time steps of 61. For this case, the modeled condensation phase transformation regime $0\div Fo_{co}$ is considered as supporting. The objective is that the temperature of the droplet's surface at the end of the the condensation regime would possibly better meet the droplet's dew point temperature but would not exceed it. It was defined by our numerical experiment that $Fo_{co}$ = 0:1583 in the '*k*' heat transfer case.

When grading the time coordinate grid, parameter *I* was changed from 11 to 61. The results of the numerical experiment show (Fig. 3.12) that the time grid for the condensation phase transition regime is optimally graded when the division number is chosen in the interval from 30 to 40. For a further numerical experiment, while choosing $I_{co,op}$=31, it is adjusted that $Fo_{co}$ = 0.161.

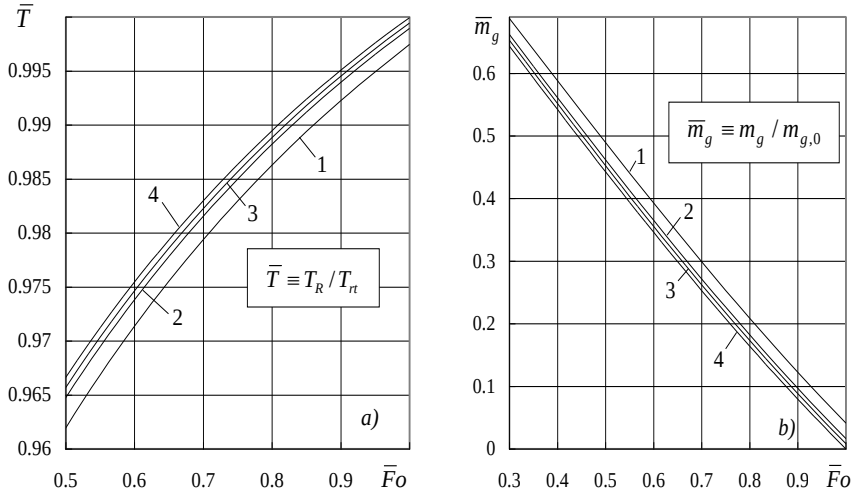


Fig. 3.12. Time coordinate grading in the numerical scheme impact for water droplet thermal a) and phase transformation b) parameters in the condensing phase transformation regime for '*k*' heat transfer case. $T_g = 1000$ K; $\bar{p} = 0.25$; $T_0 = 290$ K; $R_0$=75·10$^{-6}$ m; $Fo_{co} = 0.1583$; $I_{co}$: (*1*) 11, (*2*) 21, (*3*) 31, (*4*) 61

In the second stage of the numerical experiment, transit phase transformation regime $0 \div Fo_{co} \div Fo_{nf}$ is modeled. For transit regime, a step defined in the first stage $I_{co}$ = 31 are kept. Our simulation starts again from $Fo_{i=1}$=0. Parameter $I_{nf,op}$ for the transit evaporation regime is defined analogously to the condensation regime, however, the research is facilitated by the fact that at the final stage of transit evaporation, the instability problem of the iterative scheme does not arise because of the nature of phase transitions when changing from transit to equilibrium evaporation.

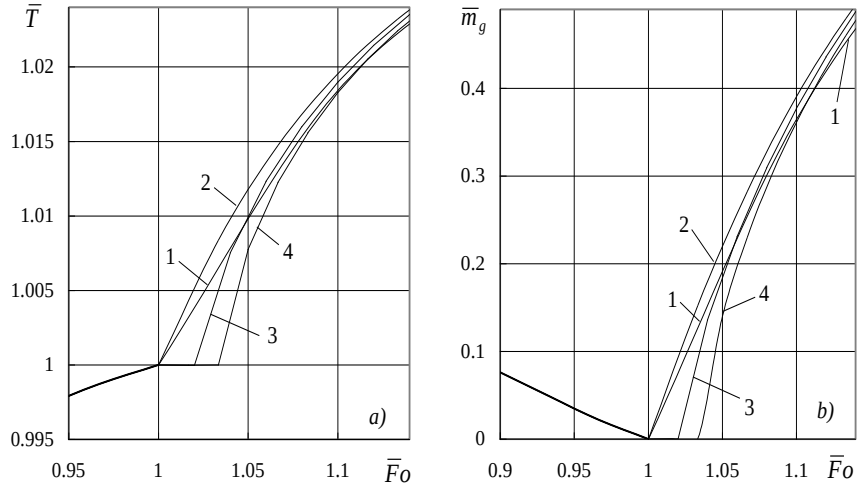


Fig. 3.13**.** Impact of time coordinate grading for water droplet surface temperature function $\overline{T} \equiv T_R / T_{dp}$ (a) and vapor density flow function $\overline{m}_v \equiv m_v / m_{v,0}$ (b) in transit evaporation in numerical scheme. $T_g$=1000 K; $\overline{p} = 0.25$; $T_0 = 290$ K; $R_0$=75·10$^{-6}$ m; $m_{v,0}$=0.1706 kg/(m$^2$s); $Fo_{co} = 0.161$; $I_{co} = 31$; $Fo_{nf}$=1.2; $T_{e,"k"}$=349.998 K; $I_{ee}$: (*1*) 10, (*2*) 30, (*3*) 50, (*4*) 60

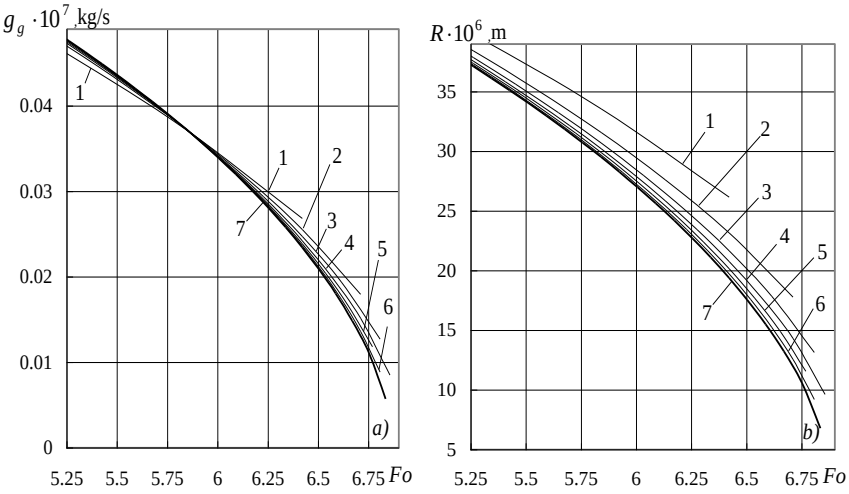


Fig. 3.14**.** Impact of parameter $I_{ee}$ for the calculated functions $R(Fo)$ and $g(Fo)$ in the droplet equilibrium evaporation regime in the '*k*' heat transfer case when $T_g$=1000 K; $\overline{p} = 0.25$; $T_0$=290 K; $R_0$=75·10$^{-6}$m; $Fo_{co}$=0.161; $I_{co}$=31; $Fo_{nf}$=1.2; $I_{ee}$=31; $Fo_{nf}$=5.8; $I_{ee}$: (*1*) 10, (*2*) 20, (*3*) 30, (*4*) 40, (*5*) 50, (*6*) 60, (*7*) 70

The transit phase transformation regime duration is defined approximately by $Fo_{nf} \cong 1.2$, and, after assessing the calculated condensation duration, $Fo_{ng} \cong 1.039$

. For the transit evaporation regime, $\Delta\overline{Fo}_i = 1/I_{ee}$. Parameter $I_{nf}$ was consistently increased from 10 to 60 by step 10.

In the modeled case, the optimal transit evaporation regime time grid is ensured by parameter $I_{ee}$ in the interval $30 \le I_{op} \le 40$. For our further numerical experiment, the division number of $I_{ee,op}$=30 was chosen. The full phase transformation regime cycle $0 \div Fo_{co} \div Fo_{nf} \div Fo_f$ is modeled in the third stage of the numerical experiment. Duration $Fo_f \approx 7$ of this cycle must be guessed at the beginning. Then, equilibrium evaporation duration is Fo≈5.8.

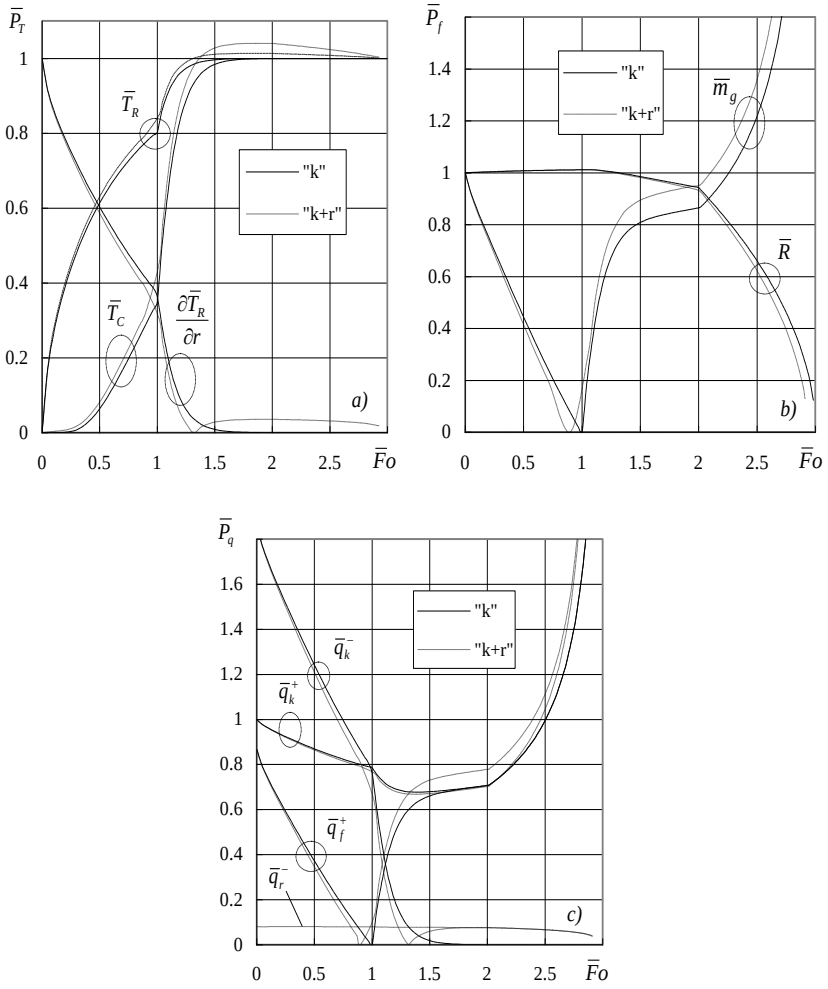


Fig. 3.15**.** Variation of water droplet: thermal (a), phase transformations (b) and energy (c) parameters in the cases of 'k' and 'k+r' heat transfer cases $T_{sr} \equiv T_g$; $T_g$=1000 K; $\overline{p} = 0.25$; $T_0$=290 K; $R_0$=75·10$^{-6}$m; $Fo_{co,"k"}$=0.161; $Fo_{co,"k+r"}$=0.145; $Fo_{pg,"k"}$=1.039; $Fo_{ee,"k"}$=5.7; $I_{co}$=31; $I_{nf}$=30; $I_{ee}$=60; $q^+_{k,0} = 483.43$ kW/m$^2$; $q^+_{k,0} = 419.83$ kW/m$^2$; $\overline{T} \equiv (T - T_0)/(T_{e,"k"} - T_0)$; $gradT_R(0) = 1527227$ K/m; $\partial\overline{T}/\partial r \equiv gradT_R(Fo)/gradT_R(Fo = 0)$; $\overline{P}_q \equiv P_q / q^+_k$

When modeling the droplet phase transformation cycle for a complex heating case by conduction and radiation '$k$+$r$', the numerical scheme grid '$k$' is maintained for defining the '$k$+$r$' heat transfer case. However, the duration of the condensation phase transformation regime that changed due to the effect of radiation must be clarified in order to avoid possible instability of the iterative scheme at the end of the first regime. Parameter $Fo_{co,"k"}$=1.45 was defined for the '$k+r$' heat transfer case with an additional numerical research $0 \div 1$ of the condensation regime. In the universal phase transformation cycle $0 \div 1 \div 2 \div 3$, while graphically interpreting droplet transfer parameter functions $P_{"k+r"}\left(\overline{Fo}\right)$, the norming parameters are kept in the case of '$k$' heat transfer case defined as $Fo_{co,"k"}$, $Fo_{nf,"k"}$ and $Fo_{ee,"k"}$ (Fig. 3.15; the dotted lines). Then, the deviation of function $P_{"k+r"}\left(\overline{Fo}\right)$ graphs from the graphs of functions $P_{"k"}\left(\overline{Fo}\right)$ illustrates the effect of more complicated heating cases than only the impact of conduction conditions on the duration of the droplet phase transformation regime and the carryover parameters within them. The droplet heat transfer case is significant to all of its transfer process parameters. This is confirmed by the tendency of the distinct droplet's thermal (Fig. 3.15 (a)), phase transformations (Fig. 3.15 (b)), and energetic (Fig. 3.15 (c)) parameter functions $\overline{P}_{"k"}\left(\overline{Fo}\right) \equiv P_{"k"}\left(\overline{Fo}\right) / P_0$ and $\overline{P}_{"k+r"}\left(\overline{Fo}\right) \equiv P_{"k+r"}\left(\overline{Fo}\right) / P_0$, although the normalizing parameters in them are identical.

The heat and phase transformations time duration coordinate of water droplets and the droplet's radial coordinate grading grid's influence on the calculated functions' graphs were evaluated. According to the summarized '$k$' and '$k$+$r$' cases of water droplet heating, the droplet's thermal parameter variation peculiarities and the optimal water droplet problem iterative scheme solutions grid formation methodology isprovided.

### 3.2. Control of numerical iterative scheme

Iterative cycles from $it \equiv 1$ to $IT$ are performed by the fastest descent method, and its control examples are presented (Fig. 3.16). An analogous requirement (59) control was executed for all the water droplets phase transformation numerical modeling cases. The droplet's surface temperature $T_{R,i,it=IT}$ attributed to the final iteration $IT$ must ensure that the calculated heat fluxes would fulfill the condition of expression (59) with a maximum allowed error of five hundredths of a percent.

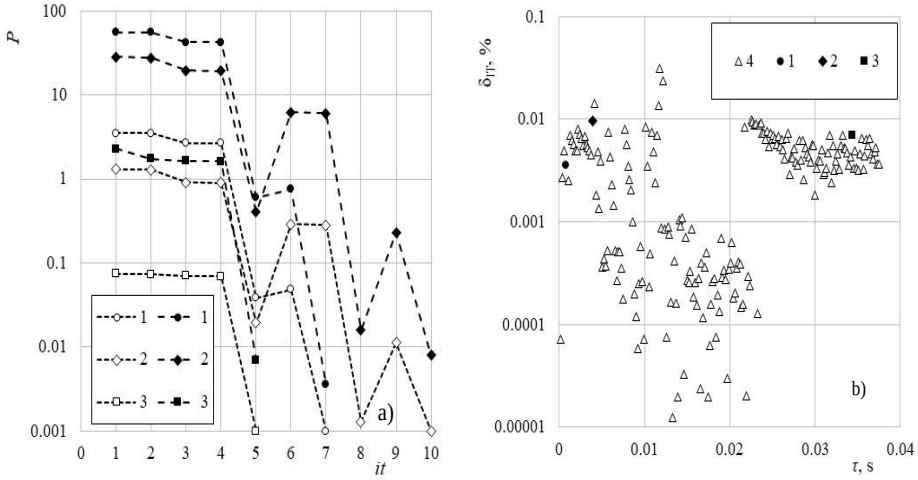


Fig. 3.16. Examples of iterative cycles $it \equiv 1 \div IT$ executed by the fastest descent method for temperature definition $T_{Ri}$ and the control of calculated heat $q_i$ flows balance condition on the droplet's surface (59) $T_g = 1133\,K$; $\bar{p}_v = 0.2$; $w_g = 15\,m/s$; $T_{l,0} = 306\,K$; $R_0 = 0.0005\,m$; $w_{l,0} = 65\,m/s$; $\tau, s$: (1) 0.00075, (2) 0.00394, (3) 0.0343; White points $P \equiv \left|T_{R,it} - T_{R,IT}\right| + 0.001, K$; black points $P \equiv \delta_{it}, \%$

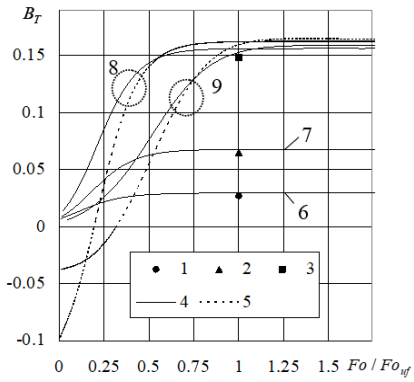


Fig. 3.17. The Spalding heat transfer parameter at the transit phase transformation regime and at the initial stage of equilibrium evaporation in "*c*" heat transfer case: (1–3) Yuen and Chen's experimental results [102]; (4–9) calculation results; $T_g$, K: (1, 6) 373, (2, 7) 473, (3, 8, 9) 673; $\bar{p}_{v,\infty}$: (4) 0, (5) 0.1; $\mathrm{Re}_0$: (6-8) 0, (9) 50; $R_0 = 100$

The peculiarities of the internal heat transfer of a droplet are defined by the regularities of Spalding heat transfer parameter function $B_T(Fo)$ (Fig. 3.17). In the condensation regime, the calculated parameter $B_T$ is negative, and its function in the expression defines the convective heating intensification due to the impact of vapor condensation. In the transitional evaporation regime, $q^-_{c,"c"} / q^+_{c,"c"} < 1$; thus, the calculated parameter $B_T$ is positive, and it shows that a part of the external convection warmth which heats the droplet does not participate in the water evaporation process. During the transitional evaporation, $q^-_c / q^+_c \to 1$ and $B_T\left(Fo = Fo_{nf}\right) = B_{T,"c"}$. In the transitional phase transformation regime, functions $B_T(Fo)$ of the Spalding heat transfer parameter depend on the humidity and temperature of the gas, as well as on the factors defining the heat transfer of the droplets. However, in the equilibrium evaporation regime, whose beginning is defined by the condition $Fo / Fo_{nf} = 1$, the temperature of the gas flow becomes the essential factor. Points $B_T(Fo)$ of graphs $B_T\left(\bar{F}o = 1\right) \equiv B_{T,"c"}$ calculated in the gas flow of different temperatures in the droplet heat transfer case 'c' correlate sufficiently well with the results of the experimental studies [103] (Fig. 3.17).

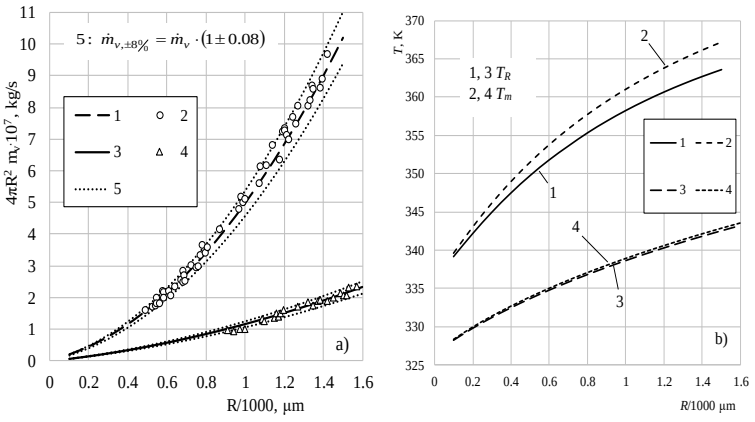

Fig. 3.18. Influence of the droplet's size and gas temperature on the vapor flow (a) and on the droplet's thermal state (b) of equilibrium-evaporated water droplets in the case of complex heating. $T_g$, K (1, 2) 1133, (3, 4) 678; $\overline{p}_v \approx 0$; $w_g = 0.01\,m/s$; $w_l = 0$ m/s ; the lines represent the modeling results; the points represent the experimental results [106]

The calculated vapor flow for water droplets of a different diameter which evaporate at equilibrium at 678 °K and 1133 °K temperature air in the complex heating case is compared with the experiment results of work [107] (Fig. 3.18 a). In order to maintain the boundary conditions of complex heating which were presented in work [106], the heat transfer model of a constant volume droplet was applied when the air flow around the droplet was at velocity 0.01 m/s, which ensures conditions $R(\tau) = R_0$ and $\mathrm{Re}(\tau) = \mathrm{Re}_0$. The existence of a radiation source having an air temperature was also foreseen. Then, in the transitional evaporation regime, a droplet warms to the calculated thermal state that ensures equilibrium evaporation (Fig. 3.18). Vapor flow is defined by the surface temperature that remains constant in equilibrium evaporation (Fig. 3.18 b). Analogous graphs were made for droplets of 2$R$ diameter, when $R \equiv 100 \div 1600\ \mu m$, and $\Delta R = 50\ \mu m$. According to these graphs, vapor flow $\dot{m}_{v,e}$ spread from equilibrium evaporating 2$R$ diameter droplet was determined for temperature cases 1133 °K and 678 °K. The calculated vapor flow $\dot{m}_{v,e}(R)$ graphs define all the experimental investigation results of work [107] for the relevant air temperatures with $\pm 8\%$ reliability, which, according to the experiment's authors, is defined within $\pm 5\%$ error limits.

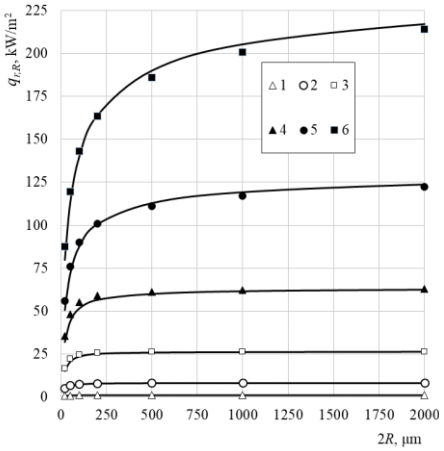


Fig. 3.19. Radiation absorption in semitransparent liquid. $T_l = 373\,K$ ;(a): $T_{sr}$, K : (1) 450, (2) 650, (3) 850, (4) 1050, (5) 1250, (6)1450 ; $R \cdot 10^6$, m : (1) 20, (2) 50, (3) 100, (4) 200, (5) 500, (6) 1000, (7) 2000 (8) 3000; Lines – numerical research; points – results of Harpole numerical investigation [111]

In this work, a comparison of radiation absorption in a semitransparent liquid with the provided numerical results of Harpole's work was also carried out [112]. In the complex "$c + r$" droplet heating case, the numerical research results correlate well with the results of work [112] (Fig. 3.19).

To prevent this, the numerical experiment is carried out in three stages. In each of them, constant parameters of the numerical scheme are kept *N, J, M*. Here, by considering size M, the dividing number of the radiation spectrum is evaluated. The time grid grading parameter *I* is chosen individually.

### 3.3. Analysis of droplet thermal state

Droplet thermal parameters are closely related with the unsteady temperature field function $T(r,\tau)$ which describes the temperature distribution inside a droplet. According to this function, the droplet's surface $T_R(\tau) \equiv T(r=R,\tau)$ and center $T_C(\tau) \equiv T(r=0,\tau)$ temperature functions important for the droplet heat transfer and phase transformations are defined. According to expression (33), the droplet mass mean temperature function $T_m(\tau)$ is described. In the real time scale, these temperature function curves are sensitive to droplet dispersity (Fig. 3.20 a.). These temperature functions in the Fourier time scale can be presented in one curve (Fig. 3.20 b).

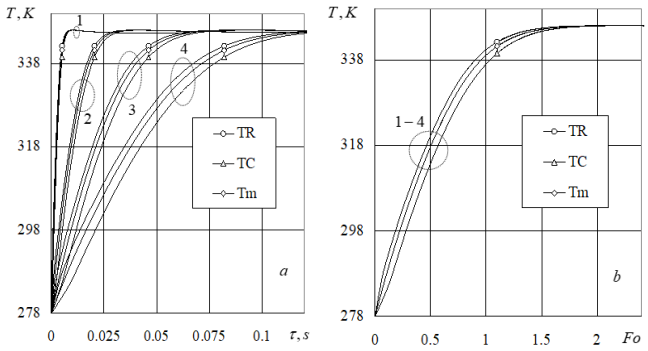


Fig. 3.20. Droplet thermal parameters $T_R(\tau)$, $T_C(\tau)$ and $T_m(\tau)$ function curves in real time (*a*) and Furrier number (*b*) timescales. $2R_0 \cdot 10^6$, m: (1) 50, (2) 100, (3) 150, (4) 200. $\mathrm{Re}_0 = 15$

The time function of the droplet's surface temperature $T_R(\tau)$ and the time function of the average mass temperature $T_m(\tau)$ are important when describing the variation in the thermal condition of the heated droplet. These temperatures are sensitive to the temperature of the dispersed water and the droplet heating process (Fig. 3.21). Figure 3.21 presents the change in the thermal state of water droplets for different droplet heating processes: curves 1 and 3 represent convective heating, curve 5 presents conductive heating, curves 2 and 4 depict complex convective and radiative heating, and curve 6 shows complex conductive and radiative heating.

The droplets with an initial temperature of 345 °K during the complex heating within a dry air flow of 1313 °K are described as cold water, but, in the case of conductive heating, they represent warm water. In the flow of humid air, at the surface of cold 306 °K initial temperature water droplets which are warming up, water vapor

condenses until the surfaces have warmed up to the dew point temperature at the time $\tau \equiv \tau_{co}$. The dew point temperature is 333.53 °K when $\bar{p}_v = 0.2$. At the moment of the change to the evaporation regime, the temperature of the droplet's central layers is lower than the dew point temperature. Droplets of hot water evaporate in the equilibrium regime and cool down, while the droplets of cold water warm up to the equilibrium evaporation thermal state expressed by temperature $T_{l,e}$ in the transitional evaporation regime. The start of the equilibrium evaporation of the cold water droplets being heated by convection is defined by their surface warming to the highest temperature $T_{l,e,c} \equiv T_R(\tau_e) = T_{R,max}$, and in the case of complex heating, they warm up to the highest temperature $T_{l,e,cr} \equiv T_m(\tau_e) = T_{m,max}$.

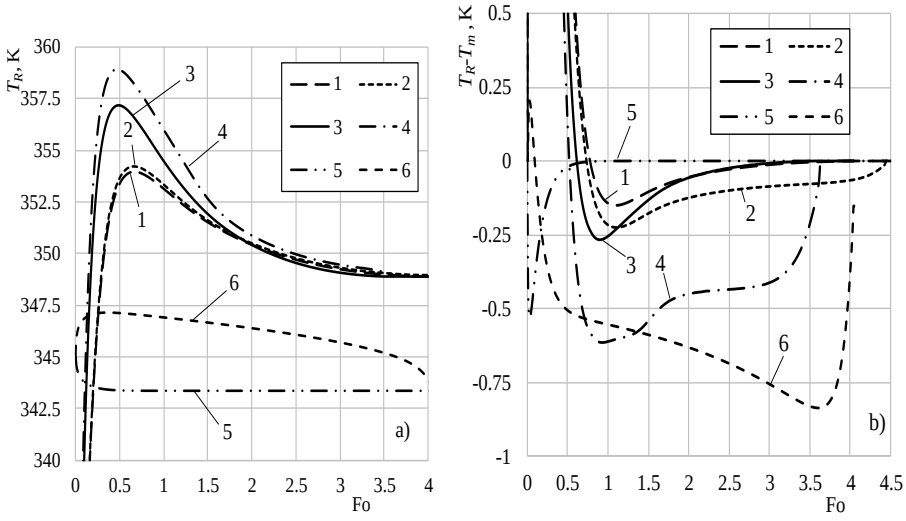


Fig. 3.21. The influence of water droplets dispersity and heating process on the variation of droplet surface temperature (a) and on the difference variation between surface temperature and droplet mass average temperature (b). $R_0 \times 10^6$, *m*: (1, 2) 50, (3, 4) 100, (5, 6) 250; $T_{l,0}$, K: (1–4) 306, (5, 6) 345; $w_{l,0}$, *m/s*: (1-4) 65, (5, 6) 0; $w_g$, m/s: (1–4) 15, (5, 6) 0; $T_g$, *K*: ; $\bar{p}_v$: (1–4) 0.2, (5, 6) 0.1; $\bar{T}_{sr}$: (1, 3, 5) 0, (2, 4, 6) 1; $Re_0$: (1, 2) 24.7, (3, 4) 98.79, (5, 6) 0; $a_0 / R_0^2$: (1, 2) 214.288 (3, 4) 13.393, (5, 6) 2.14288

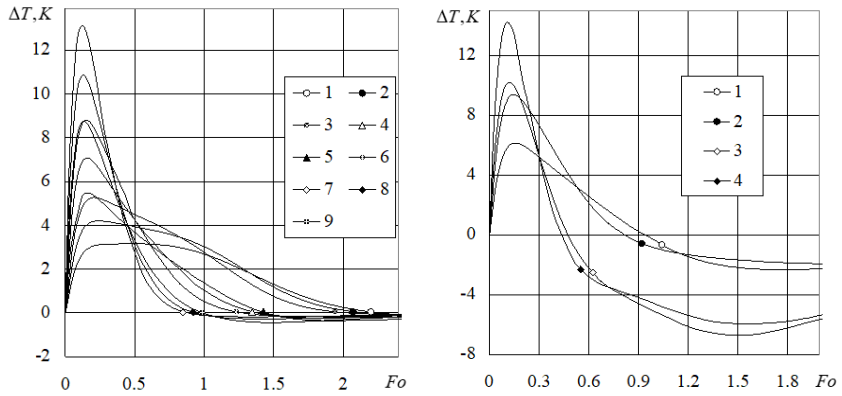


Fig. 3.22. a) Impact of gas humidity and temperature on the slipping droplet's non-isothermality $\Delta T = T_R - T_C$ at the transitional phase transformation regime in 'c' heating case $\mathrm{Re}_0 = 50$; $T_g$, K (1–3) 533, (4–6) 833, (7–9) 1133; $\overline{p}_{g,\infty}$: (1, 4, 7) 0, (2, 5, 8) 0.15, (3, 6, 9) 0.3. b) The impact of gas humidity and temperature on slipping droplet non-isothermality $\Delta T = T_R - T_C$ in transitional phase transformation regime and in the initial stage of equilibrium evaporation in "$c + r$" heat transfer case. $\mathrm{Re}_0 = 50$; $T_g$, K (1, 2) 833, (3, 4) 1133; $\overline{p}_{g,\infty}$: (1, 3) 0, (2, 4) 0.3

In warming and cooling droplets, non-isothermality rises (Fig. 3.22). During the initial stage of the condensation regime, temperature difference $\Delta T_{R,C}$ in the droplet grows and reaches the first peak independently from the droplet's heating pattern. Then, temperature difference $\Delta T_{R,C}$ in the water droplets that are warming in low temperature gases may grow by up to 10 °K (Fig. 3.22 a), while in high temperature gases, it may increase by up to 12 °K. After that, $\Delta T_{R,C}$ in the droplet rapidly decreases. Temperature difference $\Delta T_{R,C}$ is insignificant for equilibrium evaporating water droplets in low temperature gases. The second $\Delta T_{R,C}$ peak forms due to the radiation impact on the evaporating and heating droplets in high temperature gases. The second peak $\Delta T_{R,C}$ is weaker than the first peak, however, there may be up to 7 °K difference (Fig. 3.22 b).

The characteristics of the variation in the droplets' thermal state are clearly displayed in the dynamics of the temperature gradient in the droplets (Fig. 3.23). In the case of complex heating, in the transitional phase change regime, the temperature gradient in a droplet changes its direction when crossing the zero value, and then reaches the maximum value (Fig. 3.23 a, curves 2, 4 and 6). However, in the case of convective heating, the temperature gradient in a droplet reaches the zero value consistently in the transitional phase change regime and changes its direction only when the droplet starts to cool down in the equilibrium evaporation regime (Fig. 3.23 a, curves 1, 3). At the initial stage of equilibrium evaporation, the temperature gradient of a droplet that is heated by using conductivity consistently approaches the zero value, and then the zero value persists (Fig. 3.23 a, curve 5); thus, the droplet of 345

°K temperature cools down to the calculated temperature 343.36 °K, and remains in the same thermal state (Fig. 3.23, curve 5).

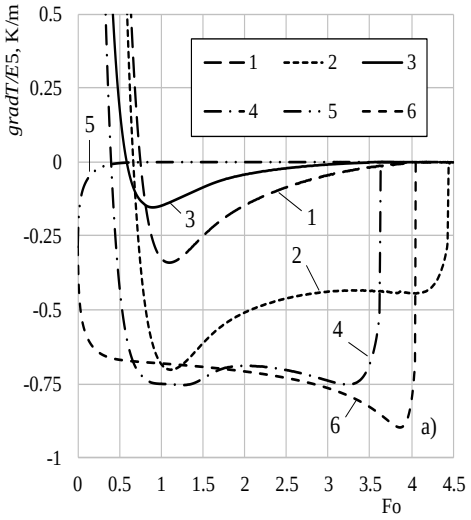


Fig. 3.23. The influence of the heating process on the dynamics in the temperature field gradient in droplets $R_0 \times E6$, *m*: (1, 2) 50, (3, 4) 100, (5, 6) 250; $T_{l,0}$, *K*: (1–4) 306, (5, 6) 345; $w_{l,0}$, *m/s*: (1–4) 65, (5, 6) 0; $w_g$, *m/s*: (1–4) 15, (5, 6) 0; $T_g$, *K*:; $\bar{p}_v$: (1–4) 0.2, (5, 6) 0.1; $\bar{T}_{sr}$: (1, 3, 5) 0, (2, 4, 6) 1; $\mathrm{Re}_0$: (1, 2) 24.7, (3, 4) 98.79, (5, 6) 0; $a_0 / R_0^2$: (1, 2) 214.288 (3, 4) 13.393, (5, 6) 2.14288

The water droplet phase transformation cycle in the Fourier time scale for the case of selected initial parameters $Re_0$, $T_0$, $T_g$, and $\bar{p}_{g,\infty}$ can be defined according to the droplet heat and mass transfer modeling results for freely chosen droplet dispersity. This creates preconditions to optimize the droplet research numerical experiment which is very important to define the optimal water spraying in a wide range of boundary conditions of heat transfer.

### 3.4 Analysis of droplet heat fluxes

The change of the droplet thermal energy state in the phase transformation cycle regimes is defined by the energy parameters functions $P_q(\tau)$ which describe the heat fluxes of the droplet surface. Unlike the case of thermal parameter functions $P_{T,"c"}(Fo)$, the energy parameters function $P_{q,"c"}(Fo)$ graph is not universal for differently sized droplets (Fig. 3.24 a). Therefore, energy parameter $P_q$ dimensionless functions $\bar{P}_{q,"c"}(Fo) = P_{q,"c"}(Fo) / P_{q,0}$ graphs are created for the universal representation of differently sized droplets (Fig. 3.24 b). It is important that the graphs of dimensionless functions $\bar{P}_{"c"}(Fo)$ are valid for all the droplets' heat and mass transfer parameters *P* including phase transformations $P_f$ and dynamics $P_D$ parameters. According to these

results, the universal droplet phase transformations cycle functions $\overline{P}_{r_c''}(Fo)$ are created for any of selected parameters *P*.

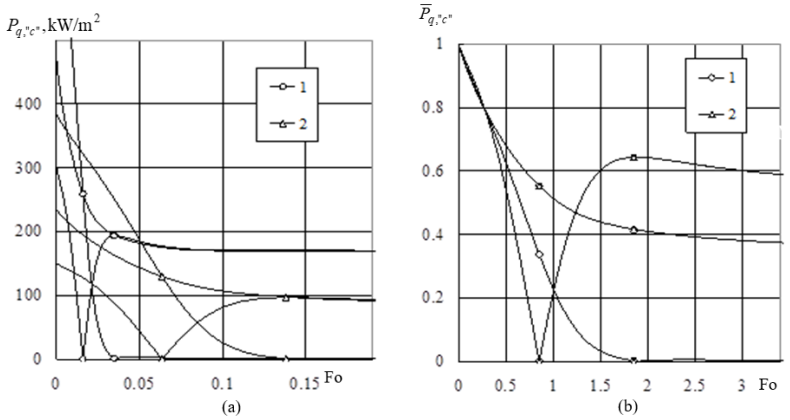


Fig. 3.24. Droplet energy $P_q$ parameters $P_q(Fo)$ and $\overline{P}_q(Fo)$function graphs (a) and (b), respectively. $P_q$: (3) $q_c^+$, (4) $q_f^+$, (5) $q_c^-$; $R_0 \cdot 10^6$, m: (1) 50, (2) 100 ; $\mathrm{Re}_0 = 30$, $\overline{p}_{v,\infty} = 0.2$ ; $T_g = 573K$

In the condensation phase, the transformation regime droplet convective heating intensity exceeds the analogous solid particle heating case when the phase transformation does not get exposed on its surface. In the transitional evaporation regime, a droplet's heating intensity is weaker than that of a solid particle, while during the regime change moment, the two intensities match (black points) (Fig. 3.25 a). The droplet slipping dynamics exert influence on the Reynolds number's variation which defines the intensity of the external convective heating (Fig. 3.25 b). A droplet slipping quickly decreases in the transitional phase change regime due to the resistance forces, whereas radiation has no significant influence on this process.

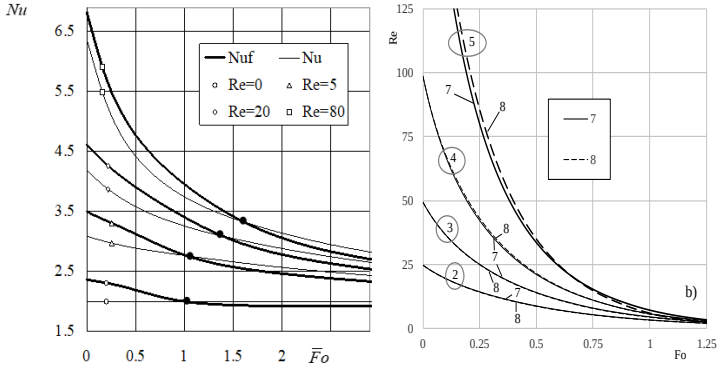


Fig. 3.25. a) In a gas flow, a slipping droplet's impact on the convective heating intensity $T_0$=278 K, $T_g$=500 K, $2R_0$=150·10$^{-6}$ m, $\overline{p}_{v,\infty} = 0.3$, $Re_0$: (*1*) 0, (*2*) 5, (*3*) 20, (*4*) 80, $w_g$≡10 m/s. b) The variation of the Reynolds number (b). $T_g$=1133 K; $R_0 \times E6$, *m :* (1) 10, (2) 25, (3) 50,

(4) 100, (5) 250, (6) 500; $q_{r,R}, kW/m^2$: (1) 39.77, (2) 53.78, (3) 63.64, (4) 71.31, (5) 77.93, (6) 81.19; $w_g = 15\ m/s$; $\bar{p}_v = 0.2$; $w_l = 65\ m/s$; $T_l = 306$ K

Water circulation intensity is sensitive regarding the droplet slipping and dispersity. A droplet's growth in the condensation regime is a suitable factor for the circulation in it, while the weakening of a droplet's slipping is a factor that reduces the water circulation in a droplet. At the beginning of the condensing regime, intensification of the convectional heat transfer is observed (Fig. 3.26 a). This means that, for some time, a droplet's growth factor that is favorable for the droplet circulation is stronger than the slipping weakening factor which represses circulation. At the balancing point of both factors $k_c^-(Fo)$, an extreme point is observed in the function graphs (Fig. 3.26 a), after which, the water circulation gets consistently suffocated in the droplet. Water circulation is defined by the friction forces at the surface of slipping droplets. Its intensity is based on the Peclet number (Fig. 3.26 b) which describes the effective thermal conductivity parameter (Fig. 3.26 a) which is an expression of the dominance of convection within a droplet compared to thermal conductivity.

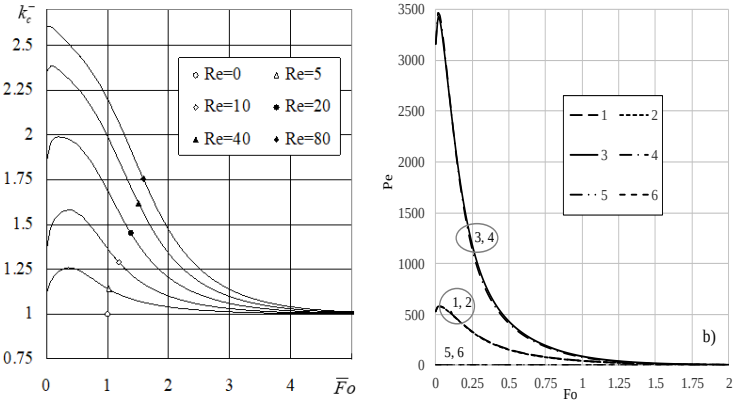


Fig. 3.26. a) Impact of a droplet slipping in air flow on the effective thermal conductivity parameter. $2R_0 \cdot 10^6$, m: (1) 50, (2) 100, (3) 150, (4) 200. $\mathrm{Re}_0 = 15$. b) Droplet slipping influence on the Peclet number ($T_g$=1133 K; $R_0 \times E6, m:$ (1) 10, (2) 25, (3) 50, (4) 100, (5) 250, (6) 500; $q_{r,R}, kW/m^2$: (1) 39.77, (2) 53.78, (3) 63.64, (4) 71.31, (5) 77.93, (6) 81.19; $w_g = 15\ m/s$; $\bar{p}_v = 0.2$; $w_l = 65\ m/s$; $T_l = 306\ K$

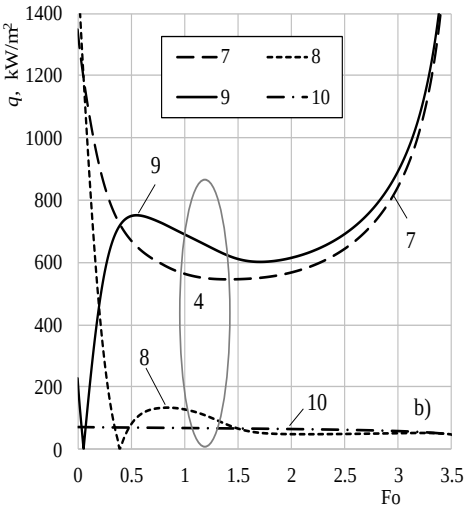


Fig. 3.27. Influence of the heating process on the variation of heat fluxes at a droplet's surface in the case of complex heating (b). Parameter $q$: (7) $q_c^+$, (8) $q_c^-$, (9) $q_f^+$, (10) $q_r$. $R_0 \times E6, m:$ (1, 2) 50, (3, 4) 100, (5, 6) 250; $T_{l,0}, K:$ (1–4) 306, (5, 6) 345; $w_{l,0}$, m/s : (1–4) 65, (5, 6) 0; $w_g$, m/s : (1–4) 15, (5, 6) 0; $T_g, K:$; $\bar{p}_v$ : (1–4) 0.2, (5, 6) 0.1; $\bar{T}_{sr}$ : (1, 3, 5) 0, (2, 4, 6) 1; $\mathrm{Re}_0$ : (1, 2) 24.7, (3, 4) 98.79, (5, 6) 0; $a_0 / R_0^2$ : (1, 2) 214.288 (3, 4) 13.393, (5, 6) 2.14288

Specific features of the variation in the energy state of cold water droplets in humid air are clearly displayed in Fig. 3.27 diagram for the heat flux variation at the surface of a droplet of 200 μm diameter. In the condensation regime, the initial energy impulse to the droplets is very strong, and it is defined by the sum of the calculated initial convective and condensation heat flux. In the process of the condensation regime, the condensation heat flux drops to zero. Hence, the convective heat flux to a droplet and the convective heat flux within the droplet become equal at moment $\tau_{co}$ of the phase change from the condensation to the evaporation regime, and the calculated heat flux in this case is shown in (Fig. 3.27, at the intersection of curves 7 and 8). Two characteristic periods can be distinguished when analyzing the specific features of convective heat flux $q_c^-$ variation in the transitional phase change regime. In the first period, $q_c^-$ consistently reaches the zero value, while, in the second period, it increases and equals the value $q_c^- \equiv q_{r,e}$ of the absorbed radiation flux in the droplet at moment $\tau_e$ (Fig. 3.28 b, the second intersection of curves 8 and 10). At the end of the first period, the temperature gradient in a droplet reaches the zero value (Fig. 3.22 a, curves 2 and 4), and it changes its direction. At the beginning of the equilibrium evaporation, the increase of $q_c^-$ is defined by the cooling droplet's enthalpy. Later, when the cooling of the droplet decreases asymptotically (Fig. 3.28, curve 4), $q_c^-$ starts to decrease as well, and the specific features of the radiation flux absorption in the droplet (Fig. 3.29 a), diminishing due to evaporation, become more relevant to its further dynamics $q_c^-(\mathrm{Fo} > \mathrm{Fo}_e)$

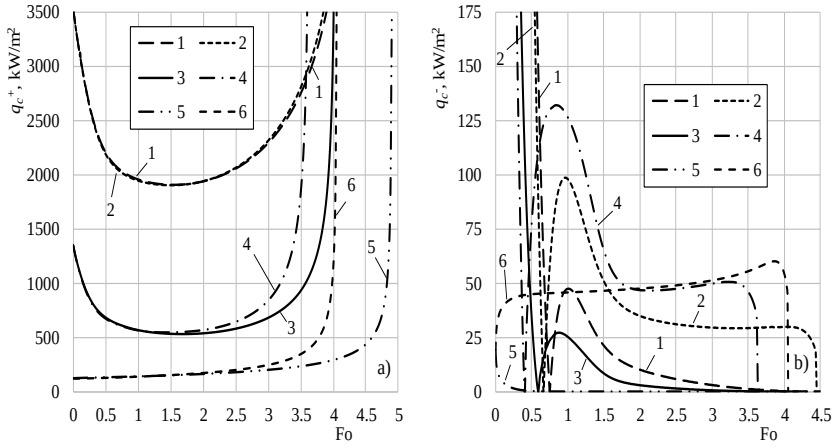


Fig. 3.28. Dynamics of the convective heat flux to the droplets (a) and within the droplets (b). $R_0 \times E6$, $m$: (1, 2) 50, (3, 4) 100, (5, 6) 250; $T_{l,0}$, $K$: (1–4) 306, (5, 6) 345; $w_{l,0}$, $m/s$: (1–4) 65, (5, 6) 0; $w_g$, $m/s$: (1–4) 15, (5, 6) 0; $T_g$, $K$:; $\bar{p}_v$: (1–4) 0.2, (5, 6) 0.1; $\overline{T}_{sr}$: (1, 3, 5) 0, (2, 4, 6) 1; $\mathrm{Re}_0$: (1, 2) 24.7, (3, 4) 98.79, (5, 6) 0; $a_0 / R_0^2$: (1, 2) 214.288 (3, 4) 13.393, (5, 6) 2.14288. $q_{c,0}^+, kW/m^2$: (1, 2) 3548.05, (3, 4) 1348.56, (5, 6) 121.06; $q_{f,0}^+, kW/m^2$: (1, 2) 908.44, (3, 4) 227.11, (5, 6) 19.2; $q_{c,0}^-, kW/m^2$: (1, 2) 4456.49, (3, 4) 1575.67, (5, 6) 140.26; $q_{r,0}, kW/m^2$: (1, 3, 5) 0, (2) 53.78, (4) 71.31, (6) 77.88

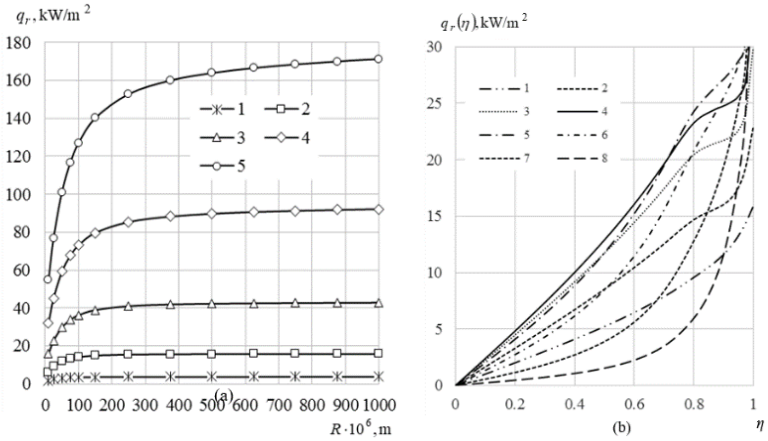


Fig. 3.29. In a semi-transparent water droplet, the absorbed radiation flux (a) and its distribution in the internal layers of the droplet (b). $T_l = 350$ K; (a): $T_{sr}$, K: (1) 573, (2) 773, (3) 973, (4) 1173, (5) 1373; (b): $R \cdot 10^6$, m: (1) 10, (2) 25, (3) 50, (4) 75, (5) 150, (6) 250, (7) 500 (8) 1000; $T_{sr} = 973$ K

In a semi-transparent water droplet, the absorbed radiation flux depends not only on the temperature of the radiating source but also on the size of a droplet (Fig. 3.29). A droplet's size defines the radiation absorption process. In the surface layers of larger droplets, the radiation absorption is intensive, and, quite suddenly, suffocating (Fig. 3.29, curves 6–8). The light refraction effects on the internal droplet surface are more significant for average-sized droplets, therefore, the radiation absorption in this case is prominently uneven (Fig. 3.29, curves 2–5). The radiation absorption in the smaller droplets is more equal again (Fig. 3.29, curve 1); however, in comparison with the case of the larger droplets, the radiation flux at the central droplet layers is relatively stronger. Therefore, for the case of combined heating, the phase transformation cycle for differently sized droplets must be simulated individually.

### 3.5 Analysis of droplet phase transformations

During the initial stage of the transitional phase change regime in an air flow, droplets of cold water of temperature 306 °K increase in size, while the warming water is expanding, and while water vapor is condensing on their surfaces (Fig. 3.30 b, curves 1–4). At the beginning of transitional evaporation, the water expansion effect is still stronger than the diminishing effect of the evaporating droplet. The dimensions of the droplet are the largest at the moment when these effects become equal. In dry air of a high temperature, droplets start diminishing immediately (Fig. 3.30, curves 5, 6).

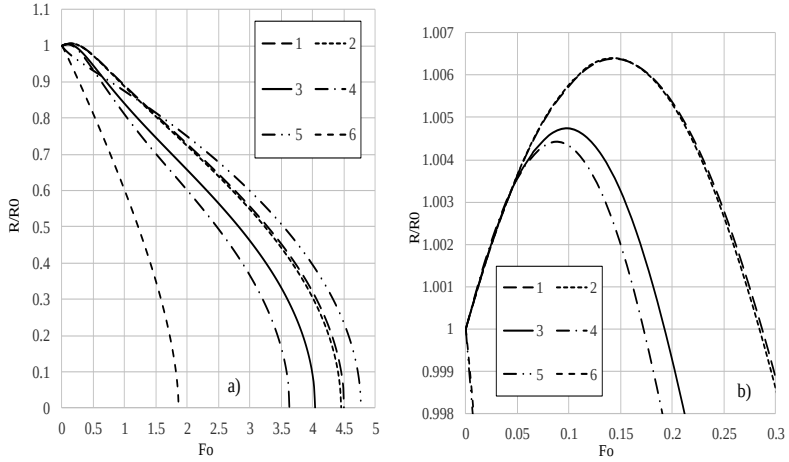


Fig. 3.30. Dynamics of the relative $R/R_0$ diameter of water droplets warming the phase change cycle (a) and in the process of transitional phase change (b). $R_{max}/R_0$: (1) 1.00636, (2) 1.00641, (3) 1.00474, (4) 1. 00443, (5, 6) 1. $R_0 \times 10^6$, $m$: (1, 2) 50, (3, 4) 100, (5, 6) 1500; $\overline{T}_{sr}$: (1, 3, 5) 0, (2, 4, 6) 1; $\mathrm{Re}_0$: (1, 2) 49.4, (3, 4) 246.98, (5, 6) 0; $T_{l,0}$, $K$: (1–4) 306, (5, 6) 358;

$w_{l,0}$, *m/s* : (1–4) 65, (5, 6) 0; $w_g$, m/s: (1-4) 15, (5, 6) 0; $T_g$=1133K; $\bar{p}_g$ : (1–6) 0.2, (7, 8) 0; $a_0 / R_0^2$ : (1, 2) 53.572, (3, 4) 2.14288, (5, 6) 0.059524

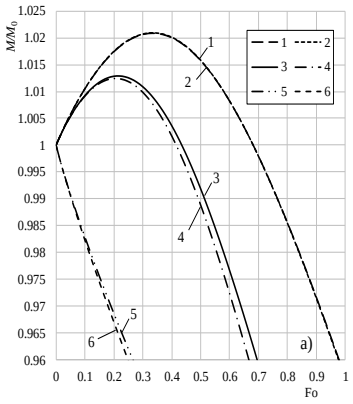


Fig. 3.31. Variation of the relative $M/M_0$ mass of water droplets warming up in 678 °K air flow in the transitional phase change regime (a) and the variation of vapor mass flux in the phase change cycle (b). $|m_{v,0}|$, kg/(m$^2$s) : (1, 2) 0.2253, (3. 4) 0.05633, (5, 6) 0.0371

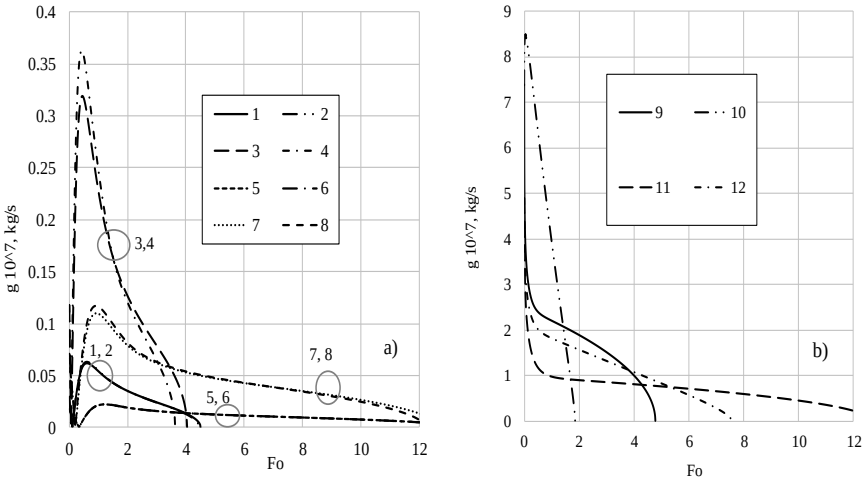


Fig. 3.32. Dependency of vapor flow rate at the surfaces of small and average size (a) and large (b) droplets on the heating process: (1, 3, 5, 7) convective heating, (2. 4, 6, 8) complex heating – convection and radiation, (9, 11) conductive heating, (10, 12) complex heating – conduction and radiation; $|\dot{m}_0| \times 10^7$, *kg/s :* (1, 2) 0.0294, (3, 4) 0.1178, (5, 6) 0.0177, (7, 8) 0.0708, (9, 10) 7.388, (11, 12) 4.896; $R_0$ *x E*6, *m :* (1, 2, 5, 6) 25, (3, 4, 7, 8) 100; (9, 10) 1500, (11, 12) 1600; $T_g$, *K* : (1–4, 9, 10) 1133, (5–8, 11, 12) 678; $T_{l,0}$, *K* : (1–8) 306, (9–12) 358; $\bar{p}_v$ : (1–8) 0.2, (9–12) 0; $w_{l,0}$, *m/s :* (1–8) 65, (9–12) 0; $w_g$, *m/s :* (1–8) 15, (9–12) 0

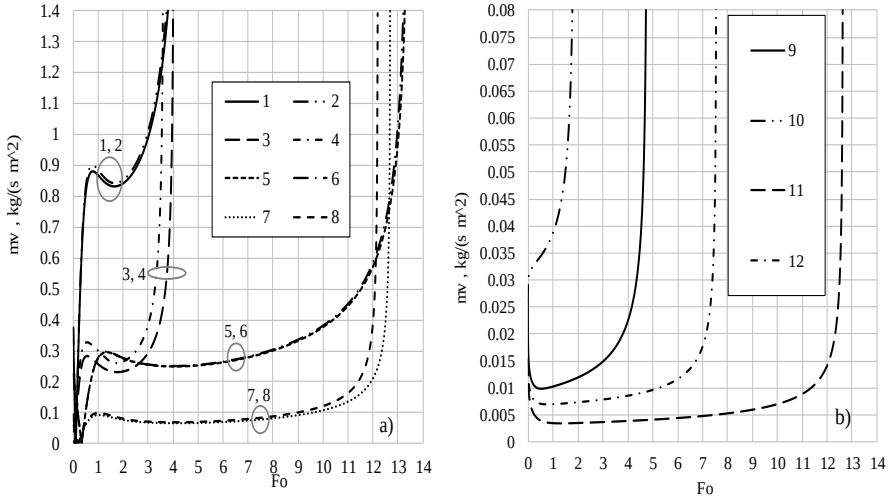


Fig. 3.33. Dependency of vapor flux at the surfaces of small and average size (a) and large (b) droplets on the heating process. $|m_{v,0}|$, $kg/(m^2 s)$: (1, 2) 0.3748, (3, 4) 0.0937, (5, 6) 0.2253, (7, 8) 0.0563, (9, 10) 0.02613, (11, 12) 0.01522. $R_0 \times 10^6$, $m$: (1, 2, 5, 6) 25, (3, 4, 7, 8) 100; (9, 10) 1500, (11, 12) 1600; $T_d$,K (1–4, 9, 10) 1133, (5–8, 11, 12) 678; $T_{l,0}$, K: (1–8) 306, (9–12) 358; $\overline{p}_g$ : (1–8) 0.2, (9–12) 0; $w_{l,0}$, m/s: (1–8) 65, (9–12) 0; $w_g$, m/s: (1–8) 15, (9–12) 0

The characteristics of droplet thermal and energy states as well as the phase change determined by the interaction of complex transfer processes define the parameter for water vapor flow rate $\dot{m}_v$, kg/s, at the droplet surface, which is important to the water dispersion technologies. The vapor flow rate at the droplet surfaceapproaches the zero value from the initial value $\dot{m}_{v,0}$ in the process of phase change when droplets evaporate (Fig. 3.31), and the vapor flux increases quickly at the final stage of evaporation (Fig. 3.32).

The initial vapor flux is defined by the temperature of the dispersed water, the droplet dispersity, and the air humidity. In the condensation regime, the vapor flux at the surface of cold water droplets decreases to zero, while, in the transitional regime, it increases to value $m_{v,e}$, which is also influenced by the droplet's heating process. At the beginning of equilibrium evaporation, $m_{v,e}$, kg/(s·m$^2$) is 0.8724, 0.8995, 0.2815, 0.3274, 0.2951, 0.2973, 0.09192 and 0.0985 for boundary conditions (1–8), respectively (Fig. 3.33 a). At the beginning of the equilibrium evaporation, the vapor flow rate $\dot{m}_e \cdot 10^7$, kg/s is 0.0615, 0.0614, 0.3171, 0.3455, 0.0221, 0.02212, 0.1097 and 0.1158, respectively (Fig. 3.33 b).

Warm water droplets instantly reach equilibrium evaporation, and, in their case, we get $\dot{m}_e \equiv \dot{m}_0$ (Fig. 3.33 a) and $m_{v,e} \equiv m_{v,0}$ (Fig. 3.33 b). During the initial stage of equilibrium evaporation, the increase in the vapor flow rate is defined by the enthalpy of the cooling droplets participating in the water evaporation process; however, it is also suppressed by the weakening intensity of the convective heating which is defined by the decrease in droplet slipping. The increase of the vapor flow rate is also directly defined by the decrease of the droplet's surface area. The result of these factors is the

extreme points formed in the diagrams of the vapor flux variation, and the rapid increase in the vapor flow rate at the final stage of droplet evaporation is defined by the decrease of the droplets' surface area.

## 4. Conclusions

On the basis of scientific literature analysis when providing physical interpretation of water droplet heat and mass transfer processes, in terms of matching their geometric, thermal and energy interpretation components, on the basis of energy state variation in phase transformations cycle analysis and extending Stefan's hydrodynamic flow influence assessment by Spalding transfer parameter based by similarity theory basis for droplet transitional processes, while adjusting the mathematical model and developing its numerical solution algorithm, while based on the optimal number of members of asset members in unsteady temperature field gradient describing in integral equation infinite series, after defining the optimal grid of radial and time coordinates in numerical scheme, when foreseeing the iterative cycle control and after basis of numerical research results reliability and after detail numerical research of the droplet warming in phase transformation, its results can be summarized by conclusions:

1. On the basis of the droplet energy state variation in the transitional regime and phase transformations as well as convectional heating fluxes ratio correction introduction for Stefan's hydrodynamic flow influence evaluated with Spalding parameter in classical expression provides universal droplet mathematical model for all droplet phase transformation regimes and enables to create a consistent solution algorithm.
2. For unsteady temperature field gradient description in an infinite integral equations series, it is necessary to evaluate no fewer than 101 members, for the droplet's radial coordinate, it is optimal to examine 41 sections, while for the time grid formation in the initial transitional phase transformation regime, it is optimal to explore 21 control time steps in the Fourier number time scale.
3. The phase transformations and the warming of water droplets sprayed in humid air flow are defined by air humidity and temperature, water temperature and droplet dispersity as well as heat transfer-specific factors. The lowest $T_{e,"k"}$ is detected in the idealized droplet heating case only involving conduction. A droplet slipping in the air flow and absorbed radiation flux raises the equilibrium evaporation temperature $T_{e,"c+r"} > T_{e,"c"} > T_{e,"k"}$. Water parameters define the transitional phase transformation processes, yet they are insignificant for equilibrium evaporation. The influence of droplet heat transfer is defined by their slipping in air and spectral radiation absorption.
4. The calculated vapor flow for large diameter water droplets which evaporate at equilibrium conditions in 678 °K and 1133 °K air temperatures in the complex heating case was compared with the experimental results whose reliability was defined with $\pm 5\%$ error limits. The calculated vapor flow for complex heating by radiation and weak convection, when Re<0.3, defines the experimental investigation results with $\pm 8\%$ reliability. In a relatively low temperature of 678 °K, the droplet evaporation rate due to the impact of radiation compared with heating only by conduction increases up to two times. In a high 1133 °K radiating

temperature environment, the equilibrium evaporation of large droplets is several times faster than that of droplets which are heated only by conduction.

5. The droplet heat transfer case defines the heating process in the transformation regime of the transitional phase:
   - The condensation phase transformation regime is defined by droplet surface warming to dew point temperature $T_{dp}$, therefore, in the central layers, the absorbed radiation is not significant for the duration of the condensation of phase transformation regimes. In the case of convection heating in an air flow slipping droplet water intensively circulates. The heat is effectively leaded inside droplet Thus, droplet surface warming in condensation regime slow down, and condensation regime duration increases.
   - In the case of convection heating, the droplet warms when unsteady temperature field gradient is positive, and when equilibrium evaporation is approaching, the non-isothermally in the droplet disappears.
   - In the case of complex heating, due to the impact of radiation heating, after a certain period of time, a negative temperature field gradient is formed. This time span of the transitional evaporation regime is divided into two periods. Only in the second period, preconditions arise for the absorbed radiation within the droplet to flow outside by internal convection into the droplet's surface layers and to participate in the droplet's evaporation process.
   - Due to friction forces, the impact of the droplet's slipping rapidly diminishes, therefore, convectional heating in terms of transitional evaporation decreases as well. However, the droplet's diameter is important for the radiation absorption; therefore, the radiation flux inside a droplet decreases only during the initial equilibrium evaporation stage.

6. The thermal state and the transitional phase transformations of water droplets sprayed in humid air flow are defined by the ratio of the dew point temperature or the equilibrium evaporation temperature with the parameters of sprayed water temperature $\overline{T}_{dp} = T_{dp} / T_{l,0}$ and $\overline{T}_e = T_e / T_{l,0}$. For the condensation regime, it is necessary to spray water when conditions $\overline{T}_{dp} > 1$ are valid, for the transitional evaporation regime, the droplet warms to $T_e$ temperature; meanwhile, when $\overline{T}_e > 1$, the droplet will warm, when $\overline{T}_e < 1$, the droplet will cool down.

## REFERENCES


1. European Parliament, Directive 2009/28/EC of the European Parliament and of the Council of 23 April 2009 on the promotion of the use of energy from renewable sources and amending and subsequently repealing Directives 2001/77/EC and 2003/30/EC (Text with EEA relevance), Available at: https://eur-lex.europa.eu/legal-content/EN/ALL/?uri=celex%3A32009L0028, Žiūrėta [2018 balandžio 23]
2. **Directive 2001/80/EC of the European Parliament and of the Council of 23 October 2001 on the limitation of emissions of certain pollutants into the air from large combustion plants** Available at: http://eur-lex.europa.eu/legal-content/EN/TXT/?uri=CELEX:32001L0080 Žiūrėta [2018 balandžio 23]
3. Zang, D., Tarafdar, S., Tarasevich, Y.Y., Choudhury, M.D., Dutta, T. (2019). Evaporation of a droplet: From physics to applications, *Physics Reports*, 804, 1-56.
4. Fuchs, N. A. (1959). Evaporation and droplet growth in gaseous media. London: Pergamon Press.
5. Sirignano, W.A. (1983). Fuel droplet vaporization and spray combustion theory, *Progress in Energy Combustion Science*, 9, 291–322.
6. Sazhin, S.S. (2014). Droplets and Sprays, Springer, Heidelberg.
7. Šlančiauskas, A., Kalpokaitė, R. (2006). Behavior of a heavy fuel oil droplet on a hot surface, *International Journal of Heat and Mass Transfer*, 49, 1050-1057.
8. Droplet evaporation, (2019). http://www.sciencedirect.com.
9. Ohogain, S., McCarton, L. (2018). A Technology Portfolio of Nature Based Solutions, Springer.
10. Sazhin, S., Shchepakina, E., Sobolev, V. (2018). Order reduction in models of spray ignition and combustion, *Combustion and Flame*, 187, 122-128.
11. Haywood, R.J., Nafziger, R., Renksizbulut, M. (1989). A detailed examination of gas and liquid phase transient processes in convective droplet evaporation, *Heat Transfer*, 111, 495-502.
12. Giusti, A., Sidey, J., Borghesi, G., Mastorakos, E. (2017). Simulations of droplet combustion under gas turbine conditions, *Combustion and Flame*, 184, 101-116.
13. Faeth, G.M. (1983) .Evaporation and combustion of sprays, *Prog Energy Combust Sci*, 9, 1–76.
14. Abramzon, B., Sirignano , W. A. (1989). Droplet vaporization model for spray combustion calculations, *International Journal of Heat and Mass Transfer*, 32, 1605–1618.
15. Vysokomornaya, O. V., Piskunov, M. V., Strizhak, A. P. (2017). Breakup of heterogeneous water drop immersed in high-temperature air, *Applied Thermal Engineering*, 2017, 127, 1340-1345.
16. Madero, E. J., Axelbaum, L. R. (2017). Spray breakup and structure of spray flames for low –volatility wet fuels, *Combustion and Flame*, 108, 102-109.
17. Bonefacic, I., Wolf, I., Blecich, P. (2017). Improvement of fuel oil spray combustion inside a 7 MW industrial furnace: A numerical study, *Applied Thermal Engineering*, 110, 795-804.
18. Vende, P.E., Trinquet, F., Lacour, S., Delahaye, A., Fournaison, L. (2018). Efficiency of water spraying on a heat exchanger: local characterization with the impacted surface. *Applied Thermal Engineering*, 128, 684-695.

19. Abdel-Salam, A. H., Simmson, J.C. (2016). State-of-the-art in liquid desiccant air conditioning equipment and systems, *Renewable and Sustainable Energy Reviews*, 58, 1152-1183.

20. Pretrel, H. (2017). Interaction between water spray and smoke in a fire event in a confined and mechanically ventilated enclosure, *Fire Safety Journal*, 91, 336-346.

21. Myers, T. M., Marshall, A. W. (2016). A description of the initial fire sprinkler spray, *Fire Safety Journal*, 84, 1-7.

22. Jenft, A., Boulet, P., Collin, A., Trevisan, N., Mauger, P. N., Pianet, G. (2017). Modeling of fire suppression by fuel cooling, *Fire Safety Journal*, 91, 680-687.

23. Breitenbach, J., Rosiman, V. I., Tropea, C. (2017). Heat transfer in the film boiling regime: Single drop impact and spray cooling, *International Journal of Heat and Mass Transfer*, 110, 34-42.

24. Wang, C., Xu, R., Song, Y., Jiang, P. (2017). Study on water droplet flash evaporation in vacuum spray cooling, *International Journal of Heat and Mass transfer*, 112, 279-288.

25. Kaltenbach, C., Laurien, E. (2018). CFD simulation of spray cooling in the model containment THAI, *Nuclear engineering and design*, 328, 359-371.

26. Tarkalson, D. D., King, B. A., Bjorneberg, D. L. 2018. Yield production functions of irrigated sugar beet in an arid climate, *Agricultural Water Management*, 200, 1-9.

27. Hopkins, I., Gall, H., Lin, H. (2016). Natural and anthropogenic controls on the frequency of preferential flow occurrence in a wastewater spray irrigation field, *Agricultural Water management*. 178, 248-257.

28. Polizos, G., Jang, G.G., Smith, D.B., List, F.A., Lassiter, M. G., Park, J., Datskos, P.G. (2018). Transparent super hydrophobic surfaces using a spray coating process, *Solar energy Materials and Solar Cells*, 176, 405-410.

29. Lee, J. G., Joshi, B. N., Samuel, E., An, S., Swihart, M. T, Lee, S. J., Hwang, K. Y., Chang, J. S, Yoon, S. S. (2017) Supersonically sprayed gas – and water sensing MIL-100 (Fe) films, *Journal of Alloys and Compounds*, 722, 996-1001.

30. Kronlund, D., Linden, M., Smatt, J. H. (2016). A sprayable protective coating for marble with water-repellent and anti-graffiti properties, *Progress in Organic Coatings*, 101, 359-366.

31. Sun, Y., Guan, Z., Gurgenci, H., Hooman, K., Li, X. (2018). Investigations on the influence of nozzle arrangement on the prie-cooling effect for the natural draft dry cooling tower, *Applied Thermal Engineering*, 130, 979-996.

32. Shapira, B., Cohen, I., Penki, R. T., Avraham, E., Aurbach, D. (2018). Energy extraction and water treatment in one system: The idea of using adesalination battery in a cooling tower, *Journal of Power Sources*, 378, 146-152.

33. Schmid, J., Zarikos, I., Terzis, A., Roth, N., Weigand, B. (2018). Crystallization of urea from evaporative aqueous solution sessile droplet at sub-boiling temperatures and surfaces with different wettability, *Experimental Thermal and Fluid Science*, 91, 80-88.

34. Zhang, X., Wu, X., Min, J., Liu, X. (2017). Modelling of sessile water droplet shape evolution during freezing with consideration of super cooling effect, *Applied Thermal Engineering*, 125, 644-651.

35. Voytkov, I., Volkov, Strizhak, P. (2017). Reducing the flue gases temperature by individual droplets, aerosol, and large water batches, *Experimental Thermal and Fluid Science*, 88, 301-316.

36. Perez, C.E., Kinney, K.A., Maestre, J. P., Hassan, Y.A., King, M. D. (2018). Droplet distribution and airborne bacteria in an experimental shower unit, *Water Research*, 130, 47-57.

37. Majeed, H., Svendsen, F. H. (2018). Effect of water wash on mist and aerosol formation in absorbtion column, *Chemical Engineering Journal*, 333, 636-648.

38. Corno, A., Morandi, S., Parozzi, F., Araneo, L., Casella, F. (2017). Experiments on aerosol removal by high-pressure water spray, *Nuclear Engineering and Design*, 311, 28-34.

39. Kim, H. K., Ko, H. J., Kim, K., Perez-Blanco, H. (2012). Analysis of water droplet evaporation in a gas turbine inlet fogging process, *Applied Thermal Engineering*, 33, 62-69.

40. Schuster, S., Benra, F. K, Brillert, D. (2017). Droplet deposition in radial turbines, *European Journal of Mechanics B/Fluids*, 61, 289-296.

41. Paepe, W., Carrero, M., Bram, S., Contino, F., Parente, A. (2017). Waste heat recovery optimization in micro gas turbine applications using advanced humidified gas turbine cycle concepts, *Applied Energy*, 207, 218-229.

42. Farokhipour, A., Hamidpour, E., Amani, E. (2018). A numerical study of $NO_X$ reduction by water spray injection in gas turbine combustion chambers, *Fuel*, 212, 173-186.

43. Mingrui, W., Nguyen, T. S., Turkson, R. F., Jinping, L., Guanlun, G. (2017). Water injection for higher engine performance and lower emissions, *Journal of Energy Institute*, 90, 285-299.

44. Gulhane, N. P., Landge, A. D., Shukla, D. S, Kale, S. S. (2015). Experimental study of iodine removal efficiency in self-priming venturi scrubber, *Annals of Nuclear Energy*, 78, 152-159.

45. Kichatov, B., Korshunov, A., Kiverin, A., Son, E. (2017). Foamed emulsion – fuel on the base of water – saturated oils, *Fuel*, 203, 261-268.

46. Jang, G. M., Kim, N. (2018). Relationships between dynamic behavior and properties of a single droplet of water- emulsified n-dodecane, *Fuel*, 220, 130-139.

47. Floyd, J., McDermott, R. (2017). Development and evaluation of two new droplet evaporation schemes for fire dynamics simulations, *Fire Safety Journal*, 91, 643-652.

48. Dombrovsky, L., Fedorets, A. A., Medvedev, A. (2016). The use of infrared irradiation to stabilize levitating clusters of water droplets, *Infrared Physics & Technology*. 75, 124-132.

49. Kirols, H. S., Mahdipoor, M., Kevorkov, D., Uihlein, A., Medraj, M. (2016). Energy based approach for undrstanding water droplet erosion, *Materials & Design*, 104, 76-86.

50. Turan, F., Cengiz, A., Kahyaoglu, T. (2015). Evaluation of ultrasonic nozzle with spray-drying as a novel method for the microencapsulation of blueberry's bioactive compounds, *Innovative Food science and Emerging Technologies*, 32, 136-145.

51. Shimziu, K., Fukunaga, H., Blajan, M. (2014). Biomedical applications of atmospheric microplasma, *Current Applied Physics*, 14, 154-161.

52. Wang, Y., Li, H., Zhao, L., Wu, B., Liu, S., Liu, Y., Yang, J. (2016). A review of droplet resonators: Operation method and application, *Optics & Laser Technology*, 86, 61-68.

53. Soares, D., Mendonca, S., Neto, E., Martinez, M. (2016). Electrical field on non-ceramic insulators and its relation to contact angles for constant volume droplets, *Journal of electrostatics*, 84, 97-105.

54. Multanen, V., Shulzinger, E., Whyman, G., Bormashenko, Y., Bormashenko, E. (2016). Electrostatical interaction between water droplets coated by cold plasma treated silicone oil. Quantification of cold plasmas charging of liquids, *Colloids and Surfaces A: Physiochemical and Engineering Aspects*, 509, 224-228.

55. Batory, D., Szymanski, W., Panjan, M., Zabeida, O., Klemberg, J. E. (2017). Plasma nitriding of Ti6Al4V alloy for improved water erosion, *Wear*, 374, 374-375.

56. Jyoti, B.V., Naseem, M., Baek, S. W. (2017). Hypergolicity and ignition delay study of pure and energized ethanol gel fuel with hydrogen peroxide, *Combustion and Flame*, 176, 318-325.

57. Qubeissi, M., Sazhin, S., Elwardany, A.E. (2017). Modelling of blended Diesel and biodiesel fuel droplet heating and evaporation, *Fuel*, 187, 349-355.

58. Sazhin, S. (2017). Modelling of fuel droplet heating and evaporation: recent results and unsolved problems, *Fuel*, 196, 69-101.

59. Maqua, C., Castanet, G., Lemoine, F. (2008). Bicomponent droplets evporation: Temperature measurements and modelling, *Fuel*, 87, 2932-2942.

60. Kristyadi, T., Depredurand, V., Castanet, G., Lemoine, F., Sazhin, S., Elwardany, A., Sazhina, E. M., Heikal, M.R. (2010). Monodisperse monocomponent fuel droplet heating and evaporation, *Fuel*, 89, 3995-4001.

61. Gavhane, S., Pati, S., Som, S.K. (2016). Evaporation of multicomponent liquid fuel droplets: Influences of component composition in droplet and vapor concentration in free stream ambience, *International Journal of Thermal Sciences*, 105, 83-95.

62. Neven, L., Walker, G., Brown, S. (2015). Sustainable thermal technologies and care homes: Productive alignment or risky investment?, *Energy Policy*, 84, 195-203.

63. Vourdas, N., Jouhara, H., Tassou, A.S., Vassilis, N. (2019). Design criteria for coatings in next generation condensing economizers, *Energy Procedia*, 161, 412-420.

64. Seem, J. E., House, J.M. (2010). Development and evaluation of optimization-based air economizer strategies, *Applied Energy*, 87, 910-924.

65. Tseng. C. C., Viskanta. R. (2007). Absorptance and transmittance of water spray/mist curtains, *Fire Safety Journal*, 42, 106-114.

66. Buchlin. J. (2017). Mitigation of industrial hazards by water spray curtains, *Journal of Loss Prevention in the Process Industries*, 50, 91-100.

67. You, W., Ryou, H. (2018). Development and application of a simplified radiative transport equation in water curtain systems, *Fire Safety Journal*, 96, 124-133.

68. Schrage, R. W. (1953). A theoretical study of interphase mass transfer. New York: Columbia University Press.

69. Johns, L.E., Beckmsnn, R.B. (1966). Mechanism of dispersed-phae mass transfer in visocous single-drop extraction systems, A.I.Ch.E. 10-16.

70. Tong, A. Y, Sirignano, W. A. (1983). Analysis of vaporizing droplet with slipping internal circulation and unsteady liquid-phase and quasi-steady gas-phase heat transfer, *ASME/JSME Thermal Engng Joint Cors Proc*,2, 481-487.

71. Miliauskas, G. (2001). Regularities of unsteady radiative-conductive heat transfer in evaporating semitransparent liquid droplets. *International Journal of Heat and Mass Transfer*, 44, 785–798.

72. Norvaišienė, K., Miliauskas, G. (2013). Išpurkšto vandens gyvavimo ciklas ir lašelių nestacionariojo garavimo sausame ore universalios trukmės diagrama, *Energetika*, 2, 57-68.

73. Shorin, S.N. (1964). Teploperedacha, Vishaja Shkola, Moskva.

74. Kuzikovskij, A.V. (1970). Dynamics of spherical particle powerful optical field, Izv. VUZ Fizika 5, 89–94.

75. Renksizbulut, M., Bussmann, M., Li, X. (1992). A Droplet Vaporization for Spray Calculations, *Particle & Particle Systems Characterization*, 9, 59-65

76. Deepak, K. M., Shamit, B. (2012). Internal circulation in a single droplet evaporating in a closed chamber, *International Journal of Multiphase Flow*, 42, 42-51.

77. Engberg, R. F., Wegener, M., Kenig, E. Y., (2014). The impact of Marangoni convection on fluid dynamics and mass transfer at deformable single rising droplets – A numerical study, *Chemical Engineering Science*, 116, 208-222.

78. Tseng, C. C., Viskanta, R. (2006). Enhancement of water droplet evaporation by radiation absorption, *Fire Safety Journal*, 41, 236-247.

79. Miliauskas, G. (2003). Interaction of the transfer processes in semitransparent liquid droplets, *International Journal of Heat and Mass Transfer*, 46, 4119–4138.

80. Li, L., Mishchenko, I. M. (2016). Optics of water microdroplets with soot inclusions: Exact versus approximate results, *Journal of Quantitative Spectroscopy & Radiative Transfer*, 178, 255-262.

81. Jiangnan, Li, Mlawer, E., Chylek, P. (2011). Parameterization of cloud optical properties for semi direct radiative forcing, Journal of Geophysical Research, 116, 1-11.

82. Brewster, M.Q. (2015). Evaporation and condensation of water mist/cloud droplets with thermal radiation, Int. J. Heat Mass Transfer. 88, 695–712.

83. Dobo, Z. (2018). Heat radiation measurement method for high pressure oxy-fuel combustion, *Measurement*, 2018, 124, 191-196.

84. Hulst, H.C. (1981). Light Scattering by Small Particles, Dover, New York.

85. Bohren, C. F., Huffman, D. R. (1983) Absorption and Scattering of Light by Small Particles, Wiley, New York.

86. Haseli, Y. (2018). Efficiency improvement of thermal power plants through specific entropy generation, *Energy Conversion and Management*, 159, 109-120.

87. Hosters, N., Klaus, M., Behr, M., Reimerders, H. (2013). Application of a partitioned field approach to transient aerothermal problems in rocket nozzles, *Computers & Fluids*, 88, 795-803.

88. Gonzalez-Portilio, L., Munoz-Anton, J., Martinez-Val, J. (2017) An analytical optimization of thermal energy storage for electricity cost reduction in solar thermal electric plants, *Applied Energy*, 185, 531-546.

89. Benajes, J., Martin, J., Garcia, A., Villata, D., Warey, A. (2015). In-cylinder soot radiation heat transfer in direct-injection diesel engines, *Energy Conversion and Management*, 106, 414-427.

90. Estrada, E., Labat, M., Lorente, S., Rocha, L. (2018). The impact of latent heat exchangers on the design of earth air heat exchanger, *Applied Thermal Engineering*, 129, 306-317.

91. Obando, J., Cadavid, Y., Ammell, A. (2015). Theoretical, experimental and numerical study of infrared radiation heat transfer in a drying furnace, *Applied Thermal Engineering*, 90, 395-402.

92. Chmielewski, A., Szolucha, M. (2016). Radiation chemistry for modern nuclear energy development, *Radiation Physics and Chemistry*, 124, 235-240.

93. Siegel, R., Howell, J. (2001). Thermal Radiaiton Heat Transfer, Tylor and Francis.

94. Hale, G. M. , Query, M. R , Rusk, A. N, Williams, D. (1972). Influence of temperature on the spectrum of water, *J. Opt. Soc. Am.*,. 62, 1103–1108.

95. Kesten, A. S. (1968). Radiant heat flux distribution in a cylindrically symmetric nonisothermal gas with temperature dependent absorbtion coefficient, JQSRT, 8(1), 419-434.

96. Dombrovsky, L. A , Sazhin, S. S , Sazhina, E. M. , Feng, G. ,. Heikal, M. R, Bardsley, M. E. A. (2001). Heating and evaporation of semi-transparent diesel fuel droplets in the presence of thermal radiation, *Fuel*, 80, 1535–1544.

97. Dombrovsky, L.A., Dembele, S., Wen, J. (2018). An infrared scattering by evaporating droplets at the initial stage of a pool fire suppression by water sprays, *Infrared Physiscs & Technology*, 91, 55-62.

98. Nakajima, T., King, D. (1989). Determination of the Optical Thickness and Effective Particle Radius of Clouds from Reflected Solar Radiation Measurements. Part I: Theory. *Journal of the Atmospheric Sciences*, 47, 15.

99. Renksizbulut, M., Yuen, M.C. (1983). Numerical study of droplet evaporation in a high-temperature stream. *J. Heat Transfer* , 105, 389–397.

100. Spalding, D.B. (1963). Convective Mass Transfer, Edward Arnold Publishers, 1963.

101. Hale, G. M., Querry, M.R., Rusk, A.N., Williams, D. (1972) Influence of temperature on the spectrum of water, *Journal of the Optical Society of America*, 62, 1103-1108.

102. Yuen, M.C., Chen, L.W. (1978). Heat-transfer measurements of evaporating liquid droplets. *Int. J. Heat Mass Transfer* 21, 537–542.

103. Volkov, R.S., Kuznetsov, G.V., Legros, J.C., Strizhak, P.A. (2016). Experimental investiga- tion of consecutive water droplets falling down through high-temperature gas zone, *Int. J. Heat Mass Transfer*, 95, 184–197 .

104. Vysokomornaya, O.V, Kuznetsov, G.V., Strizhak, P.A. (2016). Evaporation of water droplets in a high-temperature gaseous medium, *Journal of Engineering Physics*, 89 , 141–151.

105. Pino, C., Felli, L. P., Fell,i M., Fernandez-Feria, R. (2011). Structure of trailing vortices: comparison between particle image velocimetry measurements and theoretical models, *Physics Fluids*, 23, 013-602.

106. Ivanov, V. M. , Smirnova, E.V. (1962). Experimental research of liquid droplets evaporation velocity in non-moving high temperature environment. *Tr. IGI*, 19, 46-58.

107. Bennen, G. (2011). Droplet Collision. In ASHGRIZ, N.Sud. *Handbook of Atomization and Sprays*. Boston, MA: Springer US.

108. Miliauskas, G., Šabanas, V. (2006). Interaction of transfer processes during unsteady evaporation of water droplets. *International Journal of Heat and Mass Transfer*, 49, 1790–1803.

109. Miliauskas, G., Norvaišienė, K. (2013). Garuojančių lašelių sudėtinės pernašos nestacionariųjų procesų sąveikos sisteminis įvertinimas. *Energetika*., 59, 26–41.

110. Miliauskas, G. (2014). Grynojo skysčio lašelių fazinių virsmų režimų universalusis ciklas 1. Ciklo sudarymo metodas ir pernašos procesų skaitinio modeliavimo metodika, *Energetika*, 60, 77-95.

111. Harpole, G. M. (1982). Radiative absorption by evaporating droplets, J.*Heat Mass Transfer*, 23, 17-26.

**List of Publications on the Theme of Dissertation**

## Publications in Referred Journals of *Thomson's Reuters* Database *Web of Science* Core Collection

1. MILIAUSKAS, G., MAZIUKIENĖ, M.; RAMANAUSKAS, V. Peculiarities of the transit phase transformation regime for water droplets that are slipping in humid gas. *International Journal of Heat and Mass Transfer*, 2016, Volume 102, Pages 302-314, ISSN 0017-9310.

2. MILIAUSKAS, G., MAZIUKIENĖ, M., RAMANAUSKAS, V., PUIDA, E. The defining factors of the phase change cycle of water droplets that are warming in humid gas. *International Journal of Heat and Mass Transfer*, 2017, Volume 113, Pages 683-703, ISSN 0017-9310.

3. MILIAUSKAS, G., MAZIUKIENĖ, M., JOUHARA H., POŠKAS R. Investigation of mass and heat transfer transitional processes of water droplets in wet gas flow in the framework of energy recovery technologies for biofuel combustion and flue gas removal. *Energy*, 2019, Volume 173, Pages 740-754, ISSN 0360-5442

## Publications in the Journals Referred in International Databases

1.MILIAUSKAS, G., MAZIUKIENĖ, M., Modeling of heat and mass transfer processes in phase transformation cycle of sprayed water into gas: 1. The calculation peculiarities of droplet phase transformations parameters. *Mechanika*, 2014, Volume 20, Pages 550-558, ISSN 1392-1207.

2.MILIAUSKAS, G., MAZIUKIENĖ, M., Modeling of heat and mass transfer processes in phase transformation cycle of sprayed water into gas: 2. Phase transformation peculiarities of a droplet heated up by convection in humid gas flow. *Mechanika*, 2015, Volume 21(1), Pages 123-128, ISSN 1392-1207.

3. MILIAUSKAS, G., MAZIUKIENĖ, M., RAMANAUSKAS, V. Modeling of heat and mass transfer processes in phase transformation cycle of sprayed water into gas: 3. Energy and thermal states analysis of slipping droplet in a humid air flow. *Mechanika*. 2015, Volume 21(5), Pages 377-383, ISSN 1392-1207.

4. MILIAUSKAS, G., MAZIUKIENĖ, M., BALČIUS, A., GUDZINSKAS, J. Modeling of heat and mass transfer processes in phase transformation cycle of sprayed

water into gas: 4. Thermal state analysis of a droplet slipping in humid air flow. *Mechanika*. 2016, Volume 22 (2), Pages 96-104, ISSN 1392-1207.

5.MILIAUSKAS, G., MAZIUKIENĖ, M., PUIDA, E. Modelling of heat mass transfer processes in phase transformation cycle of sprayed water into gas: 5. Numerical modelling optimization of phase transformation cycle for droplets slipping in gas flow. *Mechanika*. 2017, Volume 23(1), Pages 22-30, ISSN 1392-1207.

6.MILIAUSKAS, G., ADOMAVIČIUS, A., MAZIUKIENĖ, M. Modelling of water droplets heat and mass transfer in the course of phase transitions. I: Phase transitions cycle peculiarities and iterative scheme of numerical research control and optimization. *Nonlinear Analysis: Modelling and control*. 2016, Volume 21(1), Pages 135-151, ISSN: 1392-5113.

7.MILIAUSKAS, G., ADOMAVIČIUS, A., MAZIUKIENĖ, M. Modelling of water droplets heat and mass transfer in the course of phase transitions. II: Peculiarities of the droplet radial coordinate and the time grid calibration. *Nonlinear Analysis: Modelling and control*. 2017, Volume 22 (3), Pages 386-403, ISSN 1392-5113.

**Publications in Conference Proceedings**

1.MAZIUKIENĖ, M., MILIAUSKAS, G., ADOMAVIČIUS, A. Lašo uždavinio skaitinio eksperimento optimizavimas lašelio terminių parametrų aspektu. *Šilumos energetika ir technologijos – 2015: konferencijos pranešimų medžiaga*, 2015 m. sausio 29-30 d., Kauno technologijos universitetas, Kaunas.

2.MAZIUKIENĖ, M., MILIAUSKAS, G. Drėgno oro sraute slystančių vandens lašelių kondensacinio fazinių virsmų režimo savitumai. *Šilumos energetika ir technologijos – 2016: konferencijos pranešimų medžiaga*, 2016 m. sausio 30-31 d., Kauno technologijos universitetas, Kaunas.

3.MILIAUSKAS, G., MAZIUKIENĖ, M., RAMANAUSKAS, V. Regularities of pure liquid droplets phase transformation cycle and its defining factors. *EMN Meeting on Droplets 2016*, May 9-13, 2016, San Sebastian, Spain.

4.MILIAUSKAS, G., MAZIUKIENĖ, M., RAMANAUSKAS, V. Interaction of heat and mass transfer processes of water droplets slipping in humid gas.: 12$^{th}$ *International conference on heat transfer, fluid mechanics and thermodynamics, HEFAT 2016*, July 11-13, 2016, Malaga, Spain.

5.MAZIUKIENĖ, M., MILIAUSKAS, G. Drėgnuose dūmuose išpurkšto vandens lašelių pereinamuosius fazinių virsmų procesus įtakojantys veiksniai ir slydimo faktoriaus vaidmuo. *Šilumos energetika ir technologijos – 2017: konferencijos pranešimų medžiaga*, 2017 m. sausio 26 d., Kauno technologijos universitetas. Kaunas.

6.RAMANAUSKAS, V., MAZIUKIENĖ, M., MILIAUSKAS, G. The combined heat and mass transit processes of water droplets in biofuel technologies.: 14-th *International conference of young scientists on energy issues, CYSENI 2017,* May 25-26 d., Lietuvos Energetikos Institutas, Kaunas.

7.MAZIUKIENĖ, M., MILIAUSKAS, G. Skaitinės iteracinės schemos pusskaidrio skysčio lašelių šilumos ir masės mainų parametrams apibrėžti savitumas ir optimalus tinklelio gradavimas. *Šilumos energetika ir technologijos – 2018: konferencijos pranešimų medžiaga*, 2018 m. vasario 1 d., Kauno technologijos universitetas. Kaunas.

8.MAZIUKIENĖ, M., MILIAUSKAS, G. Drėgnose dujose šylančių vandens lašelių šilumos ir masės mainai pereinamųjų fazinių virsmų režime. *20-oji Lietuvos jaunųjų mokslininkų konferencija,* 2017 m. kovo 20 d., Vilniaus Gedimino Technikos Universitetas, Vilnius.

SL344. 2019-06-17, 12,25 leidyb. apsk. l. Tiražas 12 egz. Užsakymas 133.
Išleido Kauno technologijos universitetas, K. Donelaičio g. 73, 44249 Kaunas
Spausdino leidyklos „Technologija“ spaustuvė, Studentų g. 54, 51424 Kaunas